MIMO Control of Climate in Livestock Production Houses

- P10-
Control & Automation
Project Report

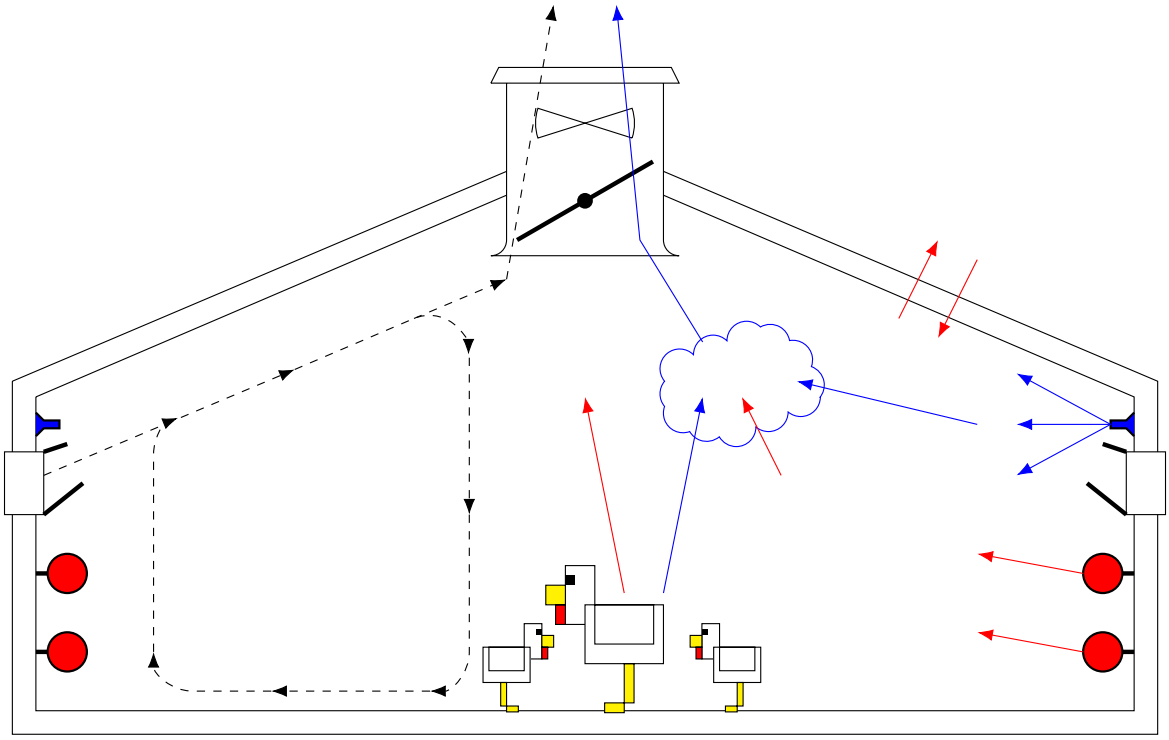

Aalborg University
Department of Electronic Systems
Fredrik Bajers Vej 7B
DK-9220 Aalborg

Department of Electronic Systems
Fredrik Bajers Vej 7
DK-9220 Aalborg Ø
http://es.aau.dk

AALBORG UNIVERSITY
STUDENT REPORT

Title:
MIMO Control of Climate in Livestock Production Houses

Theme:
CA4 - Control of Complex Systems

Project Period:
Spring Semester 2022

Project Group:
Group 1031

Participant(s):
Jóannes Højgaard Reynskor
Mads Jacob Riisager

Supervisor:
Jan Dimon Bendtsen

Page Numbers: 89 without formalities
Appendix: 16

Date of Completion:
June 1, 2022

Synopsis:

This project examines the dynamics of a livestock production house and the requirements for the poultry inside. The goal is to design an MIMO controller capable of keeping the climate inside the production house at references specified by the farmer. For this project the internal temperature is defined as the most important state and it should be kept at reference with a 2 °C margin of error.
The project is made in collaboration with SKOV A/S, who has supplied data from a production house located at Mosegaarden as well as providing an Air Physical Laboratory to be used as a test facility for the MIMO controller.
A non-linear model is derived for the production house, where data from the Mosegaarden and from the laboratory is used for parameter estimation. Using the model an Extended Kalman Filter (EKF) is designed and used as an state observer. For the controller an Linear Quadratic Regulator (LQR) and Linear Quadratic Integrator (LQI) is designed.
Testing in the laboratory resulted in a successful test, where the LQI kept the temperature at reference inside the 2 °C margin of error.

Preface

This report was written in LaTeX and has been shared online in-between the group members using Overleaf licensed to all students at Aalborg University.

Citations is marked in square-brackets with a number corresponding to a source in the bibliography, e.g. [1].

Throughout the report, decimal separators will be noted with a dot ".", e.g. 100 mV corresponds to 0.1 V.

Special thanks goes to SKOV A/S, who provided guidance and access to their Air Physical Laboratory located in Glyngøre.

Contents

Part I

Preliminary Study

Chapter 1

Introduction

To meet the future food demand of the world, the FAO (Food and Agriculture Organisation of the United Nations) has placed the increase of agricultural production as one of the most important challenges for the 21st century [2]. One way of increasing agricultural production is to make the current production more efficient.

In a modern livestock production house almost all aspects of the livestock's climate is measured and controlled. The goal is to produce as much product as possible using the least amount of resources. For livestock production the product is often meat, but it can also be milk, eggs or feathers. Here the resources would be feed, bedding, heating, electricity etc.

All livestock have climate critical boundaries, which describe the interval of temperature, humidity, airspeed etc. in which their production is maximised. Different species of livestock have different requirements for these boundaries. Such as cows which are more impervious to changing airspeed, whereas poultry is more sensitive. In this report the focus will be on poultry for the purpose of having real world numbers for use during controller design.

Poultry is responsible for 35.44 % of the worlds meat production in 2020 [3]. In UK 73 % of the production occurs inside livestock production houses and in the USA the percentage is 99 % [4][5].

With a large population of poultry living in close quarters the climate has a profound effect on their growth rate. The temperature, humidity and ventilation air speed affects the eating habits of the animals. If they feel cold, they will eat more and convert the food into energy to keep warm, or if they feel warm they will stop eating all together and not gain weight. In both cases the yield of the poultry is reduced, increasing the expenditures for the farmer. [6]

To keep the climate at a optimal level, which are further described in section 2.2 and section 2.3, a climate controller is installed in most modern production houses.

This project is made in collaboration with SKOV A/S, who specialises in making climate controllers for production houses, which keeps the conditions inside the climate critical boundaries for a specific species of livestock. Currently their climate controller consist of a combination of SISO controllers, each controlling one aspects of the climate. SKOV wishes to replace this system with a single MIMO controller able to keep an optimal climate for the livestock.

The approach in this report will be to firstly design a model of a production house and then use this model to design a MIMO climate controller. The controller will then be tested at a test facility located at SKOV A/S in Glyngøre, where the physics of both a production house and poultry and be simulated.

For the climate inside the production house each country have their own requirements by law. This report only focuses on designing a controller which can keep the climate at the specifications set by its user. Therefore the legal aspects will not be discussed.

Chapter 2

Problem Analysis

In this chapter different aspects of the problem is presented with the goal of finding a final problem statement. The following aspects are in focus:

- The inner workings of a modern production house.
- The requirements for the well being of the livestock, in this case poultry.
- The air physical laboratory located at SKOV A/S at which all tests in this project will be conducted.
- The current controller utilised by SKOV A/S.

It is important for the reader to understand the inner workings of a modern production house together with the livestock requirements, to further understand the usefulness of the air physical laboratory, and how it can be used to test equipment and controllers before they are installed in real production houses.

2.1 Modern production house

To understand the usefulness of the air physical laboratory located at SKOV A/S, the basics of a modern real world production house must be explained. Production houses are designed differently depending on the livestock, but this section will only introduce the ones used for broilers, since they are the focus of this project. Furthermore only production houses produced by SKOV A/S will be mentioned.

In Figure 2.1 four types of production houses sold by SKOV A/S are illustrated. What characterises a modern production house compared too an normal barn/stable is that the internal environment is controlled.

Through ventilation both temperature and humidity as well as harmful gasses can be adjusted. Heating can be added through heaters along the walls and humidity can be increased using sprinklers. The sprinklers can furthermore be used to cool the production house through phase-change in hotter seasons or regions.

Thereby the optimal climate for the livestock is created maximising profit for the farmer and reducing the use of resources. The optimal climate will further be described in section 2.2.

For easy control of the inner climate the whole production house is build with with a control aspect in mind. Therefore all objects which could disturb the air flow and create turbulence are moved to the outside, thereby creating a smooth surface inside.

By avoiding turbulence the air inside the production house can be said to be uniformly distributed, and thereby the temperature and humidity can be assumed to be the same throughout, simplifying control and reducing the number of sensors required.

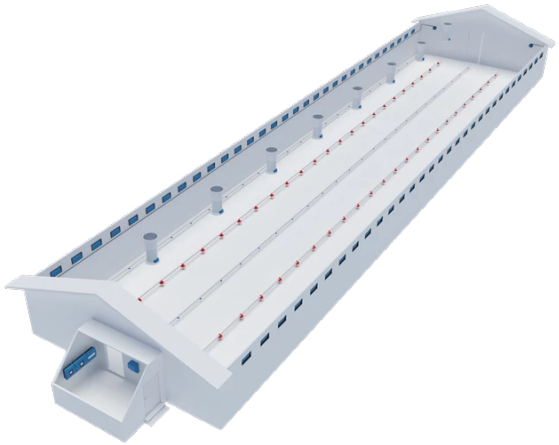

(a) LPV system [7].

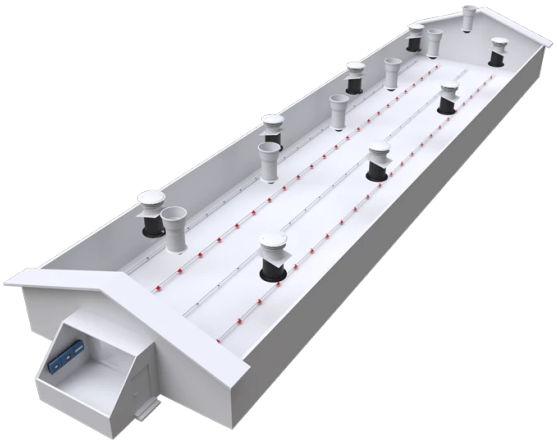

(b) Equal Pressure System [8].

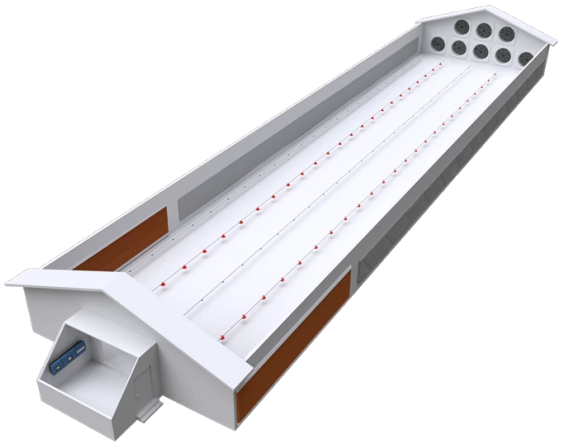

(c) Tunnel System [9].

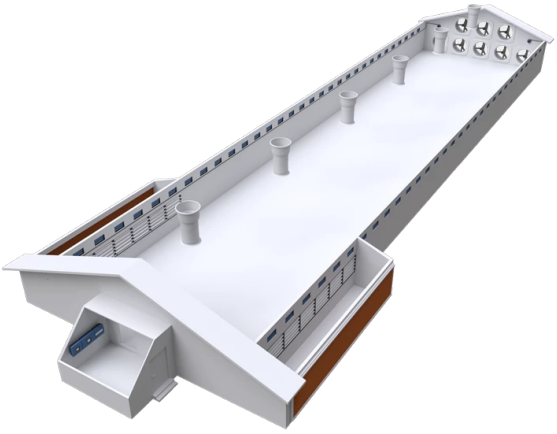

(d) Combi-Tunnel System [10].

Figure 2.1: Four types of production houses sold by SKOV A/S [11].

For all four systems air flow is created by generating a negative pressure inside the production house, thereby forcing air to be pushed inside the production house. The variation between the systems are then the placement of air inlets and outlets.

Both the LPV and Equal Pressure system have chimneys generating the negative pressure, but the LPV system has air inlets along the side on the building, while the Equal Pressure utilises secondary chimneys on the roof as illustrated in Figure 2.1a and Figure 2.1b. Both of these systems are designed for temperate climates. [7][8]

The Equal Pressure system is furthermore designed for free-range chickens, which have access to the outside through pop-holes alongside the walls. The Equal Pressure System design prevents air from entering through these pop holes, and thereby the poultry will not move away from the pop holes resulting in a uniform livestock distribution. [7][8]

The tunnel system utilises fans mounted on the end of the building to create the negative pressure. The air inlets are them placed along the side or the end of the building. The air inlets are furthermore lined with cooling pads making the tunnel system useful in hotter climates. These cooling pads works by letting air pass through running water, which cools

the air before it enters the production house. The tunnel system is illustrated in Figure 2.1c. [9]

The combi-tunnel shown in Figure 2.1d utilises all of the above mentioned techniques in combination, thereby making the production house robust to greater change in temperature. This could be areas with high temperatures during the day and low temperatures during the night. [10]

With a basic understanding of how modern production houses work, next the optimal climate and livestock requirements will be described followed by the air physical laboratory.

2.2 Optimal Climate Considerations

In the introduction the optimal climate for a specific species of livestock was mentioned. In this report a optimal climate is defined as the climate which maximises profit for the farmer. This does not always equals maximising the growth of the livestock. [6, p. 9-11]

Two factors important for a optimal climate is the stress of the livestock and the draught that it feels. Stress can impair the livestock's immune system, increase aggressive behaviour, cause physiological changes (ex. stomach ulcers for pigs) and increase mortality, which ultimately reduces the yield. [6, p. 9-11]

The feeling of draught is affected by three factors inside the production house:

- Temperature
- Humidity
- Airspeed

An increase in either airspeed or humidity will make the livestock experience the current temperature as colder. This can cause stress, and furthermore overeating since the livestock will want to increase their own heat production, which at the same time reduces protein production. Thereby resulting in reduced profit. [6, p. 9-11]

On the other hand, if the livestock becomes too hot, they will experience heat stress and stop eating all together, reducing their growth, which again reduces profit. Therefore the experienced temperature needs to be kept inside an interval, which varies from animal to animal. [6, p. 9-11]

It should be noted that if the air speed inside the production house does not exceed $0.2\,\mathrm{m\,s^{-1}}$, then the effects of draught is minimal and can be ignored [6, p. 8].

The air quality in the production house is furthermore an important aspect. Livestock and their excrement produces gasses, which can be toxic (ammonia, hydrogen sulphide and carbon monoxide) or replace oxygen, thereby causing suffocation (methane, nitrous oxide and carbon dioxide). [6, p. 49-51][12]

In the next section the requirements for livestock will be described. As mentioned in the introduction, this report focuses on poultry, therefore only their requirements are listed.

2.3 Poultry Requirements

The production starts with the farmer placing live chicks inside the livestock production house, with a maximum age of 1 day. The poultry then grows from a chick weighing around 40 g to a fully grown chicken weighing between 2150 g–2200 g in a span of around 37 days. [6, p. 25]

Beforehand the farmer has littered bedding for the poultry. The bedding is responsible for absorbing the moisture from the excrement produced by the poultry and can be reused 1-2 times for multiple groups of poultry.

The temperature requirement of poultry varies with age. When the poultry is first placed the temperature requirement is around 33 °C, with a variation tolerance of roughly 2 °C. A rule of thumb is to reduce the temperature 0.5 °C pr. day afterwards, until a temperature of 18 °C is reached. See Table 2.1 for more detail. [6, p. 23-27]

Poultry is more robust towards changes in humidity than temperature, however it should never be under 50 % relative humidity for day-old chicks, since they can become dehydrated and die before finding a water source. For bigger chicks the recommendations is a upper limit of 70 %–75 % relative humidity, but this is to prevent wet bedding. See Table 2.1 for more detail. [6, p. 23-27]

Wet bedding can cause burns to the poultry's feet called foot pad lesions, when mixed with ammonia. Furthermore wet bedding will increase the microbial activity in the bedding further increasing the release of ammonia. [6, p. 23-27]

The light levels is furthermore a requirement that needs consideration. For normal day operation the law in Denmark states a requirement of 20 lx. A normal light schedule has 8 h of nighttime followed by 16 h of daytime when the poultry is between 6 and 12 days old. Then nighttime can be reduced to 4.5 h in the age between 13 and 28 days old, and finally between 29 days and 5 days before slaughter the nighttime period can be reduced to 1.5 h. [6, p. 23-27]

Table 2.1: Requirements for poultry [6, p. 26].

Age [days]	Weight [g]	Feed Consumption [$kg\,kg^{-1}$]	Mortality Rate [%]	Temp. [°C]	Relative humidity [%]
1	42			33	50
7	175		1.0	30	50
14	444		1.6	28	56
21	843		2.2	25	64
28	1370		2.8	22	72
35	1985	1.63	3.4	18	75
36	2076	1.65			
37	2168	1.67			
38	2260	1.69			
39	2351	1.70			
40	2442	1.72	3.5	17	75

2.4 Production house vs. Laboratory

Many factors play a role in the growth of poultry, and if not controlled properly the factors may end up killing the poultry or reduce the yield of the production.

Therefore SKOV A/S has constructed an Air Physical Laboratory at their headquarters in Glyngøre, Denmark. In this laboratory it is possible to simulate all conditions present in modern production houses, but without any risk of endearing any livestock or reducing a farmers yield.

The external environment for different parts of the world or different seasons can further be simulated together with the heat and water vapour output of the livestock themselves. This system will therefore be used in this project for testing the controller designed in chapter 6. An overview of the system is given in section 2.5.

2.5 System Overview - Air Physical Laboratory

In this section an overview of the laboratory will be given as well as a description of all the equipment, which will be used for simulating a full production house. The controller and model designed during this project will be tested/verified in the laboratory. Illustrations of the laboratory can be seen in Figure 2.2 and Figure 2.3.

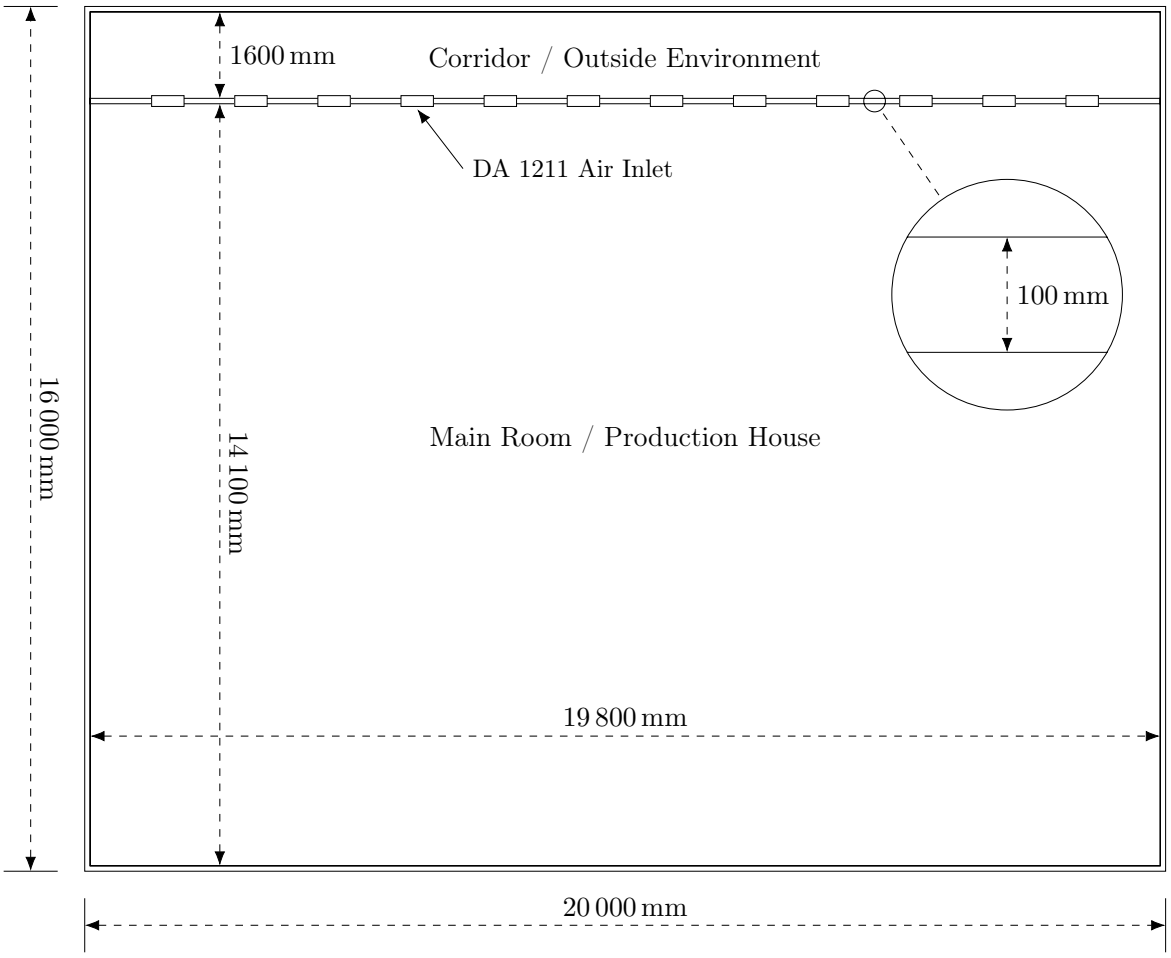

Figure 2.2: Illustration of the air physical laboratory viewed from above.

As illustrated in Figure 2.2 the air physical laboratory consists of two rooms. The main room used for simulating the production house measures 19 800 mm × 14 100 mm. A small corridor measuring 19 800 mm × 1600 mm is used for simulating an outside climate. Between the two rooms is a wall where air inlets can be mounted, which are described further in subsection 2.5.1. All walls consist of 100 mm PIR panels which is short for polyisocyanurate and is used as fire retardant insulation.

The angle of the roof inside the main room can be changed by raising or lowering the roof on one side as illustrated in Figure 2.3. The angle range is 0°–15° with the lowest end of the roof moving between 250 cm–650 cm. It is further possible to lower and raise the roof on both sides, so a flat roof can be achieved at any height in the range 250 cm–650 cm.

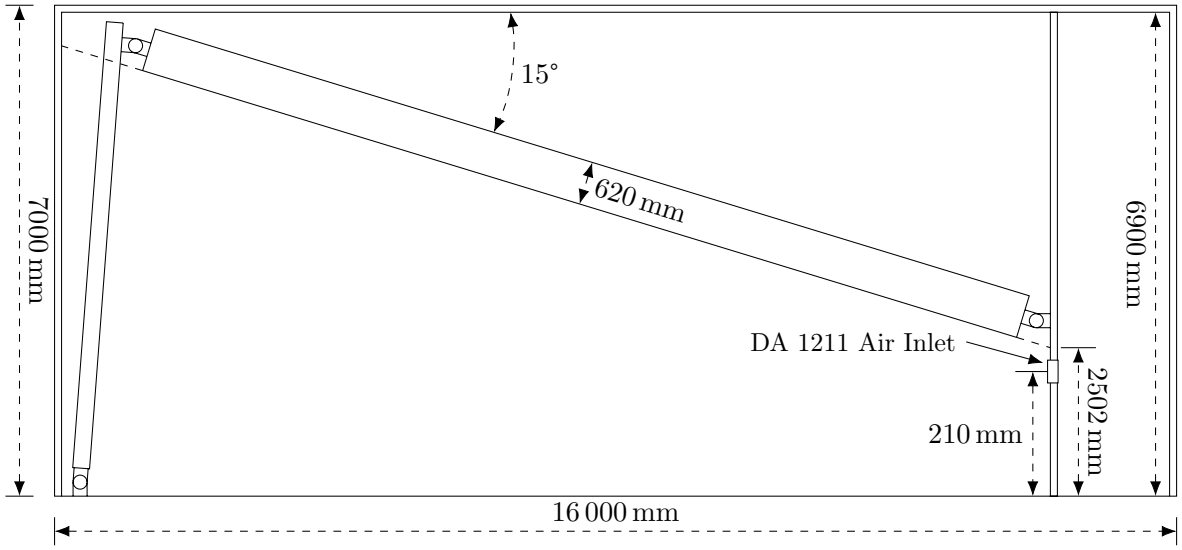

Figure 2.3: Illustration of the air physical laboratory viewed from the side.

2.5.1 Air Inlet

In the air physical laboratory the wall between the corridor and main room can be outfitted with a series of DA 1211/1911 flange inlets [13]. During this project the inlet used is the DA 1211 seen in Figure 2.4, which has a length of 600 mm, while the DA 1911 have a length of 835 mm. A DA 1211 anti freeze model also exists, but is only used in places with extremely low outside temperatures and is therefore not relevant for our tests in the air physical laboratory.

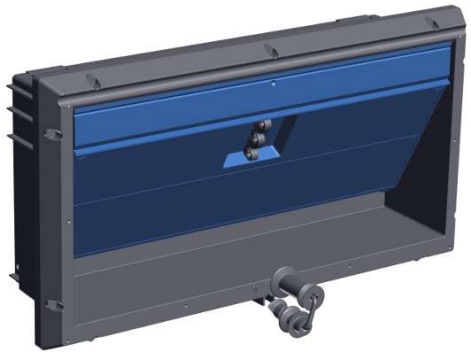

Figure 2.4: The DA 1211 air inlet produced by SKOV A/S [13].

An air direction baffle can be added to the top of all DA 1211 air inlets. The purpose being to direct the air to follow the roof of the production house and avoid adhesion to the wall. Otherwise adhesion to the wall could cause turbulence, when the air hits the corner between the wall and roof. If two rows of inlets are used the baffle can only be mounted on the top row. However in the case for this project only one row of air inlets will be used. [13]

A total of 12 DA 1211 inlets are mounted 210 cm above the floor as shown in Figure 2.5 and illustrated in both Figure 2.2 and Figure 2.3.

Figure 2.5: Image of the placement of the DA 1211 air inlets inside the air physical laboratory.

The position of the inlet flaps (the blue flap in Figure 2.4), which controls the angle of inlet air jet into the production house is controlled with a pulley-system powered by a DA 174 pulley motor. The motor takes a step-less 0 V–10 V control signal and has a pulling length of 380 mm. An illustration of the DA 174 can be seen in Figure 2.6. [14]

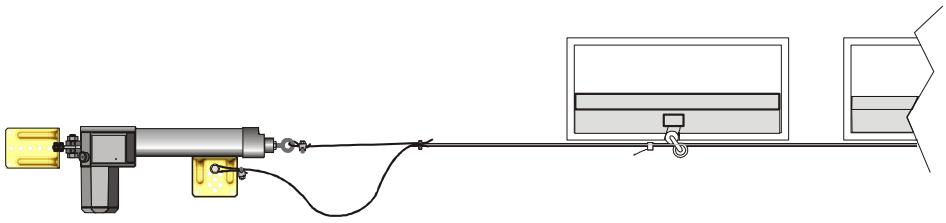

Figure 2.6: Illustration of a DA 174 mounted vertically connected to air inlets via a pulley system. [14]

2.5.2 Air Outlet

For the air outlet two DA 820 chimneys are used. The purpose for the air outlet is to create a vacuum inside the production house, which sucks air in via the air inlets. Therefore the airspeed created by the airflow in the air outlet is not considered, only the vacuum it creates is. [15]

SKOV have informed that each DA 820 is capable of delivering a flow rate of 23 200 $m^3\,h^{-1}$, which is linearly controlled by a 0 V–10 V. They can be controlled in parallel, so only one control signal is required.

Figure 2.7: DA 820 Chimney [15].

2.5.3 Humidification & Cooling

For humidification the laboratory can be outfitted with sprinklers, which spray water into the room. This functionality can furthermore be used to cool the room, when the water phase changes into vapour. Each sprinkler head can output $6.3\,\mathrm{L\,h^{-1}}$.

The flow rate is controlled by a single pump, which can only be turned on and off, meaning the flow rate will have to be controlled with a low frequency PWM signal.

2.5.4 Heating

For heating in a normal production house, long pipes called spiraflex would be used. These would be mounted to the sides of the production house below the air inlets, and through them hot water would be pumped. These pipes have a large surface area, allowing for large transfer of heat from the water to the air inside the production house. [16]

Figure 2.8: Spiraflex pipes used for heating in production houses [16].

The spiraflex is however not used in the air physical lab. The heat input will instead be simulated with 55 kW fan heaters. These are linearly PID controlled with a signal of 0 V–10 V.

2.5.5 Poultry Simulation

Pipes transporting hot water can be placed on the floor of the laboratory and act as floor heating, simulating the heat output of the poultry. For simulating the water vapour from the poultry the sprinklers will be used.

2.5.6 Sensors

For sensors inside the air physical laboratory only the type DOL 114 will be used. The DOL 114 both measures temperature and humidity. Since there are no real poultry inside the laboratory no gasses like ammonia or carbon dioxide will build up, and therefore they can be ignored during the test in the laboratory. [17]

The DOL 114 sensor outputs a 0 V–10 V signal for both the humidity and temperature. See Table 2.2 for more information. The DOL 114 sensor will be used both inside the main room of the laboratory and the corridor simulating the outside, so the controller can get both the current inside and "outside" temperature and humidity readings.

Table 2.2: DOL 114 output values. RH is relative humidity. [17]

	Humidity	Temperature
Measurement Range	0 %–100 % RH	−40 °C–60 °C
Accuracy	RH 40 %–85 % at 0 °C–40 °C: ±2 %	10 °C–40 °C: ±0.5 °C
	RH 10 %–95 % at 0 °C–40 °C: ±3 %	−30 °C–60 °C: ±1.5 °C
Output signal	0.1 V $\%^{-1}$ RH	0.1 V $°C^{-1}$; 0 °C at 4 V

In a real world production house it would be necessary to measure the levels of carbon dioxide inside the production house using a DOL 119 climate sensor [18]. A DOL 53 climate sensor could furthermore measure the levels of ammonia, but in the majority of cases this is not necessary since steady and constant ventilation already keeps the levels of ammonia low [19].

Furthermore a DOL 16 light sensor can be used to control the light levels inside the production house. As mentioned in section 2.3 this can be used to control the day and night cycle for the poultry and thereby increase production. [20]

2.6 SKOV current controller

In Figure 2.9 the current controller implemented by SKOV is illustrated. It consist of six SISO controllers working together to control the climate inside the production house. Three inputs to the system is controlled by the six controllers. Ventilation marked as green, heating marked as red and humidification marked as blue.

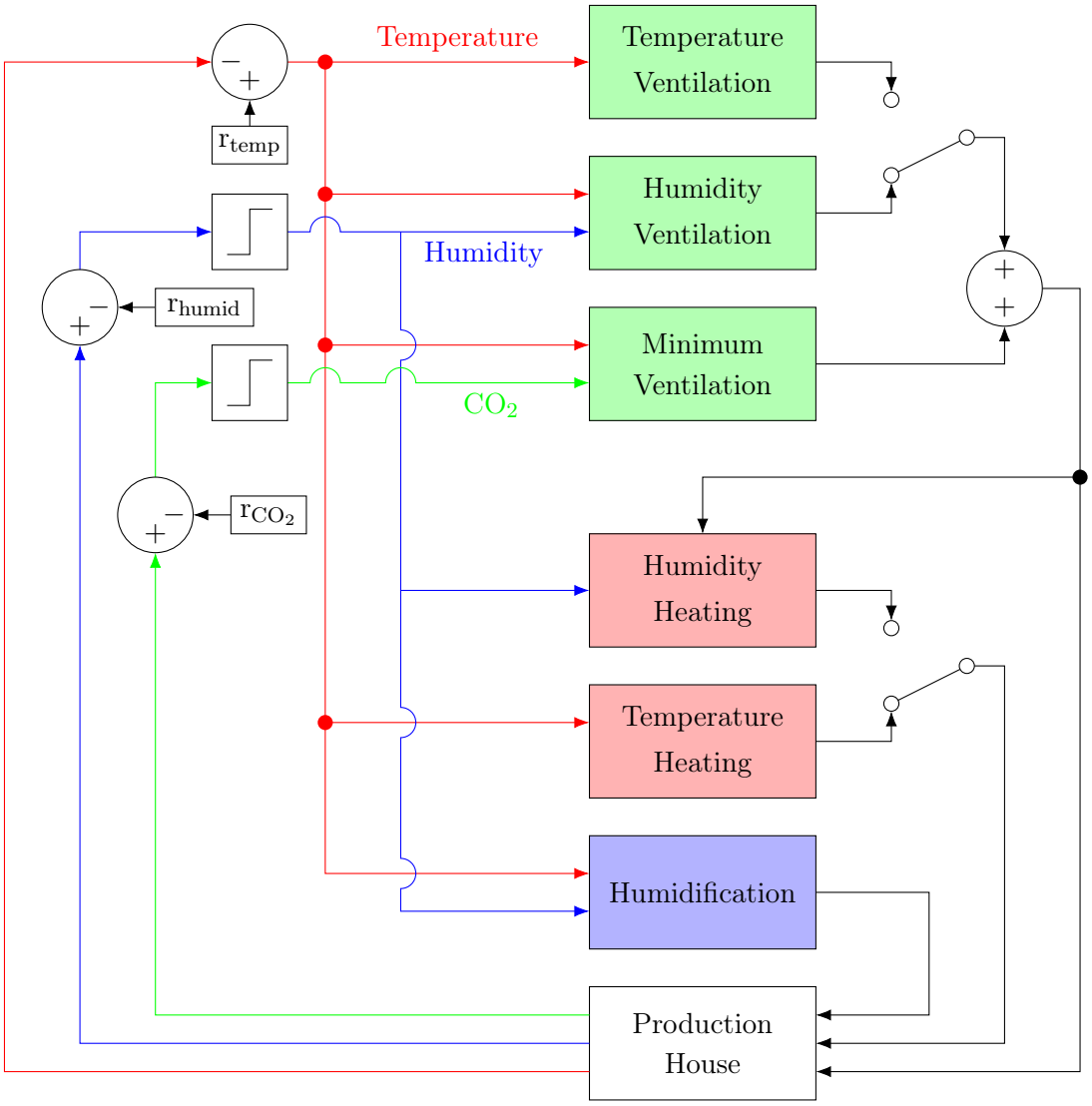

Figure 2.9: Block Diagram over the current controller implemented by SKOV.

The controllers are not all activated at the same time. Heating and ventilation can either be set to control the temperature or humidity, but not both concurrently. So if both heating and ventilation tried to control the temperature at the same time they would work against each other, since they do not have the means of knowing what the other part is doing. The decision of which controller controls which state is made by the farmer and illustrated as switches in Figure 2.9.

For the current system only the temperature are set to follow a reference. Humidity and CO_2 levels are a maximum allowed level specified by the farmer. A minimum ventilation controller is added to avoid a build up of harmful gasses.

Even though the controllers all are SISO controllers, some of them have a discrete input for safety. All ventilation and humidification blocks receives the current temperature as a discrete input (ignoring the ventilation block, which only receives the temperature). The discrete input is used as a constraint to ensure that the temperature does not get below a critical point, where the animals can experience cold stress. If the temperature gets to low,

ventilation and humidification is turned off.

Another control block which receives a secondary input is the "Humidity Heating". Although given its name, this controller does not heat the room, but rather cools it using sprinklers. The air speed affects the effectiveness of the cooling and is therefore added as a disturbance. "Humidity Heating" is used in seasons or world regions when and were the climate is hot and active cooling is required.

2.6.1 Shortcomings of the current controller

Light Schedule

It is known that poultry produces more heat and water vapour in the day time than in the nighttime. Since the light in the production house runs on a schedule, this could be added to the control structure as an input, thereby giving the controllers the possibility to predict and act on future increases and decreases in heat and vapour production. Currently the light level is not included in SKOV's control structure.

SISO Control Disadvantage

Since all controllers in the current control structure are SISO controllers, they all suffer from the disadvantage that they can only control one state of the climate inside the production house. Since all states affects each other some of the controllers will end up fighting each other. Therefore one state has to be prioritised, in this case it is the temperature state as described previously.

The temperature is affected by both the heating, ventilation and humidification. But only one of the control blocks actively uses the temperature as a reference at a given time. The rest just shuts off completely if the temperature reaches a critical point. Here it would be more effective to have a MIMO controller that can account for the interactions between states, and use ventilation, humidification and heating in combination to create an ideal climate inside the production house.

Adjustment of the air inlets

As described in subsection 2.5.1 the air inlets flap position is controlled via a pulley system actuated by a linear actuator. In the current control structure, the linear actuator is manually adjusted by the farmer, and the farmer decides how much the actuator affects the position of each inlet flap by adjusting the pulley system.

Since the ventilation controllers cannot adjust the air inlets, they must instead limit the range of the chimney ventilators as to avoid generating turbulence inside the production house. If however the ventilation controllers could adjust the air inlet positions to avoid turbulence, the controller would be able to utilise a larger range of ventilation throughput from the chimney ventilators.

This could be implemented in two ways. The cheapest way would be to add the current manual linear actuator into the current control structure. A more expensive way would be to add a actuator to each individual air inlet, thereby giving the ventilation controller the ability to adjust each air inlet individually.

2.7 Final Problem Statement

Based on the findings in the problem analysis a problem statement has been formulated.

The goal is to design a MIMO controller based on the wish from SKOV A/S, that is able to keep the climate inside of the production house at the references defined by the farmer.

In section 2.3 a tolerance of 2 °C is mentioned for the poultry. Therefore a deviation of 2 °C is allowed for the temperature inside of the production house. The temperature is furthermore the most important state, since the poultry is more robust to changes in humidity than temperature.

Additionally it was found in Table 2.1, that the poultry will experience a temperature range of 17 °C–33 °C during their lifetime.

The problem statement is therefore as follows:

"How can a MIMO climate controller for a poultry production house be designed, which keeps the internal temperature at a reference between 17 ℃–33 ℃ *with a maximum deviation of* 2 ℃*."*

Part II

System Analysis

Chapter 3

System Model

In this chapter a model of the production house environment will be designed. An overview of the system inside the production house can be seen in Figure 3.1.

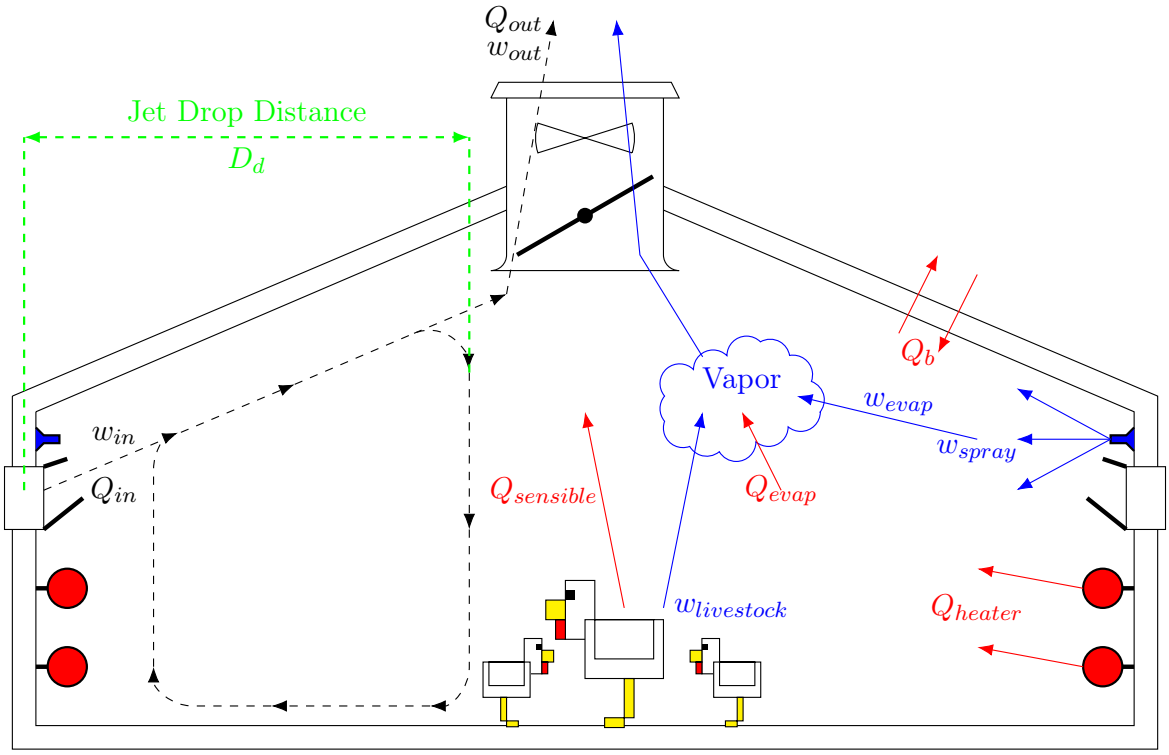

Figure 3.1: Illustration of a cross-section of a production house. Heat transfer is illustrated in red and water flow in blue. All variables are described in section 3.1 and 3.2 or can be found in Appendix A.

As seen in Figure 3.1 there are four main aspects to consider in creating a model. The ventilation, the heater, the water sprinkler and the poultry. The ventilation replaces the air and transports water vapour out of the production house. The heater inputs heat to increase the temperature and the sprinkler inputs water which can be used to lower the temperature through evaporation. Lastly the poultry is one of the main disturbances, since they produce both heat and water vapour.

Using these four main aspects, a model for the production house is designed in section 3.2. Figure 3.1 will be referenced throughout.

A fifth aspect is the jet drop distance marked with green, but as it will be explained in section 3.1 it is only used to ensure the air does not become turbulent inside the production house. Therefore it is not included in the model derived in section 3.2.

3.1 Air Flow Model

In this section a model for the jet drop distance for the air entering the production house is presented. Looking at Figure 3.1 the jet drop distance D_d is illustrated to be the distance the inlet air travels before hitting the floor.

The model is based on previous work [12]. The jet drop distance is used to check if the air current in the production house is laminar or if it is turbulent.

If the airflow in the production house is laminar the air mixture will be homogeneous meaning there is no stratification of the air. Thereby it can be assumed that the air temperature is the same everywhere. However, if the airflow becomes turbulent it will no longer be homogeneous.

A homogeneous temperature throughout the production house reduces the amount of temperature sensors needed. Furthermore the model does not need to account for the air movement caused by difference in temperature or air pockets with lower or higher temperatures, making the model less complex.

The goal with the air flow model is therefore to give the controller a state, which can be used to adjust the ventilation so as to avoid turbulent airflow.

3.1.1 Airflow Pattern

To accurately model the temperature inside of the livestock production house the airflow pattern must be considered as it is a key factor in controlling the temperature. The airflow pattern of a production house with given dimensions can be described using the corrected Archimedes Number Ar_c. Ar_c is then used to describe the drop distance of the air jet.

Archimedes Number

The Archimedes Number Ar is a dimensionless variable which can be used to describe the motion of fluids or gasses affected by differences in density.

In the case of this project it will be used to describe the drop distance of an air jet entering a livestock production house. From the drop distance the direction of the circulation of air inside the production house can be determined as illustrated in Figure 3.2.

Using the results from [12] the corrected Archimedes number is given in Equation 3.1, which takes into account the imperfect shape of the air inlet in production houses. Imperfect refereeing to that the inlets are not aerodynamically shaped.

$$Ar_c = \frac{g \cdot C_d \cdot a \cdot b \cdot W \cdot H \cdot (W + H) \cdot (T_s - T_a)}{q_{inlet,i}^2 \cdot (T_s + T_a)}, \tag{3.1}$$

where

g	$[\mathrm{m\,s^{-2}}]$	gravitational acceleration,
C_d	$[\cdot]$	discharge coefficient,
a	[m]	vertical dimension of the inlet,
b	[m]	horizontal dimension of the inlet,
W	[m]	width of the livestock production house,
H	[m]	height of the livestock production house,
T_s	[K]	livestock production house temperature,
T_a	[K]	ambient temperature outside,
$q_{inlet,i}$	$[\mathrm{m^3\,s^{-1}}]$	volumetric airflow through inlet no. i.

Given a Archimedes number of above 70 ($Ar_c > 70$) the air jet follows the roof of the production house and gives a stable airflow/circulation. This is furthermore known as the Coandă effect [21]. Below 30 ($Ar_c < 30$) the airflow is still stable, but the air jet drops early creating a circulation in the opposite direction. Between these values ($30 < Ar_c < 70$) the airflow becomes unstable. All scenarios is illustrated in Figure 3.2. [12]

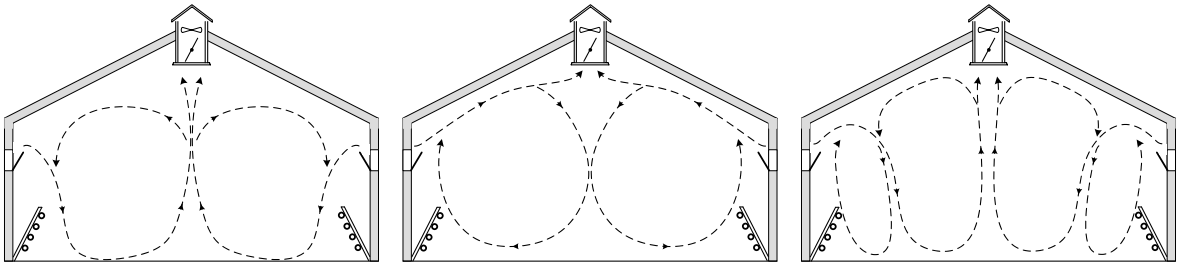

(a) $Ar_c > 70$ (b) $Ar_c < 30$ (c) $30 < Ar_c < 70$

Figure 3.2: Cross-section view of airflow inside livestock production house given different intervals of Ar. [12]

3.2 Humidity & Temperature Models

In this section both the mass balances and energy balances for the production house will be derived. Both balances are important for determining the current temperature inside the production house, because of their correlation illustrated as

$$\text{temperature} = \frac{\text{energy}}{\text{mass} \cdot \text{specific heat capacity}}.$$

For the modelling some assumptions about the system has been made.

- The air speed inside the production house does not exceed $0.2\,\mathrm{m\,s^{-1}}$ and can be delimited to zero as mentioned in section 2.2. [6, p. 8]
- The volumetric air flow through the inlets and outlets of the production house is equal.
- The air inside the production house is regarded as an ideal gas.
- The humidity and temperature inside the production house is considered uniformly distributed.

3.2.1 Mass Balance

For the internal system (the air) of the production house a mass balance is derived. The mass balance is parted into a mass balance for the water vapour, the water and the dry air derived in Equation 3.2, Equation 3.19 and Equation 3.20 respectively.

From Figure 3.1 it is seen that water vapour is added through ventilation input, evaporation from the poultry and evaporation of the water added through the sprinklers. Water vapour is removed from the system through the ventilation output. This mass balance is derived in Equation 3.2.

$$\frac{d}{dt}M_v(t) = w_{v,in} - w_{v,out} + w_{evaporation} + w_{livestock} \cdot n_{broilers}, \tag{3.2}$$

where

M_v	[kg]	mass of water vapour inside the production house,
$w_{v,in}$	$[\mathrm{kg\,s^{-1}}]$	flow rate of water vapour into the production house,
$w_{v,out}$	$[\mathrm{kg\,s^{-1}}]$	flow rate of water vapour out of the production house,
$w_{evaporation}$	$[\mathrm{kg\,s^{-1}}]$	rate of water evaporating,
$w_{livestock}$	$[\mathrm{kg\,s^{-1}}]$	rate of water vapour from the livestock, (See subsection 3.2.3)
$n_{broilers}$	$[\cdot]$	number of broilers in production house.

For the mass flow of water vapour into and out of the production house, an expression for the flow rate is derived in Equation 3.3 and Equation 3.4 respectively.

$$w_{v,in} = w_a \cdot \frac{x_a}{x_a + 1}, \tag{3.3}$$

$$w_{v,out} = w_a \cdot \frac{x_s}{x_s + 1}, \tag{3.4}$$

where

w_a	$[\mathrm{kg\,s^{-1}}]$	flow rate of air into the production house,
x_a	$[\frac{\text{kg water vapour}}{\text{kg dry air}}]$	absolute humidity of the outside air (sensor reading),
x_s	$[\frac{\text{kg water vapour}}{\text{kg dry air}}]$	absolute humidity of the production house air.

The expression $\frac{x_a}{x_a+1}$ in Equation 3.3 represents the proportion of the air flow being water vapour. This is derived using the fact that the absolute humidity is calculated in thermodynamics by dividing the mass of water vapour with the mass of dry air as seen in Equation 3.5.

$$x = \frac{M_v}{M_d} \Leftrightarrow M_d = \frac{M_v}{x} \tag{3.5}$$

where

M_d	[kg]	mass of dry air inside the production house.

The total mass of air is naturally given as the mass of dry air and mass of water vapour combined. Using this and the expression of M_d in Equation 3.5 an expression for the water vapour contained in air is derived in Equation 3.6.

$$M = M_d + M_v \Leftrightarrow M = \frac{M_v}{x} + M_v \Leftrightarrow M_v = M \cdot \frac{x}{x+1} \tag{3.6}$$

As mentioned x_a is a sensor reading, but both w_a and x_s can be derived. First the flow rate of air is derived in Equation 3.7 and then the absolute humidity in Equation 3.8.

$$w_a = \rho_s \cdot \dot{V}(t) \tag{3.7}$$

where

ρ_s	$[\mathrm{kg\,m^{-3}}]$	general density of air,
$\dot{V}(t)$	$[\mathrm{m^3\,s^{-1}}]$	volumetric flow rate of air into and out of the production house.

$$x_s(t) = \frac{M_v(t)}{\rho_s \cdot V_s - M_v(t)} \tag{3.8}$$

where

V_s	$[\mathrm{m^3}]$	volume of the production house.

The water vapour gained from evaporation of water from the sprinkler system is given as $w_{evaporation}$ and derived in Equation 3.9 [22].

$$w_{evaporation} = h_m(\gamma_{ws} - \gamma_s) \cdot A_m, \tag{3.9}$$

where

h_m	$[\mathrm{m\,s^{-1}}]$	mass transfer coefficient,
γ_{ws}	$[\mathrm{mol\,m^{-3}}]$	molar concentration of water vapour at saturation,
γ_s	$[\mathrm{mol\,m^{-3}}]$	molar concentration of water vapour at current humidity x_s,
A_m	$[\mathrm{m^2}]$	surface area of a mist.

Note that for molar concentration the normal procedure would be to use c, but c is in this report reserved for representing the specific heat capacity, which uses the same nomenclature. So instead γ will be used for representing the molar concentration.

The concentration of water vapour is derived in Equation 3.10 [22].

$$\gamma_{ws} - \gamma_s = \frac{\aleph_v}{R \cdot T_s} \cdot (p_{ws} - p_s) \tag{3.10}$$

where

$\aleph_v$	$[\mathrm{g\,mol^{-1}}]$	molar mass of water vapour,
R	$[\mathrm{J\,K^{-1}\,mol^{-1}}]$	the universal gas constant,
T_s	[K]	temperature of air in the production house (aka. the stable),
p_{ws}	[Pa]	pressure of water vapour at saturation,
p_s	[Pa]	pressure of water vapour at current humidity x_s.

The pressure of water vapour at saturation can be expressed as in Equation 3.11 [23]. The original equation was for Celsius, but is here converted to Kelvin.

$$p_{ws} = \frac{\exp\left(34.494 - \frac{4924.99}{(T_s - 273.15) + 237.1}\right)}{((T_s - 273.15) + 105)^{1.57}} = \frac{\exp\left(34.494 - \frac{4924.99}{T_s - 36.05}\right)}{(T_s - 168.15)^{1.57}} \tag{3.11}$$

Then by rewriting an expression for the absolute humidity found in [24] the pressure at the current humidity x_s is derived in Equation 3.12

$$p_s = \frac{p_0 \cdot x_s}{x_s + \lambda_{wd}}, \tag{3.12}$$

where

p_0	[Pa]	standard air pressure at sea level,
λ_{wd}	[·]	ratio between the molar mass of water and dry air.

The mass transfer coefficient is derived in Equation 3.13 [22].

$$h_m = \frac{\text{sh} \cdot D_v}{d_{drop}}, \tag{3.13}$$

where

sh	[·]	ratio between the natural diffusion and forced convection (Sherwood number),
D_v	[$\text{m}^2\,\text{s}^{-1}$]	mass diffusion coefficient of vapour,
d_{drop}	[m]	diameter of a drop.

The Sherwood number is a ratio between the natural diffusion and forced convection, where the forced convection is the movement of air across a droplet. The Sherwood number for a sphere is derived in Equation 3.14 [22].

$$\text{sh} = 2 + 0.6 \cdot \text{Re}^{1/2} \cdot \text{Sc}^{1/3}, \tag{3.14}$$

where

Re	[·]	Reynolds number,
Sc	[·]	Schmidt number.

The equations for the Reynolds number [25] and Schmidt number [26] can be seen in Equation 3.15 and Equation 3.16 respectively.

$$\text{Re} = \frac{\rho_s u_r d_{drop}}{\mu_s} \tag{3.15}$$

$$\text{Sc} = \frac{\mu_s}{\rho_s D_v} \tag{3.16}$$

where

u_r	[$\text{m}\,\text{s}^{-1}$]	flow speed air relative to droplet,
μ_s	[$\text{N}\,\text{s}\,\text{m}^{-2}$]	general viscosity of air.

The Reynolds number is used to describe if a flow is laminar or turbulent, where a higher value equals more turbulence [27]. The Schmidt number is a ratio between the momentum diffusion and mass diffusion of the droplets [28]. Since the air speed inside the production

house is delimited to be zero, the Reynolds number also becomes zero, whereby the Sherwood number can be found to be equal to 2 as seen in Equation 3.17.

$$\mathrm{sh} = 2 + 0.6 \cdot 0^{1/2} \cdot \mathrm{Sc}^{1/3} = 2. \tag{3.17}$$

An expression for A_m is derived in Equation 3.18.

$$A_m = A_d \cdot \frac{M_w}{M_{drop}}, \tag{3.18}$$

where

A_d	$[\mathrm{m}^2]$	surface area of a water droplet,
M_w	[kg]	mass of water inside the production house,
M_{drop}	[kg]	mass of water droplet.

Note that since the mass of the water droplet is used to estimate its surface area A_m, the area is underestimated because the mass shrinks faster than the area.

Next we have the mass balance of the water. From Figure 3.1 it is seen that the mass of water depends on the amount sprayed into the production house from the sprinklers subtracted the amount lost to evaporation derived in Equation 3.9.

$$\frac{d}{dt} M_w(t) = w_{spray} - w_{evaporation}, \tag{3.19}$$

where

w_{spray}	$[\mathrm{kg\,s}^{-1}]$	flow rate of water from the sprinkler system.

Lastly the mass balance of dry air inside the production house is calculated simply as the difference between the total mass of air and the mass of water vapour in Equation 3.20.

$$M_d(t) = \rho_s \cdot V_s - M_v(t). \tag{3.20}$$

3.2.2 Energy Balance

In this section a energy balance for the production house is derived. The progress from [12] will be used. In their work, they separately modelled the temperature change caused by ventilation and the the temperature change caused by heating. Here they will be combined and extended with the addition of cooling spray.

Firstly a general energy balance for the production house is derived in Equation 3.21 based on Figure 3.1.

Figure 3.1 shows that energy is added to the production house through the ventilation input, the heater and from the poultry. It further shows that energy is removed through the ventilation output, the energy required for the sprinkler water to evaporate and the heat exchange with the building itself.

$$\frac{d}{dt}U_s(t) = Q_{in}(t) - Q_{out}(t) - Q_{evap} + Q_{heater}(t) - Q_b(t) + Q_{sensible}(t), \tag{3.21}$$

where

U_s	[J]	internal energy inside the production house,
Q_{in}	[J s^{-1}]	heat transfer from the air outside to the production house air,
Q_{out}	[J s^{-1}]	heat transfer from the production house air to the outside air,
Q_{evap}	[J s^{-1}]	heat loss in production house air from water evaporation,
Q_{heater}	[J s^{-1}]	heat transfer from heater to production house air,
Q_b	[J s^{-1}]	heat transfer from the production house air to the production house walls,
$Q_{sensible}$	[J s^{-1}]	heat transfer from the broilers to the production house air. [See subsection 3.2.3]

The energy going in and out of the production house because of ventilation is derived in Equation 3.22 and Equation 3.23.

$$Q_{in}(t) = w_{d,in}(t) \cdot T_a(t) \cdot c_d + w_{v,in}(t) \cdot T_a(t) \cdot c_v, \tag{3.22}$$
$$Q_{out}(t) = w_{d,out}(t) \cdot T_s(t) \cdot c_d + w_{v,out}(t) \cdot T_s(t) \cdot c_v, \tag{3.23}$$

where

$w_{d,in}$	[kg s^{-1}]	mass flow of dry air into the production house,
$w_{d,out}$	[kg s^{-1}]	mass flow of dry air out of the production house,
T_a	[K]	temperature of the air outside,
c_d	[J kg^{-1} K^{-1}]	specific heat capacity of dry air,
c_v	[J kg^{-1} K^{-1}]	specific heat capacity of water vapour.

Using w_a, $w_{v,in}$ and $w_{v,out}$ from Equation 3.7, Equation 3.3 and Equation 3.4 respectively, a expression for $w_{d,in}$ and $w_{d,out}$ is derived in Equation 3.24 and Equation 3.25 by finding the difference.

$$w_{d,in} = w_a - w_{v,in} = \rho_s \cdot \dot{V}(t) - w_{v,in} \tag{3.24}$$
$$w_{d,out} = w_a - w_{v,out} = \rho_s \cdot \dot{V}(t) - w_{v,out} \tag{3.25}$$

The energy from the heater is derived in Equation 3.26 based on work from [12].

$$Q_{heater}(t) = h_{sh} \cdot P_{sh} \cdot l_{sh} \cdot (T_{sh,out}(t) - T_s(t)), \tag{3.26}$$

where

h_{sh}	[W m^{-2} K^{-1}]	convection heat transfer coefficient between the heater and air,
P_{sh}	[m]	outer perimeter of the heater,
l_{sh}	[m]	length of the stable heater,
$T_{sh,out}$	[K]	temperature of the water exiting the heater.

$T_{sh,out}$ is dependant on the flow rate of water through the heater, the inlet temperature of the water entering the heater and the temperature in the livestock production house. $T_{sh,out}$ is derived in Equation 3.27.

$$\frac{d}{dt}T_{sh,out}(t) = \frac{w_{sh}(t) \cdot c_{pw} \cdot (T_{sh,in}(t) - T_{sh,out}(t)) - h_{sh} \cdot P_{sh} \cdot l_{sh} \cdot (T_{sh,out}(t) - T_s(t))}{l_{sh} \cdot (\rho_i \cdot c_{pi} \cdot A_i + \rho_w \cdot c_{pw} \cdot A_w)}, \tag{3.27}$$

where

w_{sh}	$[\mathrm{kg\,s^{-1}}]$	water flow rate through the heater,
c_{pw}	$[\mathrm{J\,kg^{-1}\,K^{-1}}]$	specific heat capacity of water,
$T_{sh,in}$	[K]	temperature of the water entering the heater,
ρ_i	$[\mathrm{kg\,m^{-3}}]$	density of iron,
c_{pi}	$[\mathrm{J\,kg^{-1}\,K^{-1}}]$	specific heat capacity of iron,
A_i	$[\mathrm{m^2}]$	cross-sectional area of iron in the heating pipe,
ρ_w	$[\mathrm{kg\,m^{-3}}]$	density of water,
A_w	$[\mathrm{m^2}]$	cross-sectional area of water in the heating pipe.

Next, an expression for the heat loss due to water evaporation Q_{evap} is derived in Equation 3.28.

$$Q_{evap} = w_{evaporation} \cdot h_e, \tag{3.28}$$

where

h_e	$[\mathrm{J\,kg^{-1}}]$	latent heat of evaporation.

Lastly, there exist a heat transfer between the production house air and the walls of the production house (the building) derived in Equation 3.29.

$$Q_b(t) = h_b \cdot A_b \cdot (T_s(t) - T_b(t)), \tag{3.29}$$

where

h_b	$[\mathrm{W\,m^{-2}\,K^{-1}}]$	heat transfer coefficient between the production house air and walls,
A_b	$[\mathrm{m^2}]$	area of the inside walls of the production house,
T_b	[K]	temperature of the production house walls.

The temperature of the production house walls T_b is depended on the temperature of the air in the production house T_s and the outside air T_a. The energy balance for T_b is derived in Equation 3.30.

$$\frac{d}{dt}T_b(t) = \frac{h_b \cdot A_b \cdot (T_s - T_b) - h_a \cdot A_b \cdot (T_b - T_a)}{M_b \cdot c_{pb}}, \tag{3.30}$$

where

h_a	$[\mathrm{W\,m^{-2}\,K^{-1}}]$	heat transfer coefficient between the production house walls and outside air,
M_b	[kg]	mass of the production house walls,
c_{pb}	$[\mathrm{J\,kg^{-1}\,K^{-1}}]$	specific heat capacity of the production house walls.

Using the energy balance in Equation 3.21 and the mass balance for M_d and M_v in Equation 3.20 and Equation 3.2, the change in temperature inside the production house is derived in Equation 3.31.

$$\frac{d}{dt}T_s(t) = \frac{Q_{in}(t) - Q_{out}(t) - Q_{evap} + Q_{heater}(t) - Q_b(t) + Q_{sensible}(t)}{(M_d + M_v) \cdot c_s} \tag{3.31}$$

where

c_s $[\mathrm{J\,kg^{-1}\,K^{-1}}]$ specific heat capacity of production house air given a humidity.

The specific heat capacity c_s is derived in Equation 3.32.

$$c_s = c_d + 1884 \cdot x_s \tag{3.32}$$

3.2.3 Broilers

This section discusses the broilers effect on the temperature and humidity inside the production house. The broiler produces heat which it exchanges with its surroundings through sensible, latent and radiation energy as illustrated in Figure 3.3.

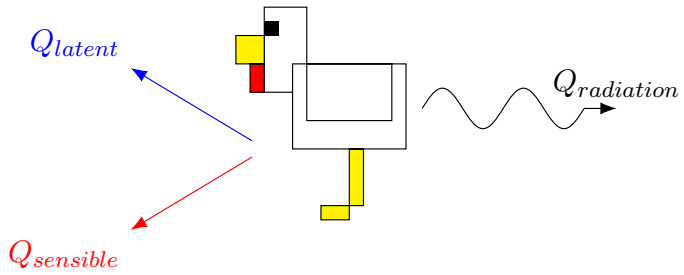

Figure 3.3: Illustration of the energy transfer from broiler.

The total energy from the broiler is then Q_{total} as shown in Equation 3.33.

$$Q_{total} = Q_{sensible} + Q_{latent} + Q_{radiation} \tag{3.33}$$

The way this interacts with the production house is that the sensible energy causes direct heat transfer between the broiler and the surrounding air and the latent energy is released from the broiler as water vapour into the production house. The radiation contribution is negligible and will be disregarded in this project.

As the broiler ages its size and heat production increases. The total heat produced by a broiler can be estimated with Equation 3.34 [29, p. 8].

$$y = 10 \cdot \sqrt{0.057 \cdot A^{1.65}} \tag{3.34}$$

where

y	$[\mathrm{J\,s^{-1}}]$	total heat produced by one broiler in 20°C production house,
A	$[week]$	age of the broiler in weeks.

The total heat production is given at 20 °C. Therefore, to account for variation in temperature inside the actual production house, a temperature correction factor is derived in Equation 3.35 [29, p. 12].

$$f_t = 4 \cdot 10^{-5}(-T_s + 20)^3 + 1 \tag{3.35}$$

where

f_t	$[\cdot]$	temperature correction factor,
T_s	[°C]	temperature in the production house .

The total heat produced can be split into sensible and latent heat using Equation 3.36. F is a ratio which gives the sensible heat directly, and the latent heat as a complement of the ratio. [29, p. 13]

$$F = -1.85 \cdot 10^{-7}(T_s + 10)^4 + 0.8 \tag{3.36}$$

where

F	$[\cdot]$	sensible heat ratio
T_s	[°C]	temperature in the production house.

The heat output of a broiler can then be estimated by combining Equation 3.34, 3.35 and 3.36 in Equation 3.37.

$$Q_{sensible} = y \cdot f_t \cdot F \tag{3.37}$$

where

$Q_{sensible}$	$[\mathrm{J\,s^{-1}}]$	sensible heat produced by one broiler corrected for by the production house temperature.

Using the complement of the sensible heat ratio the latent heat can further be found. Since a energy and mass balance is used for the model of the production house, the latent energy is further converted into a water vapour flow given in Equation 3.38.

$$w_{livestock} = \frac{Q_{latent}}{h_e} = \frac{y \cdot f_t \cdot (1 - F)}{h_e} \tag{3.38}$$

where

$w_{livestock}$	$[\mathrm{kg\,s^{-1}}]$	water vapour produced by one broiler corrected for by the production house temperature.

Currently both $Q_{sensible}$ and $w_{livestock}$ are constant throughout the day. In the real world however the output from the broiler varies, since it is more active in the day than at night. This activity is controlled by adjusting the light inside the production house. The difference between day and night for the broiler output is 4 dB. [30]

Therefore an additional heat correction factor has been made to include the effect of lighting. Here we assume that data used in [29] to calculate Q_{total} had lighting but it showed the average output.

To make the output of the broiler further dependent on the light level a cosine curve is used. It is cut at the top and bottom as illustrated in Figure 3.4, and then scaled such that the mean is equal to 1 and the peak to bottom difference is 4 dB.

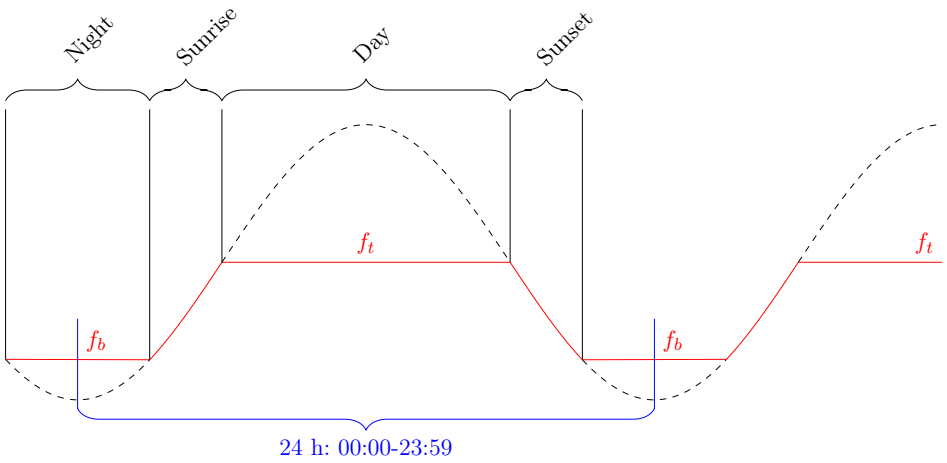

Figure 3.4: Illustration of the light-cycle scalar used for modelling the dynamic heat production from poultry.

This cosine curve is then used as a additional correction factor derived in Equation 3.39 for the heat and water vapour production.

$$f_{lux}(t) = \begin{cases} f_b & 0 < t < 4 \\ -\cos(2 \cdot \pi \cdot fs \cdot t) & 4 < t < 4.5 \\ f_t & 4.5 < t < 19.5 \\ -\cos(2 \cdot \pi \cdot fs \cdot t) & 19.5 < t < 20 \\ f_b & 20 < t < 24 \end{cases} \tag{3.39}$$

where

f_{lux} [·] light correction factor.

Adding the light correction factor in Equation 3.39 to Equation 3.37 and Equation 3.38, new expressions for $Q_{sensible}$ and $w_{livestock}$ is derived respectively in Equation 3.40 and Equation 3.41

$$Q_{sensible} = y \cdot f_t \cdot F \cdot f_{lux} \tag{3.40}$$

$$w_{livestock} = \frac{y \cdot f_t \cdot (1 - F)}{h_e} \cdot f_{lux} \tag{3.41}$$

The time intervals for night, sunrise, day and sunset used in Equation 3.39 are for broilers between 6 and 12 days old. As mentioned in section 2.3 the intervals changes depending of the age of the broiler. With this addition of the light correction factor the increase in day time and thereby increase in heat and water vapour production can be taken into account in the model.

Lastly it should be noted that in [29] it is not stated if the length of the days inside the production houses were changed with age or not as described as normal practise in section 2.3. If it were changed, it would affect the activity levels of the poultry, and thereby their heat and vapour output.

3.3 Final Model

Combining the mass balance from subsection 3.2.1 and the energy balance from subsection 3.2.2 on a state space form, the final model is derived in Equation 3.42.

The corrected Archimedes number from section 3.1 has not been included in the final state space model. The reason being that is does not directly influence the temperature or humidity inside the production house, but rather gives a indication if the air flow is turbulent or not. Additionally the air flow is not expected to exceed $0.2\,\mathrm{m\,s^{-1}}$. This is further touched upon in chapter 8.

$$\begin{aligned}\begin{bmatrix}\dot{M}_v\\ \dot{M}_w\\ \dot{T}_{sh,out}\\ \dot{T}_b\\ \dot{T}_s\end{bmatrix} =& A_1\begin{bmatrix}T_{sh,out}\\ T_s\\ T_b\end{bmatrix} + A_2\begin{bmatrix}w_{evap}(M_w,T_s,x_s)\\ w_{live}(A,T_s)\cdot f_{lux}(t)\end{bmatrix} + A_3\begin{bmatrix}w_{evap}(M_w,T_s,x_s)\\ T_{sh,out}\\ T_s\\ T_b\\ q(A,T_s)\cdot f_{lux}(t)\end{bmatrix} k(x_s)\\ &+ B_1\begin{bmatrix}w_{spray}\end{bmatrix} + B_2\begin{bmatrix}T_{sh,in}\\ T_{sh,out}\end{bmatrix} w_{sh} + B_3\begin{bmatrix}\rho(x_a)\\ \rho(x_s)\\ T_a k(x_s)\\ T_a\rho(x_a)k(x_s)\\ T_s k(x_s)\\ T_s\rho(x_s)k(x_s)\end{bmatrix}\dot{V}(t)\\ &+ D\begin{bmatrix}T_a\end{bmatrix}\end{aligned} \tag{3.42}$$

The addends are then defined as seen in Equation 3.43, 3.44, 3.45, 3.46, 3.47,3.48 and 3.49.

$$A_1 = \begin{bmatrix}0 & 0 & 0\\ 0 & 0 & 0\\ -\frac{h_{sh}P_{sh}}{\rho_i c_{pi}A_i+\rho_w c_{pw}A_w} & \frac{h_{sh}P_{sh}}{\rho_i c_{pi}A_i+\rho_w c_{pw}A_w} & 0\\ 0 & \frac{h_b A_b}{M_b c_{pb}} & -\frac{h_b A_b+h_a A_b}{M_b c_{pb}}\\ 0 & 0 & 0\end{bmatrix} \tag{3.43}$$

$$A_2 = \begin{bmatrix} 1 & n_{broilers} \\ -1 & 0 \\ 0 & 0 \\ 0 & 0 \\ 0 & 0 \end{bmatrix} \tag{3.44}$$

$$A_3 = \begin{bmatrix} 0 & 0 & 0 & 0 & 0 \\ 0 & 0 & 0 & 0 & 0 \\ 0 & 0 & 0 & 0 & 0 \\ 0 & 0 & 0 & 0 & 0 \\ -h_e & h_{sh}P_{sh}l_{sh} & -h_{sh}P_{sh}l_{sh} - h_bA_b & h_bA_b & n_{broilers} \end{bmatrix} \tag{3.45}$$

$$B_1 = \begin{bmatrix} 0 \\ 1 \\ 0 \\ 0 \\ 0 \end{bmatrix} \tag{3.46}$$

$$B_2 = \begin{bmatrix} 0 & 0 \\ 0 & 0 \\ \frac{c_{pw}}{l_{sh}(\rho_i c_{pi} A_i + \rho_w c_{pw} A_w)} & -\frac{c_{pw}}{l_{sh}(\rho_i c_{pi} A_i + \rho_w c_{pw} A_w)} \\ 0 & 0 \\ 0 & 0 \end{bmatrix} \tag{3.47}$$

$$B_3 = \begin{bmatrix} 1 & -1 & 0 & 0 & 0 & 0 \\ 0 & 0 & 0 & 0 & 0 & 0 \\ 0 & 0 & 0 & 0 & 0 & 0 \\ 0 & 0 & 0 & 0 & 0 & 0 \\ 0 & 0 & c_d\rho_s & c_v - c_d & -c_d\rho_s & c_d - c_v \end{bmatrix} \tag{3.48}$$

$$D = \begin{bmatrix} 0 \\ 0 \\ 0 \\ \frac{h_a A_b}{M_b c_{pb}} \\ 0 \end{bmatrix} \tag{3.49}$$

Some states were not possible to isolate. For now they are therefore defined as functions as seen below.

$$\rho(x) = \frac{x \cdot \rho_s}{x + 1} \tag{3.50}$$

$$k(x) = \frac{1}{(c_d + 1884 \cdot x)\rho_s V_s} \tag{3.51}$$

$$x_s = \frac{M_v}{\rho_s V_s - M_v} \tag{3.52}$$

$$w_{live}(x_1, x_2) = \frac{\sqrt{0.057 \cdot x_1^{1.65}} \cdot \left(4 \cdot 10^{-4} \cdot (-x_2 + 20)^3 + 10\right) \cdot \left(0.2 + 1.85 \cdot 10^{-7} \cdot (x_2 + 10)^4\right)}{h_e} \tag{3.53}$$

$$w(x_1, x_2, x_3) = \frac{\aleph_v}{R \cdot x_2} \left(\frac{\mathrm{sh} \cdot D_v A_d \cdot x_1}{d_{drop} M_{drop}} \cdot \frac{\exp\left(34.494 - \frac{4924.99}{x_2 - 36.05}\right)}{(x_2 - 168.15)^{1.57}} - \frac{p_0 \cdot x_3}{x_3 + \lambda_{wd}} \right) \tag{3.54}$$

$$q(x_1, x_2) = \sqrt{0.057 \cdot x_1^{1.65}} \cdot \left(4 \cdot 10^{-4} \cdot (-x_2 + 20)^3 + 10\right) \cdot \left(-1.85 \cdot 10^{-7} \cdot (x_2 + 10)^4 + 0.8\right) \tag{3.55}$$

Chapter 4

Parameter Estimation

In this chapter the parameters for the model designed in chapter 3 will be estimated. The chapter will explain the data used for estimation, the method utilised and the results.

4.1 Open vs. Closed Loop Parameter Estimation

Any data from a production house will be for a closed loop system, since a controller actively generates the inputs to the system based on the outputs. The goal is to generate parameters only for the open loop system G, but if there is not enough excitement of the system, clearly demonstrating the dynamics [31], the parameters generated will be for the closed loop system $G(1 + (r - G)D)^{-1}$ as illustrated in Figure 4.1.

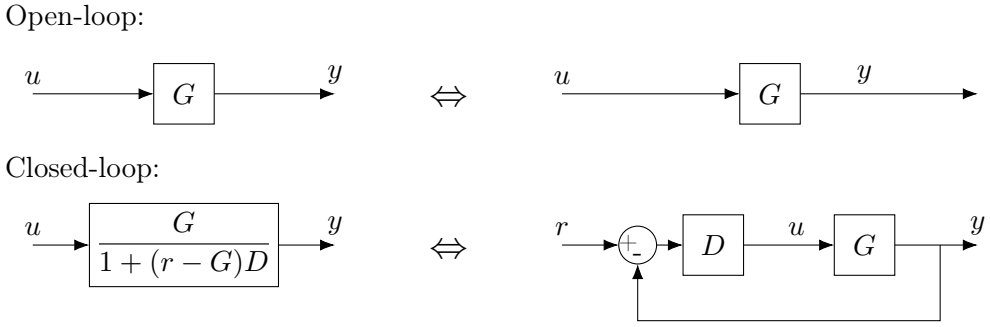

Figure 4.1: Open vs. closed loop parameter estimation.

Therefore it is necessary to ensure that the data used for parameter estimation has enough excitement.

4.2 Data Analysis

SKOV A/S has supplied a data set from a active production house at Mosegaarded farm. Here a data set for both the summer and winter period was supplied. In the summer period both, heating, ventilation and spray cooling is utilised, whereas the spray cooling is not utilised in the winter period. Furthermore there is more excitement and variation in the summer data. Therefore the summer data set will be used for training data and the winter data set for validation. The data is measured with 2 minute intervals. The summer set has 38 days of measurements and the winter set has 28 days of measurements.

4.2.1 Summer Data Set

The dynamic behaviour inside the production house is best represented by big changes or spikes in the data set. Therefore, ranges in the data with these characteristics have been identified for use in parameter estimation. These ranges are marked with green and can be seen together with the summer data in Figure 4.2, 4.3 and 4.4.

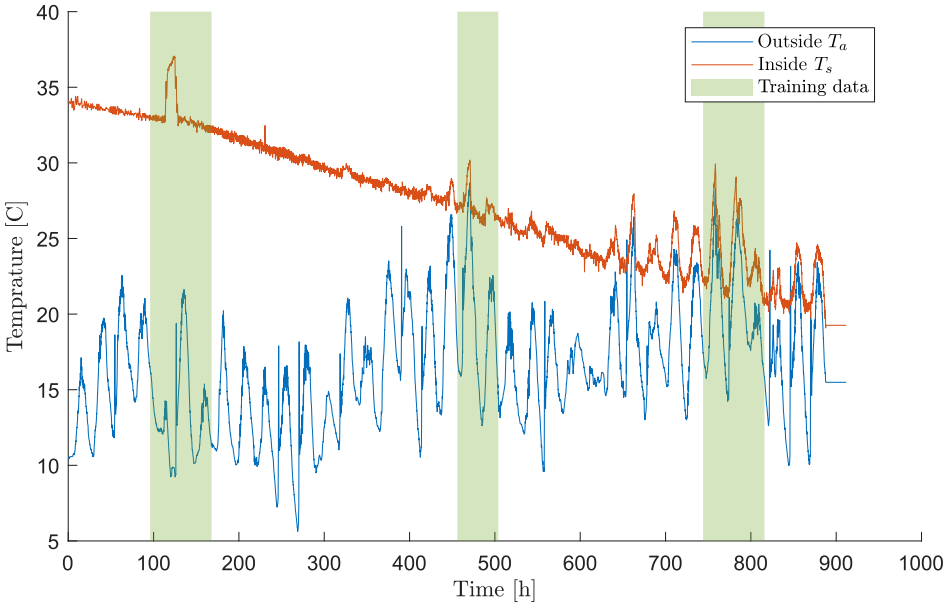

Figure 4.2: The measured temperature inside and outside Mosegaarden Production house in the summer.

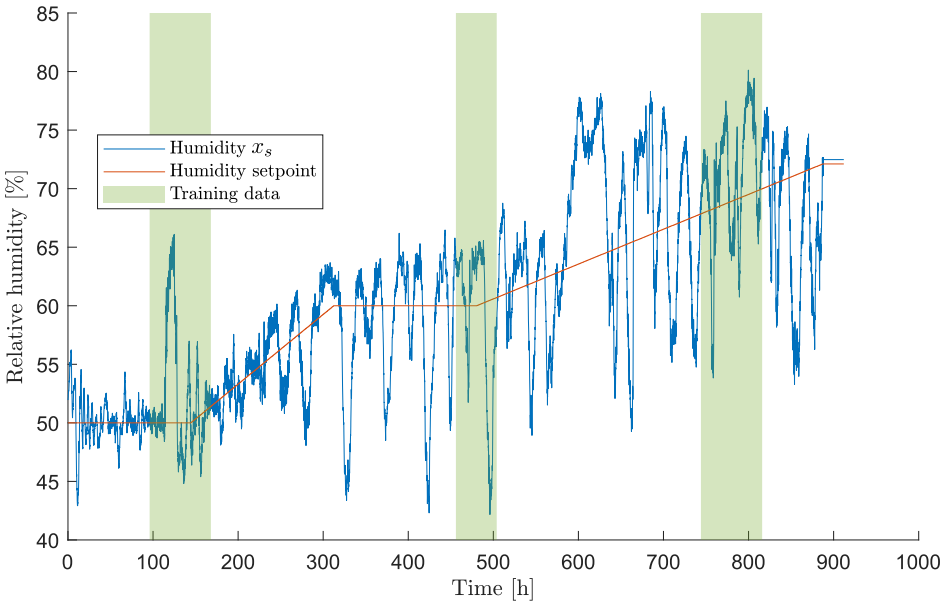

Figure 4.3: The measured relative humidity inside Mosegaarden Production house in the summer.

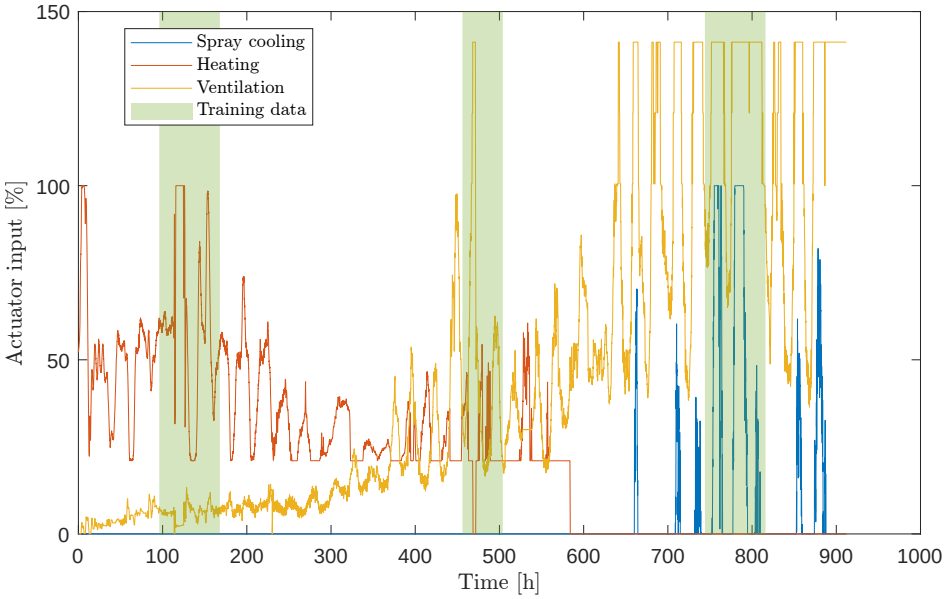

Figure 4.4: Actuator control signal in percentage of maximum throughput in the summer.

In Figure 4.2 the temperature inside the production house T_s and the temperature outside of the production house T_a are plotted. Figure 4.3 plots the humidity x_s inside of the production house and Figure 4.4 plots the actuator inputs affecting the climate inside the production house.

Figure 4.2 shows how the current controller utilised by SKOV A/S are able to keep the temperature T_s somewhat steady, while the temperature outside fluctuates. Though the temperature T_s clearly is still affected by the spikes in the temperature T_a.

In Figure 4.3 notice the setpoint for the humidity . As described in section 2.3 it follows the requirement that chicks must have at least 50 % relative humidity, after which the setpoint slowly rises to a setpoint of first 60 % between day 14 and 21 and then lastly 70 %–75 %.

The reason for the setpoint being kept at 60 % for a period is to keep a minimum biological process going in the bedding. In section 2.3 is was described that the poultry will experience food pad lesions if the bedding is too wet. The biological process keeps the bedding warm, which evaporates the water. If the biological process dies, then more heating is required to keep the water evaporating, which increases the expense of the farmer. Though as also mentioned in section 2.3, this biological process produces ammonia, which increases the risk of food pad lesions. Therefore the process is balanced between keeping the bedding warm without producing too much ammonia.

When the setpoint is then changed to 70 %–75 % after day 21 the reason is that it is expensive to keep it any lower. To keep it lower requires more ventilation, which cools down the production house increasing the need for heating.

It should be noted that the information about water evaporating from the bedding is not included in the model designed in chapter 3.

Looking at the three spike ranges chosen of parameter estimation it can be seen that in the last two ranges in Figure 4.2, that T_s reacts to the spikes in T_a, but in the first range there

does not seem to be a correlation. However if comparing Figure 4.2 and 4.4 it can be seen that the spike in temperature T_s in the first range matches with an increase in the heating input. The heating input furthermore affects the humidity x_s in the production house, which has an increase matching that of the temperature T_s as seen in Figure 4.3.

Going back to the two last ranges and comparing Figure 4.2 and 4.4 it can be seen that the controller tries to correct the temperature spikes by increasing ventilation in the production house. And looking at the last range the controller furthermore activates the spray cooling system in an attempt to counteract the spike in the outside temperature. Here both the ventilation and spray cooling actuators are saturated. The saturation introduces a lot of excitement in the system, and shows more of the plant dynamics than the controller dynamics.

Based on these arguments the system shows enough excitement to demonstrate the dynamics of the system and can therefore be used for closed loop parameter estimation.

4.2.2 Winter Data Set

In Figure 4.5, 4.6 and 4.7 the data from the winter set is plotted. In Figure 4.5 it is seen that the fluctuations in the temperature T_a has no visible effect on the temperature T_s, which is stable. The humidity x_s is additionally found to be stable around the setpoint as shown in Figure 4.6.

Furthermore looking at the inputs plotted in Figure 4.7 it is seen that the production house uses minimal ventilation and no spray cooling during the winter. Mainly heating is utilised for adjusting the temperature T_s.

Thereby it can be concluded that the winter data set does not demonstrate enough system dynamics to be used for parameter estimation, and is therefore only used for validation.

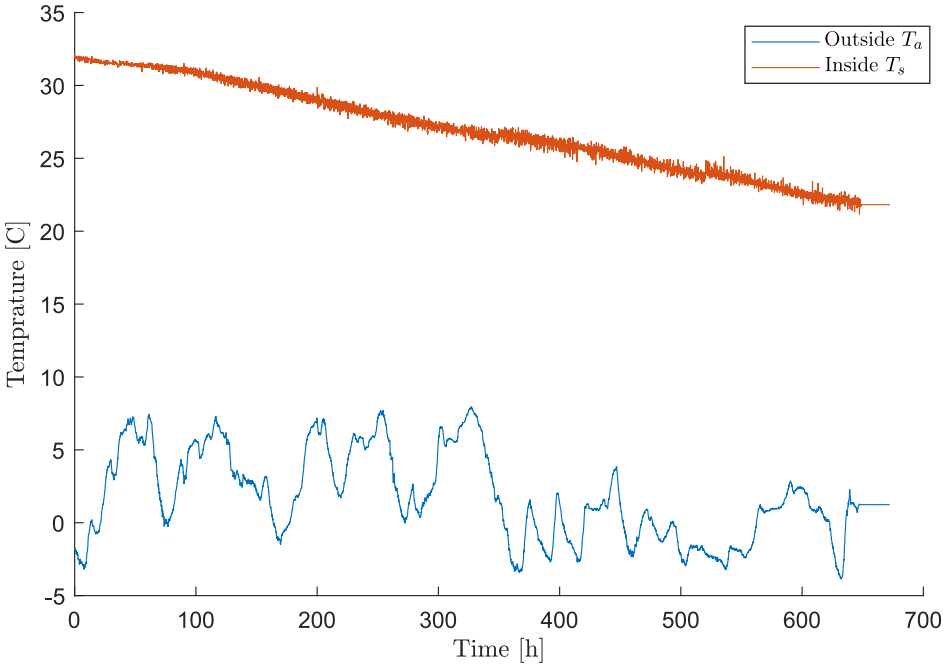

Figure 4.5: The measured temperature inside and outside Mosegaarden Production house in the winter.

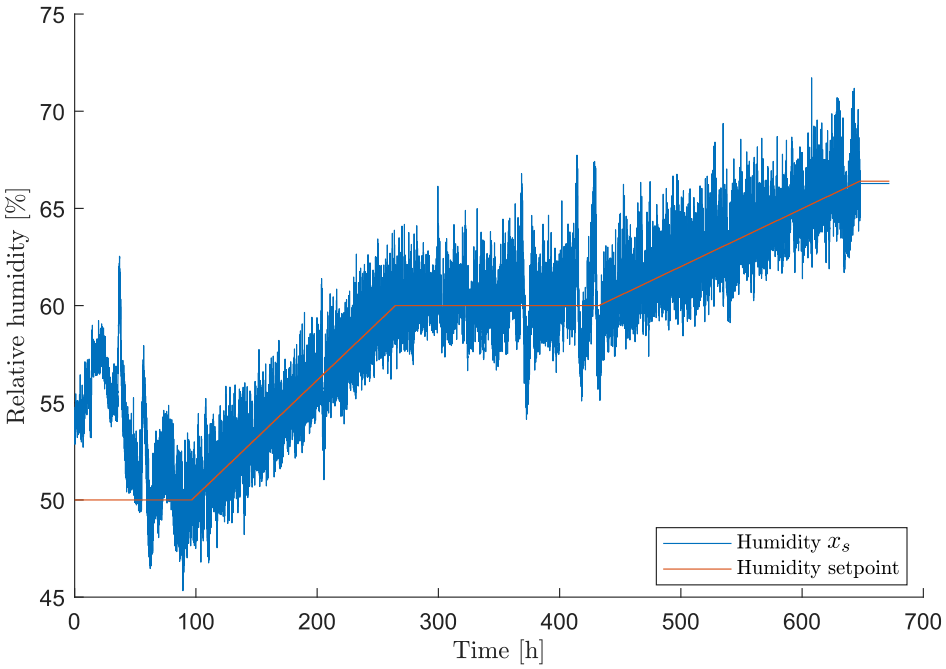

Figure 4.6: The measured relative humidity inside Mosegaarden Production house in the winter.

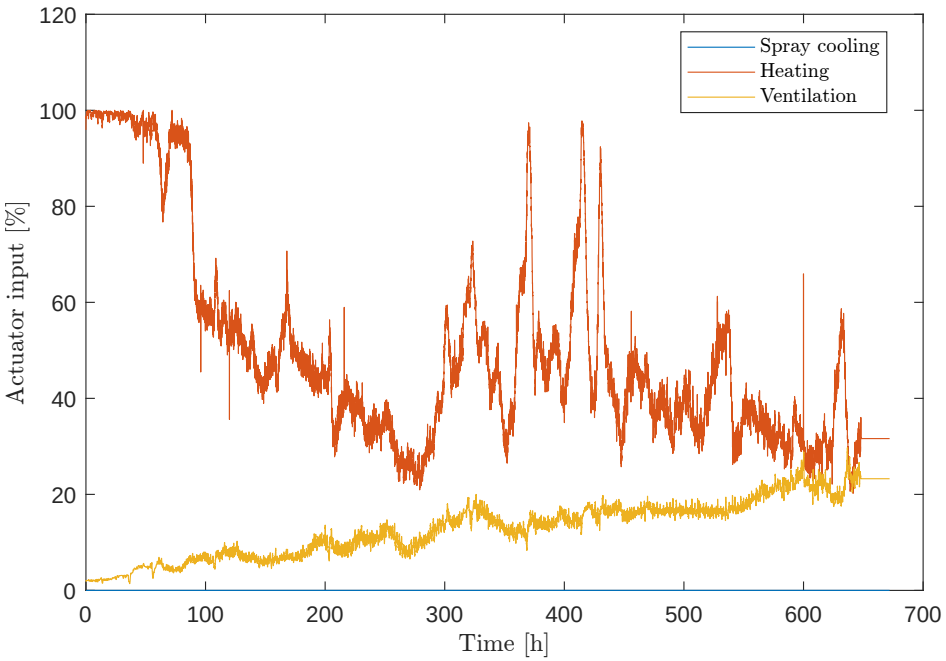

Figure 4.7: Actuator control signal in percentage of maximum throughput in the winter.

4.3 Parameter Estimation Method

For parameter estimation is has been decided to utilise a grey-box approach. From the Matlab System Identification Toolbox the command `nlestgray`[32] is used, since the model designed in chapter 3 is non-linear.

The System Identification Toolbox estimates parameters by setting the error between the model output and the measured output as a cost function. This cost function is a weighted sum of squares of the errors given in Equation 4.1. [33]

$$V(\theta) = \frac{1}{N}\sum_{t=1}^{N} e^T(t,\theta)W(\theta)e(t,\theta), \tag{4.1}$$

where

N	$[\cdot]$	number of data samples,
$e(t,\theta)$	$[\cdot]$	the error between the model and measured output,
t	$[\cdot]$	discrete time t,
θ	$[\cdot]$	vector of parameters to be estimated,
W	$[\cdot]$	positive semi-definite weighting matrix.

The weight matrix is chosen so that size of the error are on a similar scale.

Then finding the parameters that solve the optimisation problem on the following form Equation 4.2.

$$\begin{aligned} &\min_{\theta} V(\theta) \\ &\text{subject to } \psi_i(\theta) = 0, i \in \varepsilon \\ &\qquad\qquad \psi_i(\theta) \geq 0, i \in \iota \end{aligned} \tag{4.2}$$

where

ψ	$[\cdot]$	nonlinear constraints,

The estimation is done using the `fmincon` method `SQP`, which is a general nonlinear constrained minimisation method [34].

4.3.1 Sequential Quadratic Programming

The idea behind `SQP` is to define a quadratic programming sub-problem around an iterator. The solution from the sub-problem is used to update the iterator, then use the new iterator to redefine the sub-problem and so on. This approach is used to solve the non-linear estimation problem in Equation 4.2 by turning it into quadratic programming form with linearized constrains as in Equation 4.3[35], that is solved using an active set method.

$$\begin{aligned} &\min_{p} V(\theta_k) + \nabla V(\theta_k)^T p + \frac{1}{2} p^T \nabla^2_{\theta\theta}\mathcal{L}(\theta_k, \lambda_k)p \\ &\text{subject to: } \nabla\psi_i(\theta_k)^T + \psi_i(\theta_k) = 0, i \in \varepsilon \\ &\qquad\qquad \nabla\psi_i(\theta_k)^T p + \psi_i(\theta_k) \geq 0, i \in \iota \end{aligned} \tag{4.3}$$

where

λ	$[\cdot]$	Lagrangian multiplier.

The Lagrangian function is defined as Equation 4.4.[35]

$$\mathcal{L}(\theta, \lambda) = V(\theta) - \lambda^T c(\theta) \tag{4.4}$$

Then the solution of Equation 4.3 is use to calculated the new iteration point as in Equation 4.5

$$\theta_{k+1} = \theta_k + p \tag{4.5}$$

4.4 Parameter Estimation Implementation

For parameter estimation all parameters from the model designed in chapter 3 are listed in Table B.1 in Appendix B together with their initial guesses and a description of where the values originates from. Some of these parameters can be lumped together and are done so for a more efficient parameter estimation process. The lumped together parameters are derived in Equation 4.6.

$$\begin{aligned}
\theta_{hsh} &= h_{sh} \cdot P_{sh} \cdot l_{sh} \\
\theta_{msh} &= l_{sh} \cdot (\rho_i \cdot c_{pi} \cdot A_i + \rho_w \cdot c_{pw} \cdot A_w) \\
\theta_{hb} &= h_b \cdot A_b \\
\theta_{ha} &= h_a \cdot A_b \\
\theta_{Mb} &= c_{pb} \cdot M_b \\
\theta_{evap} &= \frac{A_d \cdot \mathrm{sh} \cdot D_v \cdot \aleph_v}{M_{drop} \cdot R \cdot d_{drop}}
\end{aligned} \tag{4.6}$$

The final parameters for estimation after being lumped together are listed in Table 4.1 together with their initial guesses and final values after parameter estimation has been completed.

As seen in Figure 4.4 all input values from the Mosegaard data set are given as a percentage of the maximum throughput of each actuator. Therefore these three inputs are multiplied with three scalars to convert into actual input:

- $\dot{V}_{max}$ for ventilation,
- $w_{sh,max}$ for heating,
- $w_{spray,max}$ for spray cooling.

These scalars are then estimated during the parameter estimation. Their initial guesses and final values are listed in Table 4.1.

Table 4.1: Parameters to be estimated with initial guess and final value.

Parameter	Initial Guess	Final Value	Unit
$\dot{V}_{max}$	1	10.387	$\mathrm{m^3\,s^{-1}}$
$w_{sh,max}$	0.2	5.1097	$\mathrm{m^3\,s^{-1}}$
$w_{spray,max}$	0.001	0.025	$\mathrm{m^3\,s^{-1}}$
$T_{sh,in}$	313.15	337.2683	K]
c_{pw}	4179.6	5264.1334	$\mathrm{J\,kg^{-1}\,K^{-1}}$
θ_{hsh}	3373.3527	2596.7907	$\mathrm{W\,K^{-1}}$
θ_{msh}	3834688.2089	4099236.5889	$\mathrm{J\,K^{-1}}$
$n_{broilers}$	8000	9690.3815	·
h_e	2453500	2721546.6591	$\mathrm{J\,kg^{-1}}$
θ_{evap}	0.06341	0.062142	$\mathrm{m^3\,K\,J^{-1}\,s^{-1}}$
λ_{wd}	0.62198	0.6253	·
p_0	101325	101527.65	Pa
c_d	1006	1094.892	$\mathrm{J\,kg^{-1}\,K^{-1}}$
c_v	1864	1766.9318	$\mathrm{J\,kg^{-1}\,K^{-1}}$
ρ_s	1.205	1.1801	$\mathrm{kg\,m^{-3}}$
V_s	9000	8482.5893	$\mathrm{m^3}$
θ_{hb}	24187.285	22713.1723	$\mathrm{W\,K^{-1}}$
θ_{ha}	3079.875	1641.7425	$\mathrm{W\,K^{-1}}$
θ_{Mb}	1000000	1031852.4179	$\mathrm{J\,K^{-1}}$

4.5 Parameter Estimation Results

Three sections of the data from the Mosegaarden summer set were chosen for parameter estimation. After the parameter estimation has completed a open-loop simulation was run with the model. The resulting fit for the simulation of these three sections are plotted in Figure 4.8, 4.9 and 4.10.

The fit percentage in the Figure 4.11 is calculated as.

$$\text{fit} = 100\left(1 - \frac{\|y - \hat{y}\|}{\|y - \text{mean}(y)\|}\right) \tag{4.7}$$

where:

fit	[%]	Fit
y	[·]	Measured output
$\hat{y}$	[·]	Model output

Figure 4.8 shows the fit for the first section. It is seen that the temperature T_s has a good fit of 57.87 %, while the humidity x_s only has a fit of 23.4 %. Though for both plots it is shown that the model captures the dynamics of the system.

Furthermore Figure 4.9 and 4.10 shows the fit to be 49.35 % and 53.7 % for the temperature T_s respectively, and −33.79 % and 2.95 % for the humidity x_s respectively.

Clearly the fit for the humidity is generally lower than that for the temperature. This can be caused by the fact that there is not enough change in the humidity throughout the data to capture the dynamics. Most of the changes in humidity are likely driven by sensor noise.

Furthermore the water evaporation from the bedding in the production house was not included in the model, which affects the accuracy of the humidity predicted by said model.

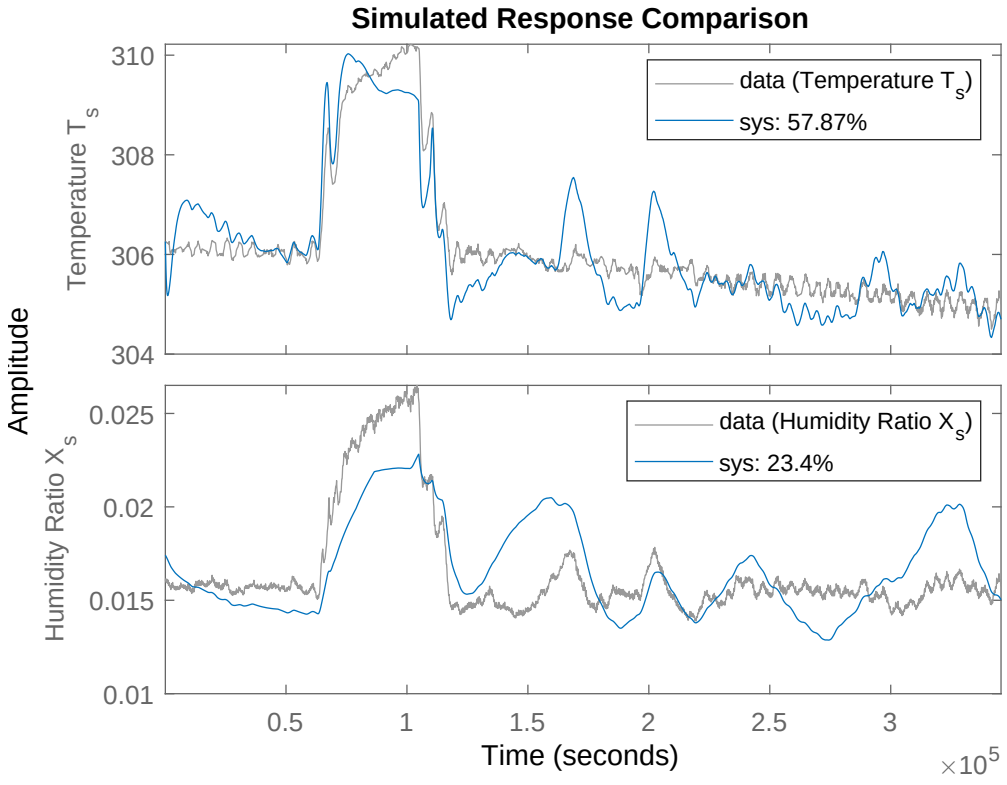

Figure 4.8: Shows the resulting fit for the first green segment in Figure 4.11.

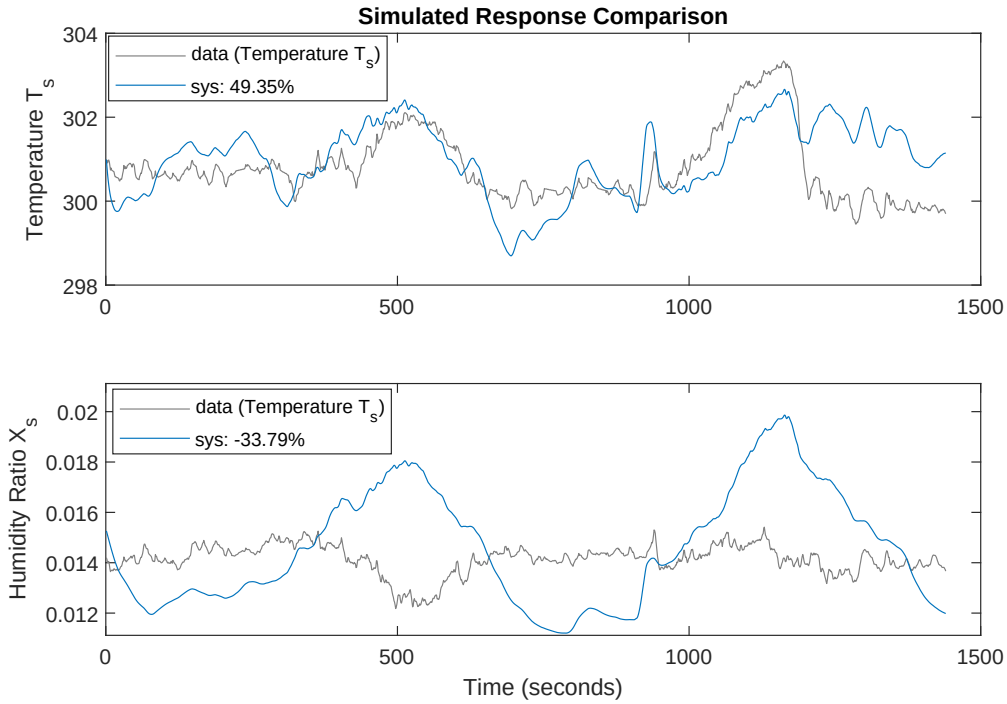

Figure 4.9: Shows the resulting fit for the second green segment in Figure 4.11.

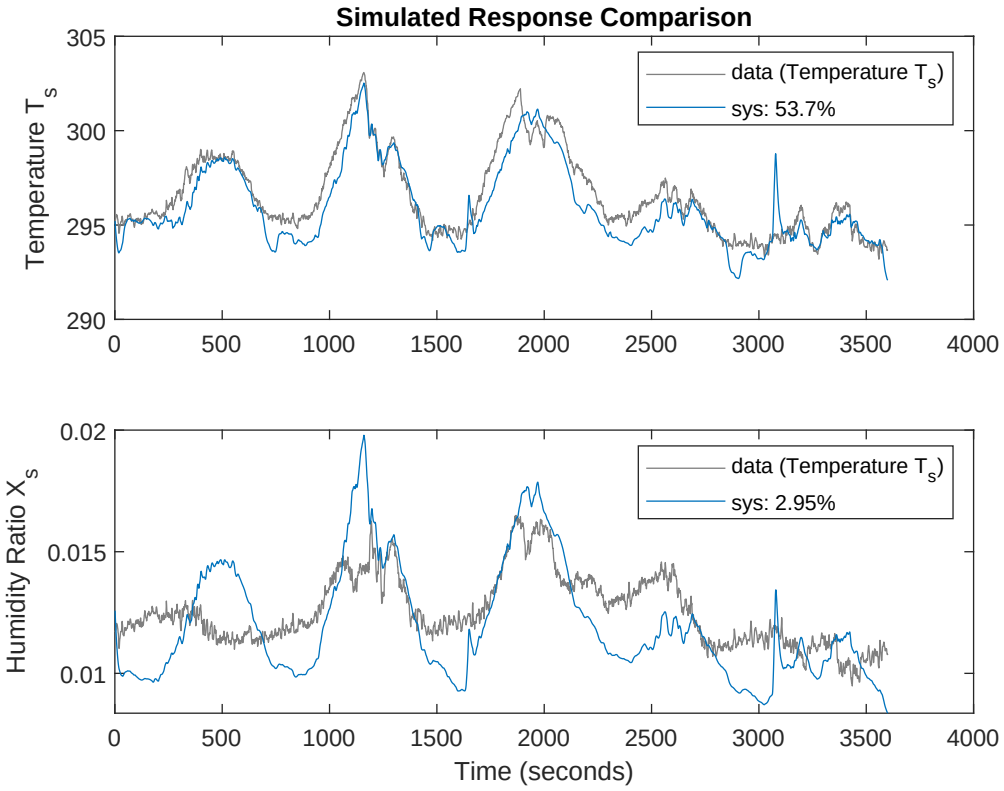

Figure 4.10: Shows the resulting fit for the third green segment in Figure 4.11.

Running a open-loop simulation for the complete summer data set from Mosegaarden a fit of 65.79 % is seen for the temperature T_s and a fit of 4.875 % is seen for the humidity x_s. This matches with what could be expected after seeing the fits for the training data. The open-loop simulation for the complete data set is plotted in Figure 4.11.

It should be noted that a reason for the temperature fit for the complete summer data set to be better than the individual fits for the training data might be caused by the fit calculation. The model output is compared to the mean of the data. Given more data the mean might fit the data worse, meaning the model get a better fit percentage without actually performing better.

In Figure 4.12 the error of the open-loop simulation is plotted. The temperature T_s has an acceptable error of 0 K–4 K with a few spikes hitting 5 K. A greater error is seen for the humidity, where the error lies between $0–4 \cdot 10^{-3}$ with spikes hitting $5 \cdot 10^{-3}$. But given that the water evaporation from the bedding were not included in the model and that the humidity data is stable making parameter prediction hard, this is an acceptable error.

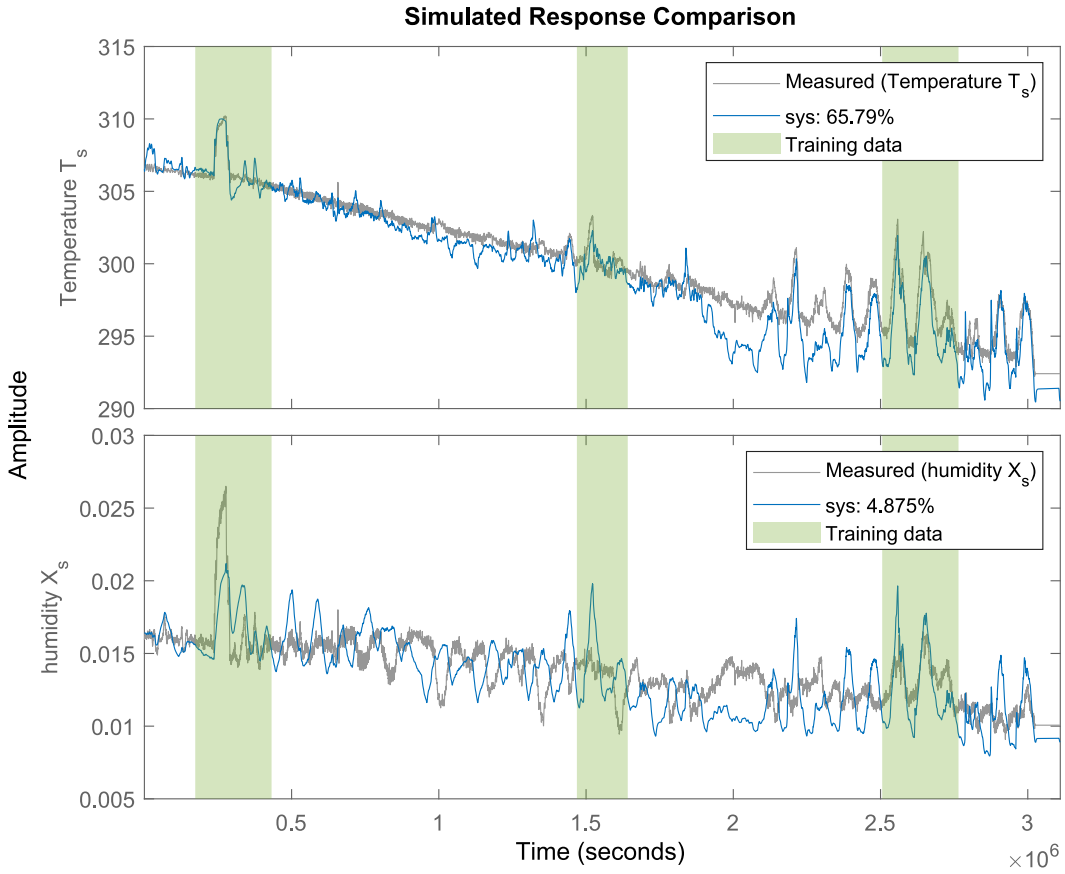

Figure 4.11: Comparison between the model and measured data given the estimated parameters in Table 4.1 for an open-loop simulation of the summer data set for Mosegaarden.

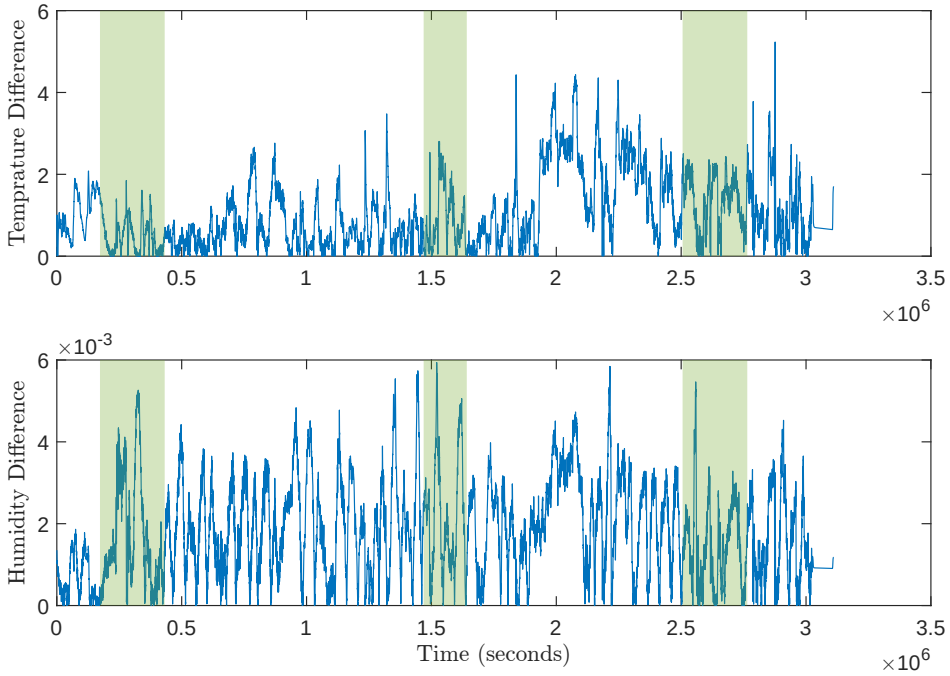

Figure 4.12: Error for the open-loop simulation for the results shown in Figure 4.11.

As mentioned in section 4.2 the winter data set were to be used for validation. Therefore a open-loop simulation using the winter data is plotted in Figure 4.13 with a plot of the error shown in Figure 4.14. The fit for the temperature T_s is 51.54 % with an error around 0 K–4 K, same as for the summer set, which is an acceptable error.

The humidity x_s however has a fit of $-153.9\,\%$, with an constant error between $0\text{–}6 \cdot 10^{-3}$. Though this is worse than for the summer set the model still captures the dynamics of the system. As the true humidity decreases, the model prediction also decreases.

Furthermore in the winter less ventilation is utilised as seen in Figure 4.7. Therefore the humidity inside of the production house x_s is less affected by the outside humidity x_a and more affected by the water vapour generated from the bedding and the poultry. Since the bedding evaporation is not included in the model, an offset is generated between the true value and the model value.

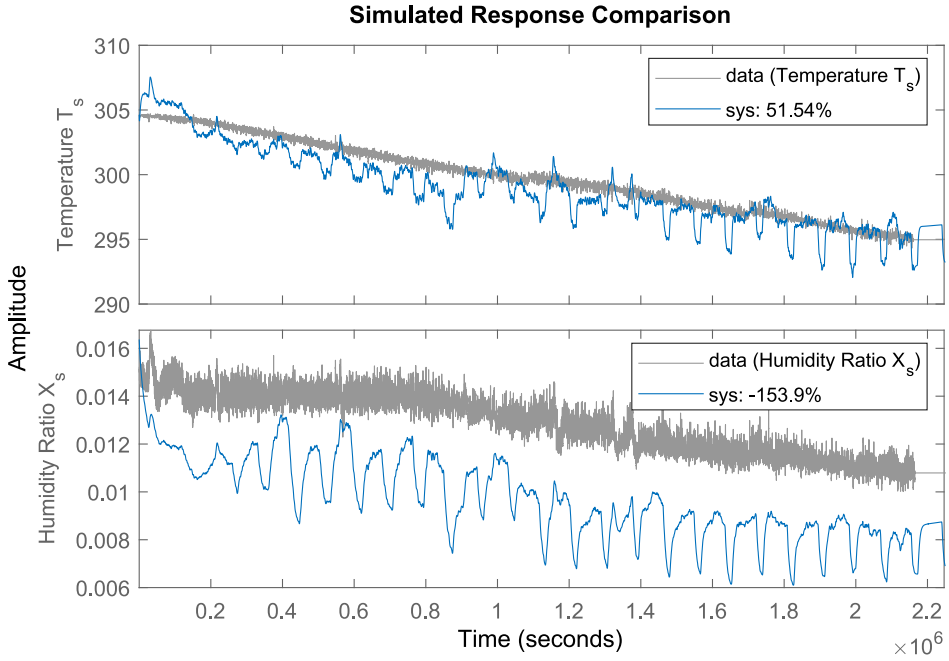

Figure 4.13: Comparison between the model and measured data given the estimated parameters in Table 4.1 for an open-loop simulation of the winter data set for Mosegaarden.

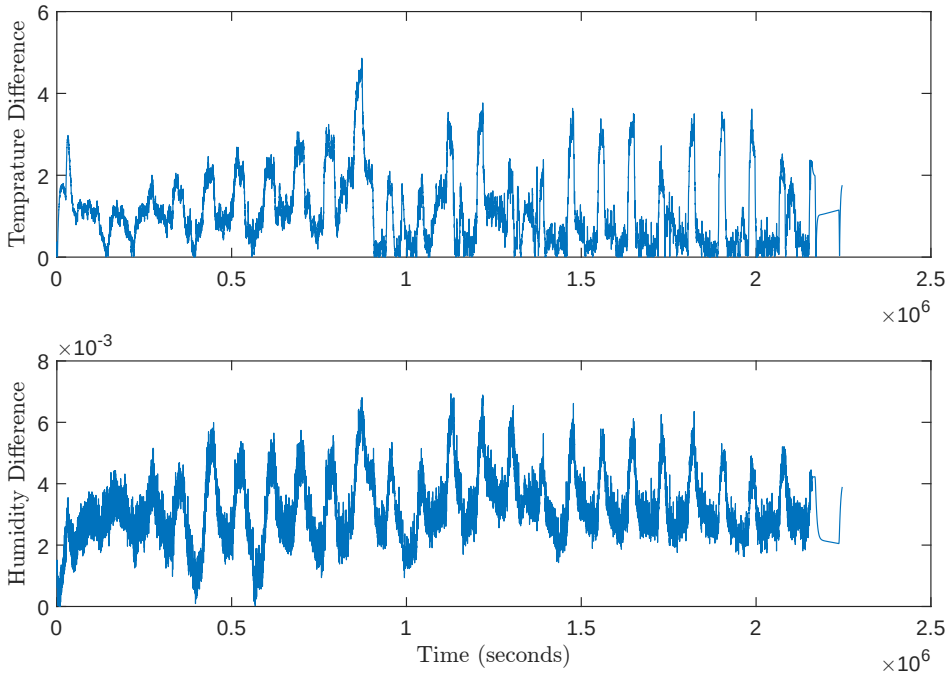

Figure 4.14: Error for the open-loop simulation for the results shown in Figure 4.13.

Based on the results presented it can be concluded that the current model can simulate a production house to a satisfactory degree and can therefore be used for controller and observer design in Part III.

Part III

Design - Control System

Chapter 5

State Observer

In chapter 3 a non-linear model for a production house was found. Here the states M_w, $T_{sh,out}$ and T_b are hidden states, which are not measured. All states are required for the LQR controller, a controller choice which will be argued for in section 6.1. Therefore a state observer is needed. For this task an Extended Kalman Filter (EKF) has been chosen as it is a nonlinear version of the standard Kalman Filter.

Initially a Luenberger Observer and a Kalman Filter were tested, but both did not perform adequately likely because of the non-linear nature of the system. Hence, the EKF was chosen.

It should further be noted that the observer designed in this chapter is tuned based on parameters and data from the Mosegaarden production house presented in chapter 4. Since the testing in chapter 7 is carried out at Air Physical Laboratory at SKOV A/S the observer will have to tuned again for this system once on location. See Appendix D for more detail.

5.1 Extended Kalman Filter

The Extended Kalman Filter used as a state estimator for a non-linear system with additive white noise is generally defined as in Equation 5.2 for a system on the form [36]

$$\begin{aligned} x_{k+1} &= f(x_k, u_k) + w_k, \qquad & w_k &\overset{i.i.d.}{\sim} \mathcal{N}(0, Q_k) \\ y_k &= h(x_k, u_k) + v_k, \qquad & v_k &\overset{i.i.d.}{\sim} \mathcal{N}(0, R_k) \end{aligned} \tag{5.1}$$

Initial conditions:

$$x_0 \sim \mathcal{N}(\hat{x}_{0|-1}, P_{0|-1})$$

Measurement update:

$$\begin{aligned} \hat{y}_{k|k-1} &= h(\hat{x}_{k|k-1}, u_k) \\ \tilde{y}_{k|k-1} &= y_k - \hat{y}_{k|k-1} \\ H_k &= \left.\frac{\partial h(x,u)}{\partial x^{\mathrm{T}}}\right|_{\hat{x}_{k|k-1}, u_k} \\ K_k &= P_{k|k-1}\, H_k^{\mathrm{T}} \left(H_k\, P_{k|k-1}\, H_k^{\mathrm{T}} + R_k\right)^{-1} \\ \hat{x}_{k|k} &= \hat{x}_{k|k-1} + K_k\, \tilde{y}_{k|k-1} \\ P_{k|k} &= (I - K_k\, H_k)\; P_{k|k-1}\; (I - K_k\, H_k)^{\mathrm{T}} + K_k\, R_k\, K_k^{\mathrm{T}} \end{aligned} \tag{5.2}$$

Time update:

$$\begin{aligned} \hat{x}_{k+1|k} &= f(\hat{x}_{k|k}, u_k) \\ F_k &= \left.\frac{\partial f(x,u)}{\partial x^{\mathrm{T}}}\right|_{\hat{x}_{k|k}, u_k} \\ P_{k+1|k} &= F_k\, P_{k|k}\, F_k^{\mathrm{T}} + Q_k \end{aligned}$$

where

x_k	$[\cdot]$	state at time k,
u_k	$[\cdot]$	input at time k,
w_k	$[\cdot]$	random dynamic disturbance at time k,
v_k	$[\cdot]$	random sensor noise at time k,
$\hat{y}_{k\|k-1}$	$[\cdot]$	output prediction at time k,
$\tilde{y}_{k\|k-1}$	$[\cdot]$	output prediction error at time k,
$\hat{x}_{k\|k}$	$[\cdot]$	state estimate at time k,
$\hat{x}_{k+1\|k}$	$[\cdot]$	state prediction at time k,
H_k	$[\cdot]$	linearisation of the output function $h(x, u)$,
F_k	$[\cdot]$	linearisation of the state function $f(x, u)$,
K_k	$[\cdot]$	Kalman gain at time k,
$P_{k\|k}$	$[\cdot]$	estimate of the state covariance at time k,
$P_{k+1\|k}$	$[\cdot]$	prediction of the state covariance at time k,
R_k	$[\cdot]$	sensor noise weighting matrix,
Q_k	$[\cdot]$	process noise weighting matrix.

5.1.1 Non-linear continuous time function to discrete time function

For the model designed in chapter 3 and chapter 4 the continuous time system is on the form

$$\begin{aligned} \dot{x} &= f_c(x, u, d) \\ y &= Cx \end{aligned} \tag{5.3}$$

The states x, inputs u and disturbances d for the system in Equation 5.3 are then

$$x = \begin{bmatrix} M_v \\ M_w \\ T_{sh,out} \\ T_b \\ T_s \end{bmatrix}, \qquad u = \begin{bmatrix} w_{sh} \\ \dot{V} \\ w_{spray} \end{bmatrix}, \qquad d = \begin{bmatrix} T_{sh,in} \\ T_a \\ x_a \\ A \\ f_{lux}(t) \end{bmatrix}. \tag{5.4}$$

All disturbances are measured, except $T_{sh,in}$ which is assumed to be constant. Therefore all disturbances are included as inputs in the EKF.

The sample time t_s is set at 120 s based on the sample time of the data from Mosegaarden presented in chapter 4.

For the discritisation of the continuous time function Forward Euler were attempted, but it were only stable up until 8 s with a 1 s time-step. For more see Appendix C.

Instead Backwards Euler were implemented as implicit discretisation. Here a solution were found by numerically solving the discritisation of the continuous time system. Backwards Euler is given in Equation 5.5.

$$\hat{x}_{k+1|k} = \hat{x}_{k|k} + t_s \cdot f_c(\hat{x}_{k+1|k}, u_k, d_k) \tag{5.5}$$

5.1.2 Modifications

Some modification for EKF were needed, so that it would fit the system. During the measurement update, the expression for H_k linearised is just the expression itself.

$$H_k = \left.\frac{\partial h(x,u)}{\partial x^{\mathrm{T}}}\right|_{\hat{x}_{k|k-1},u_k} = H \tag{5.6}$$

Including this modification a new EKF is formulated in Equation 5.7, where the changes is marked with red.

$$\begin{aligned}
&\text{Initial conditions:}\\
&\qquad x_0 \sim \mathcal{N}(\hat{x}_{0|-1}, P_{0|-1})\\
&\text{Measurement update:}\\
&\qquad \hat{y}_{k|k-1} = H\hat{x}_{k|k-1}\\
&\qquad \tilde{y}_{k|k-1} = y_k - \hat{y}_{k|k-1}\\
&\qquad K_k = P_{k|k-1}\,H^{\mathrm{T}}\left(H\,P_{k|k-1}\,H^{\mathrm{T}} + R_k\right)^{-1}\\
&\qquad \hat{x}_{k|k} = \hat{x}_{k|k-1} + K_k\,\tilde{y}_{k|k-1}\\
&\qquad P_{k|k} = (I - K_k\,H)\,P_{k|k-1}\,(I - K_k\,H)^{\mathrm{T}} + K_k\,R_k\,K_k^{\mathrm{T}}\\
&\text{Time update:}\\
&\qquad \hat{x}_{k+1|k} = \hat{x}_{k|k} + t_s \cdot f_c(\hat{x}_{k+1|k}, u_k, d_k)\\
&\qquad F_k = \left.\frac{\partial f(x,u)}{\partial x^{\mathrm{T}}}\right|_{\hat{x}_{k|k},u_k}\\
&\qquad P_{k+1|k} = F_k\,P_{k|k}\,F_k^{\mathrm{T}} + Q_k
\end{aligned} \tag{5.7}$$

It is furthermore not possible to linearise the non-linear discrete time function $f(x_k, u_k, d_k)$ directly. Therefore the continuous time function $f_c(x, u, d)$ will first be linearised in subsection 5.1.3 and then discretised in subsection 5.1.4.

5.1.3 Model Linearisation

For linearisation of the continuous time function $f_c(x, u, d)$ jacobian linearisation is utilised. Here $f_c(x, u, d)$ is linearised around specific operating points called equilibrium points. Given a non-linear differential equation

$$\dot{x}(t) = f_c(x(t), u(t), d(t)),$$

the jacobian linearisation is derived in Equation 5.8. [37]

$$A_c := \left.\frac{\partial f_c}{\partial x}\right|_{\substack{x=\bar{x}\\u=\bar{u}\\d=\bar{d}}} \in \mathbf{R}^{\mathbf{n}\times\mathbf{n}} \quad , \quad B_c := \left.\frac{\partial f_c}{\partial u}\right|_{\substack{x=\bar{x}\\u=\bar{u}\\d=\bar{d}}} \in \mathbf{R}^{\mathbf{n}\times\mathbf{m}} \tag{5.8}$$

where $\bar{x}$, $\bar{u}$ and $\bar{d}$ are the equilibrium points for the states, inputs and disturbances respectively. These points are defined as equilibrium if the condition

$$f_c(\bar{x}, \bar{u}, \bar{d}) = 0_n,$$

is satisfied. [37]

The new continuous time linearised system is then on the form

$$\begin{aligned} \frac{d\delta x}{dt} &= A_c \delta x + B_c \delta u, \\ \delta x &= x - \bar{x}, \\ \delta u &= u - \bar{u}. \end{aligned} \tag{5.9}$$

The linearisation is performed in Matlab with the function `jacobian(f,v)`, which computes the jacobian matrix of `f` with respect to the variable(s) `v`. [38]

Next linear continuous time system will be discretised.

5.1.4 Discretization

The linear system is discretised assuming zero-order hold on the input u. Given the linear state space system

$$\dot{x}(t) = Ax + Bu,$$

the discretisation is derived in Equation 5.10 and 5.11. [39, p. 106]

$$A_k = e^{At_s}, \tag{5.10}$$

$$B_k = A^{-1}(A_k - I)B, \tag{5.11}$$

$$\tag{5.12}$$

where A is required to be invertible and t_s is the sample time. The linearised discretised state space then becomes

$$\delta x_{k+1} = A_k \delta x_k + B_k \delta u_k. \tag{5.13}$$

5.1.5 $\mathbf{Q_k}$ and $\mathbf{R_k}$ weighting matrices

The two weight matrices Q_k and R_k describes the processes noise and sensor noise, respectively. It is possible to estimate R_k from measured data, whereas Q_k is normally used as a tuning parameter.

The main purpose of the two matrices is to determine if the model or the measurements are to be trusted more than the other. If there is more noise in the model than the measurements, the measurements are trusted more if disputes in results should arise and vise versa.

It is furthermore possible to find suitable Q_k and R_k matrices through trial and error, which is the method used for this project. Both matrices there found to be identify matrices of suitable sizes.

5.2 Performance

In this section the performance of the EKF observer will be presented. In Figure 5.1, 5.2, 5.3, 5.4 and 5.5 the results for the states M_v, M_w, $T_{sh,out}$, T_b and T_s are plotted respectively. In all plots are included a test based on simulation and a test based on real world data from Mosegaarden. For M_v and T_s the real world data measurement are plotted together with the estimate, but for M_w, $T_{sh,out}$ and T_b this is not the case since they are hidden states. The simulations are done with input data from Mosegaarden.

In Figure 5.1 the estimate for M_v is shown to fit the data from both simulation and real world. Furthermore the dynamics of the system are captured to a satisfactory degree. Even given that the estimate for the real world data starting point is around 20 kg bigger than the measurement it quickly stabilises.

In Figure 5.2 the estimate of M_w is shown to fit the simulation data well. Furthermore both the estimate for simulation and real world data are shown to capture the dynamics of the system. Given that M_w is a hidden state it is satisfactory to see it matching the simulation dynamics. The same is true for $T_{sh,out}$ and T_b in Figure 5.3 and 5.4

Like for M_v, Figure 5.5 shows that the estimate of T_s for both simulation and real world measurements fits and captures the dynamics of the system. Even given that the starting point of the estimate for the measured data is around 5 K–6 K higher, it quickly stabilises.

Based on the fact that the EKF observer both fits can captures the dynamics of the true measurements for the measured states, it can be concluded that the estimates for the hidden states are acceptable, since they too capture the dynamics of the system.

A block diagram of the final EKF is to be found in Figure 5.6. Next is the design of the controller in chapter 6.

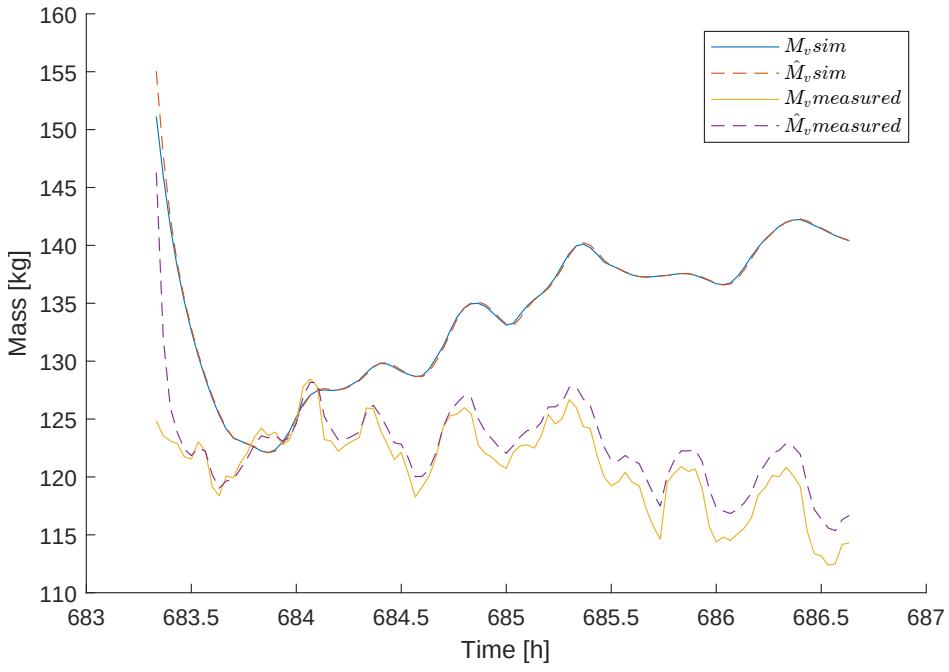

Figure 5.1: Estimate of M_v given data from simulation and real world data from Mosegaarden.

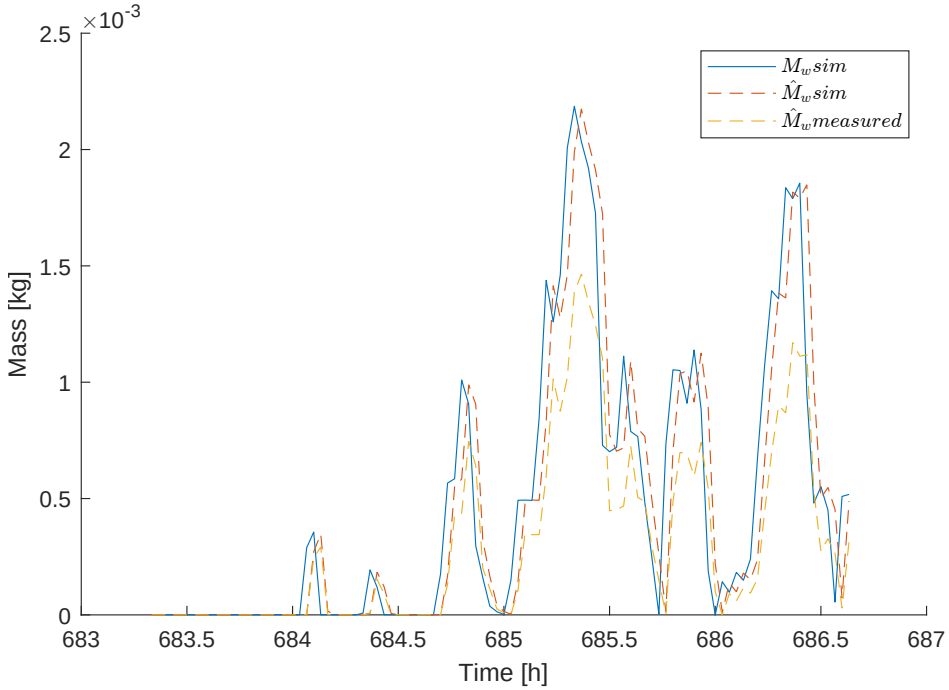

Figure 5.2: Estimate of M_w given data from simulation and real world data from Mosegaarden.

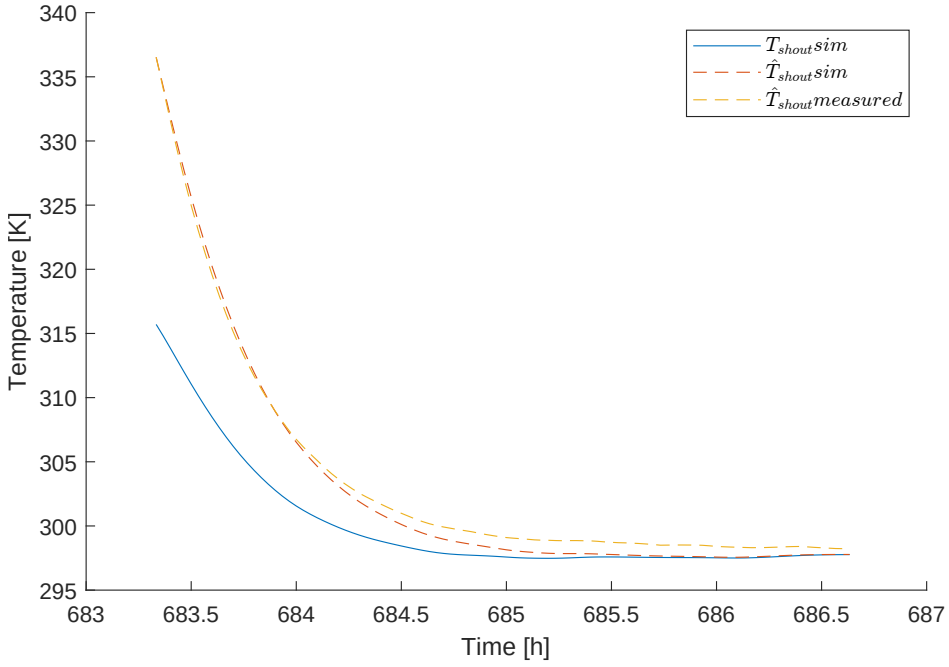

Figure 5.3: Estimate of $T_{sh,out}$ given data from simulation and real world data from Mosegaarden.

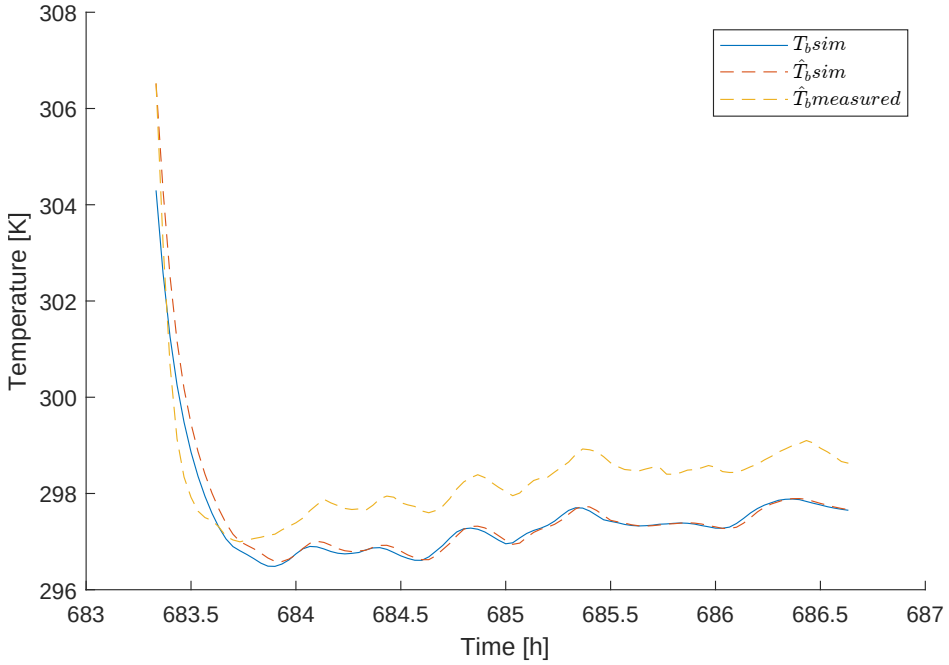

Figure 5.4: Estimate of T_b given data from simulation and real world data from Mosegaarden.

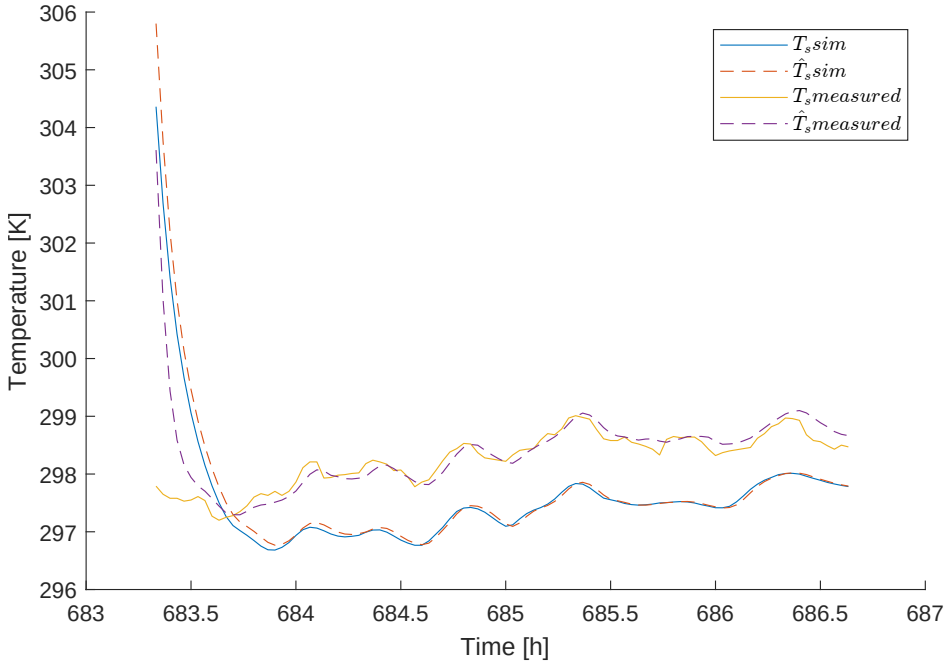

Figure 5.5: Estimate of T_s given data from simulation and real world data from Mosegaarden.

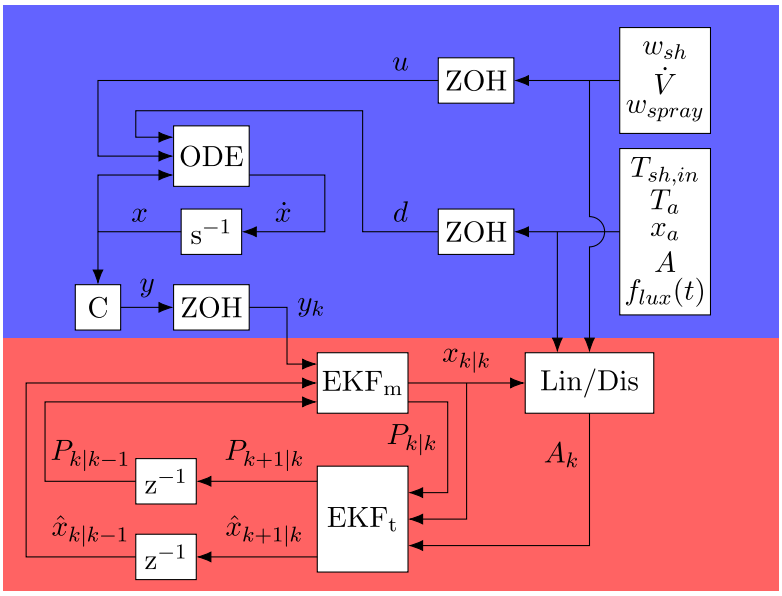

Figure 5.6: Block diagram for the EKF.

Chapter 6

Control Strategy

In this chapter the choice and design of controller will be covered. An LQR controller has been chosen and firstly the reasoning for this choice will be presented. This is followed by the design of said controller, tuning and lastly performance.

It should be noted that the controller is this chapter is tuned for the normal production house based on the parameters found in chapter 4. Since the testing will not take place at a production house, but instead at the Air Physical Laboratory at SKOV A/S, the controller will need to be tuned again based on parameters for the laboratory. Which will further be touched upon in section 6.1 and more details of the process can be found in Appendix D.

6.1 Control Strategy Selection

For this project is has been chosen to design a Linear Quadratic Regulator (LQR) to be used as a MIMO controller for climate control inside a production house. In combination with the EKF designed in chapter 5, the final controller becomes an Linear Quadratic Gaussian Regulator (LQG).

An LQR controller is a light-weight controller which does not require much computing power to run. It reacts to the current states of the system by generating actuator inputs which aim to pull the states to a reference specified by the user.

In the general cost function for LQR in Equation 6.3 there are a Q and R matrix which determines the cost/importance of the states and actuator inputs, respectively. One of the advantage of the LQR controller is that the user easily can tune the controller by adjusting these matrices.

This is positive, because the controller will be implemented for testing at the Air Physical Laboratory at SKOV A/S. No complete data set has been available for the laboratory, so to tune the controller for the tests the following steps are necessary:

- Generate data for the dynamics of the laboratory by exiting the states,
- Repeat the parameter estimation with the new data,
- Repeat tuning of the EKF with the new parameters,
- Repeat tuning of the controller gain K by adjusting Q and R with the new parameters.

The laboratory is only available for one week, therefore having a quick-to-tune controller is crucial.

A disadvantage of the LQR controller is, that if the model used for its design does not fit the real world, then the LQR cannot optimally control the system.

6.2 Linear Quadratic Regulator Design

In this section the design of the Linear Quadratic Controller is covered. The controller is designed based on the model from chapter 3 and the parameters found in chapter 4.

The LQR works together with the EKF effectively becoming a Linear Quadratic Gaussian (LQG) controller. An overview of the complete control structure is illustrated in Figure 6.1.

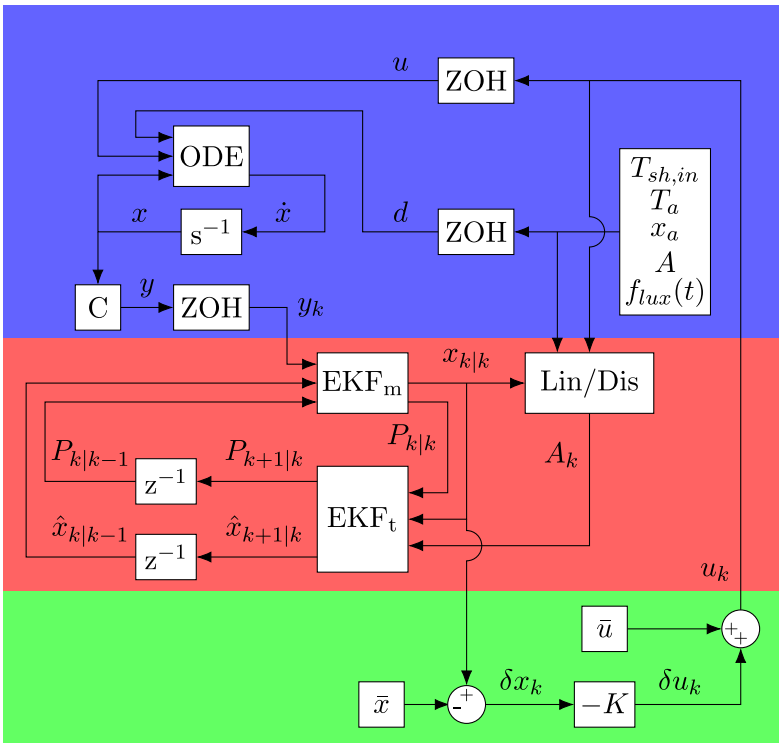

Figure 6.1: Block Diagram over the EKF, LQR and simulation setup.

For a system on the form

$$x_{k+1} = Ax_k + Bu_k \tag{6.1}$$

a closed-loop control feedback gain matrix K on the form in Equation 6.2 can be found using LQR.

$$u_k = -K \cdot x_k \tag{6.2}$$

The values of the K matrix are found, so that u_k minimises the the cost function defined in Equation 6.3 [39].

$$J = \sum_{k=1}^{\infty} (x_k^T Q x_k + u_k^T R u_k) \tag{6.3}$$

where

Q	$[\cdot]$	is the state weight matrix,
R	$[\cdot]$	is the input weight matrix.

Equation 6.3 shows that the weight of the cost of the states are defined by Q and for the inputs defined by R.

The cost function is minimised by finding the S matrix that solves the discrete time algebraic Riccati equation in Equation 6.4 [39, p. 371]. This is done numerically.

$$A^T SA - S - (A^T SB)(B^T SB + R)^{-1}(B^T SA) + Q = 0 \tag{6.4}$$

The solution for S is then used to calculate the feedback gain matrix K in Equation 6.5 [39, p. 371].

$$K = (B^T \cdot S \cdot B + R)^{-1}(B^T \cdot S \cdot A) \tag{6.5}$$

The calculation of the feedback gain matrix K and the S matrix is based on a linear discrete time model. Since the model designed in chapter 3 is a non-linear continuous time model, it needs to be linearised and discretised, which were covered in subsection 5.1.3 and subsection 5.1.4, respectively.

As mentioned in subsection 5.1.3, the operating points of the linearised system becomes the new zeros. The resulting gain matrix K will therefore take the error between the operating points and the true value as an input and output a small signal actuator input $\tilde{u}$. Therefore the operating points u_{ss} must be added to the actuator inputs $\tilde{u}$ before they enter the system as illustrated in Figure 6.2.

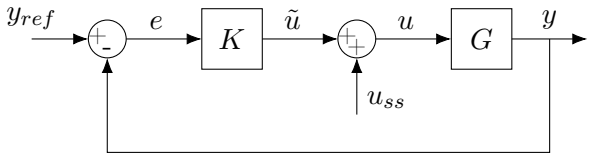

Figure 6.2: System Control structure for a linearised system.

6.3 Tuning of the Linear Quadratic Regulator

For tuning the LQR controller there are three parameters there can be adjusted:

- The operating points, which the model is linearised around,
- The Q matrix for the states,
- The R matrix for the inputs.

The N matrix is not utilised in this project and will therefore be set equal to zero.

The operating points chosen will function as the reference for each state and input. The Q and R matrices will then determine the weight of the error for each of these references.

6.3.1 Operating Points

All states and inputs with their determined operating points are listed in Table 6.1.

Table 6.1: List of the operating points with values used for LQR tuning based on data from Mosegaarden.

Variable	Operating Point	Unit
M_v	125	kg
M_w	0	kg
$T_{sh,out}$	311.15	K
T_b	297.15	K
T_s	298.15	K
w_{sh}	0	$\mathrm{kg\,s^{-1}}$
V_{dot}	0.15	$\mathrm{m^3\,s^{-1}}$
w_{spray}	0	$\mathrm{kg\,s^{-1}}$
T_a	288.15	K
x_a	0.0064	$\frac{\text{kg water vapour}}{\text{kg dry air}}$
$T_{sh,in}$	333.15	K
f_{lux}	1	·
A	50	*days*

For the operating points the production house temperature T_s is the most important state and the state which is the main goal of the controller to keep at reference. For the simulations shown in section 6.4 the reference temperature is set to 25 °C.

The other temperatures $T_{sh,out}$, T_b and T_a are from the data set from Mosegaarden. This is also the case for M_v.

M_w, w_{sh} and w_{spray} are all set to zero as the operating points represent a final state we want to reach. If the reference for the temperature is reached no heating or cooling should ideally take place.

The ventilation V_{dot} is set a $0.15\,\mathrm{m^3\,s^{-1}}$ as there will always be a minimum ventilation inside the production house to keep harmful gasses at a minimum.

$T_{sh,in}$ there found through parameter estimation, and f_{lux} and A are set to match daylight time with 50 days old poultry, while x_a is set to 0.0064 $[\frac{\text{kg water vapour}}{\text{kg dry air}}]$.

Furthermore the hidden states T_b, $T_{sh,out}$ and M_w are not meant to be driven to any specific reference. Therefore their values are also their equilibrium points.

6.3.2 *Q* and *R* matrices

As mentioned in the beginning of this section the Q and R matrices determines the weight of each state and input, respectively. When choosing a starting value for these matrices, one possibility it to use Bryson's Rule defined in Equation 6.6 and 6.7 [39, p. 400].

$$Q = \operatorname{diag}\left\{\frac{1}{x_{1,\max}}, \frac{1}{x_{2,\max}}, \ldots, \frac{1}{x_{n,\max}}\right\} \qquad \text{for } n > 0 \text{ states,} \tag{6.6}$$

$$R = \operatorname{diag}\left\{\frac{1}{u_{1,\max}}, \frac{1}{u_{2,\max}}, \ldots, \frac{1}{u_{m,\max}}\right\} \qquad \text{for } m > 0 \text{ inputs.} \tag{6.7}$$

Bryson's Rule define each weight as a product of the maximum allowed range of the state or input that the weight represents. It is a valid starting point, but manual tuning may still be required.

Using Bryson's Rule as a starting point, the Q and R matrices was tuned to their final values presented in Equation 6.8 and 6.9.

$$x^T Q x = \begin{bmatrix} M_v & M_w & T_{sh,out} & T_b & T_s \end{bmatrix} \begin{bmatrix} 0 & 0 & 0 & 0 & 0 \\ 0 & 0 & 0 & 0 & 0 \\ 0 & 0 & 0 & 0 & 0 \\ 0 & 0 & 0 & 0 & 0 \\ 0 & 0 & 0 & 0 & 100 \end{bmatrix} \begin{bmatrix} M_v \\ M_w \\ T_{sh,out} \\ T_b \\ T_s \end{bmatrix} \tag{6.8}$$

$$u^T R u = \begin{bmatrix} w_{sh} & \dot{V} & w_{spray} \end{bmatrix} \begin{bmatrix} 100 & 0 & 0 \\ 0 & 10 & 0 \\ 0 & 0 & 10 \end{bmatrix} \begin{bmatrix} w_{sh} \\ \dot{V} \\ w_{spray} \end{bmatrix} \tag{6.9}$$

As seen in Equation 6.8 the weight of all states except T_s are set equal to zero, since they are not important for the well being of the poultry. The inputs however all have an effect on the temperature T_s and therefore also the poultry. In Equation 6.9 it is seen that V_{dot} and w_{spray} are weighted the same, while w_{sh} is weighted higher with a factor of 10.

The results are presented in section 6.4.

6.4 LQG simulation results

Using the weighting matrices Q and R defined in Equation 6.8 and 6.9 a gain matrix K was generated. Combined with the observer designed in chapter 5 an LQG controller was created. Using the summer data from Mosegaarden described in subsection 4.2.1 a simulation was run with the temperature reference set to 25 °C. The results from the simulation are plotted in Figure 6.3, 6.4 and 6.5.

In Figure 6.3 it is seen that the temperature T_s is being kept consistently close to the reference inside the 2 °C margin defined in the problem statement in section 2.7. Unfortunately, the controller seems unable to cool down the production house, when the outside temperature T_a is greater than the reference. The controller seems to try to use the ventilation for cooling and not the water spray as seen in Figure 6.5. Therefore it is not able to get the temperature T_s lower than T_a, since it is only pumping in air from the outside. Furthermore when the temperature T_a gets to low, the temperature T_s dips below the 2 °C margin.

The humidity is kept above the reference, but is not consistently keeping close to the reference as seen in Figure 6.4. Though it should be noted, that the Q weighting matrix weights the humidity as zero, while the temperature is at 100.

Given the results it has been decided to add an integral part to the controller creating an LQI with the purpose of tracking the error for better performance. This is described in section 6.5.

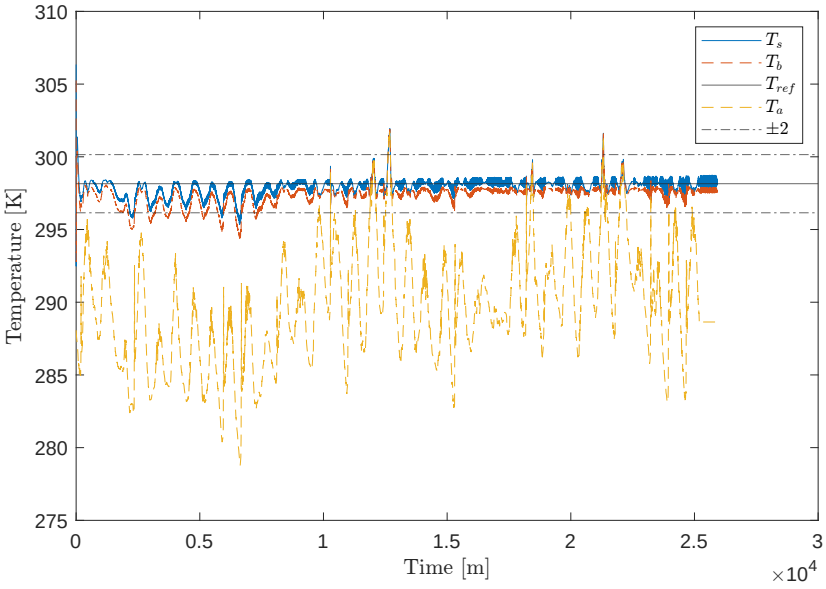

Figure 6.3: Temperature results from LQG simulation with Mosegaarden summer data set.

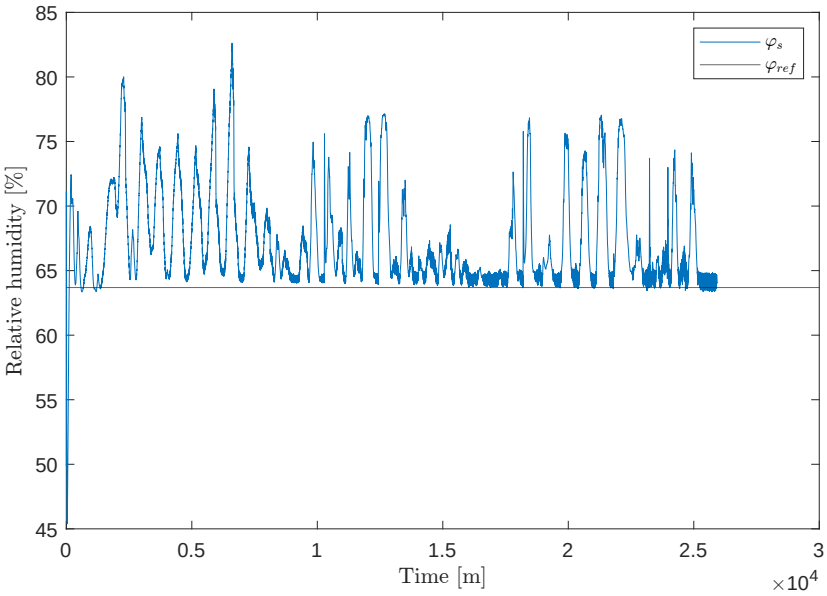

Figure 6.4: Humidity results from LQG simulation with Mosegaarden summer data set.

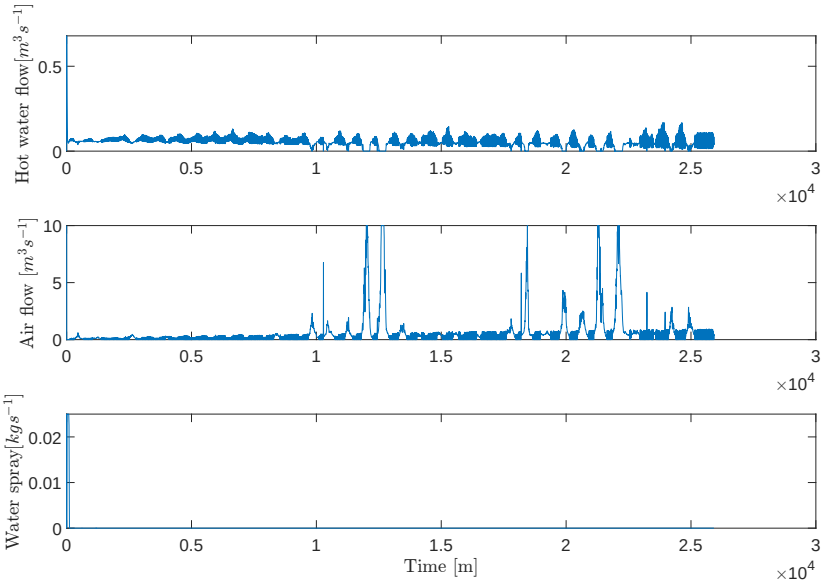

Figure 6.5: Inputs from LQG simulation with Mosegaarden summer data set.

6.5 LQI design

Integral action can be introduced by augmenting the states and matrices with an accumulated error term. Using the error e_k found in Equation 6.10 a new A and B matrix is defined in Equation 6.11.

$$e_{k+1} = r_k - Cx_k + e_k \tag{6.10}$$

$$\begin{bmatrix} x_{k+1} \\ e_{k+1} \end{bmatrix} = \underbrace{\begin{bmatrix} A & 0 \\ -C & 1 \end{bmatrix}}_{A_{aug}} \begin{bmatrix} x_k \\ e_k \end{bmatrix} + \underbrace{\begin{bmatrix} B \\ 0 \end{bmatrix}}_{B_{aug}} u_k \tag{6.11}$$

e_k is viewed as a state, therefore the Q weighting matrix is extended to account for the new state. These new matrices and weights can be used to compute a LQI controller gain $[K, K_i]$, the same way that the LQR controller was computed by solving the Riccati equation.

With integral action there is a windup problem that occurs when a system input is saturated. This causes the integral error to build up without affecting the input. Once the input is no longer saturated it takes a long time for the error to decrease, causing a big overshoot and bad performance in general. A simple way to do anti-windup is to do clamping, where the error integration is disabled when a input is saturated.

Implementing an integral results in the final controller structure illustrated in the block diagram in Figure 6.6.

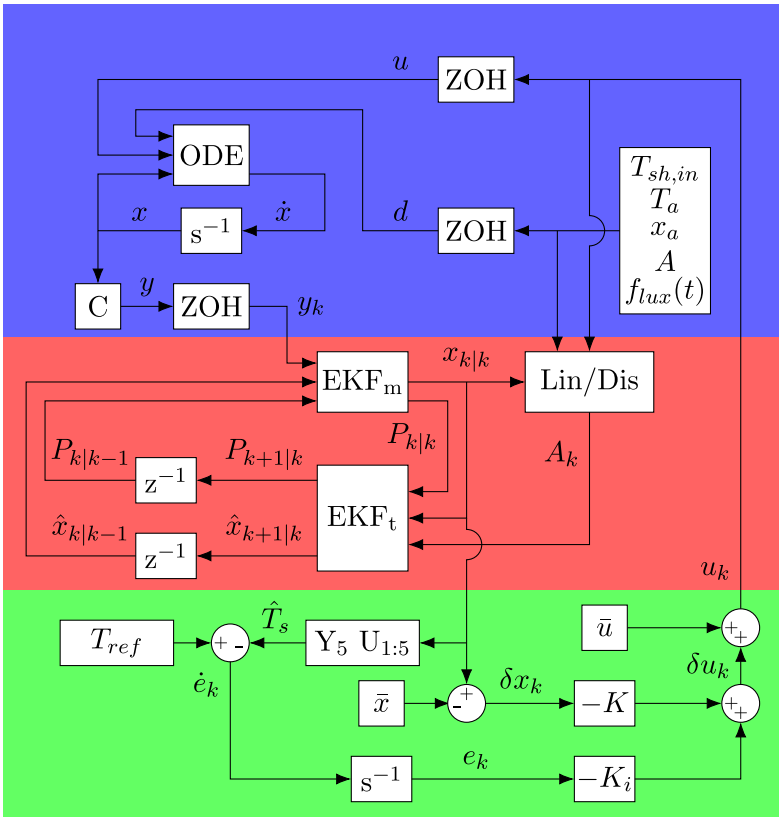

Figure 6.6: Block Diagram over the EKF, LQI and simulation setup.

6.6 LQI simulation results

Using the same setup as for the LQG in section 6.4, the summer data set from Mosegaarden is used to simulate the performance of the LQI. The weighting matrices are defined as $Q = \text{diag}(0, 0, 0, 0, 100, 1)$ and $R = \text{diag}(100, 10, 10)$. As before the temperature reference is set to 25 °C and the results are plotted in Figure 6.7, 6.8 and 6.9.

In Figure 6.7 it is seen that the temperature T_s follows the reference closely inside the 2 °C margin of error. Furthermore the LQI actively tries to counteract the increase and decreases in the temperature T_a, which is does with greater success than the LQG. Looking at the LQI inputs in Figure 6.9 and comparing them to the LQG inputs in Figure 6.5 it is additionally seen that the LQI utilises all actuators dynamically to control the temperature.

The humidity in Figure 6.8 is still not keeping consistently close to reference, but it oscillates less extremely compared to the LQG. Though the humidity seems too have a greater bias with the LQI than the LQG.

Again it should be noted, the humidity is weighted at zero, while the temperature T_s is at 100. Therefore it is to be expected, that the humidity performs worse than the temperature.

Given that the temperature T_s lies inside the margin of error of 2 °C it can be concluded that the LQI performs well. In the next chapter the implementation of the controller will be described.

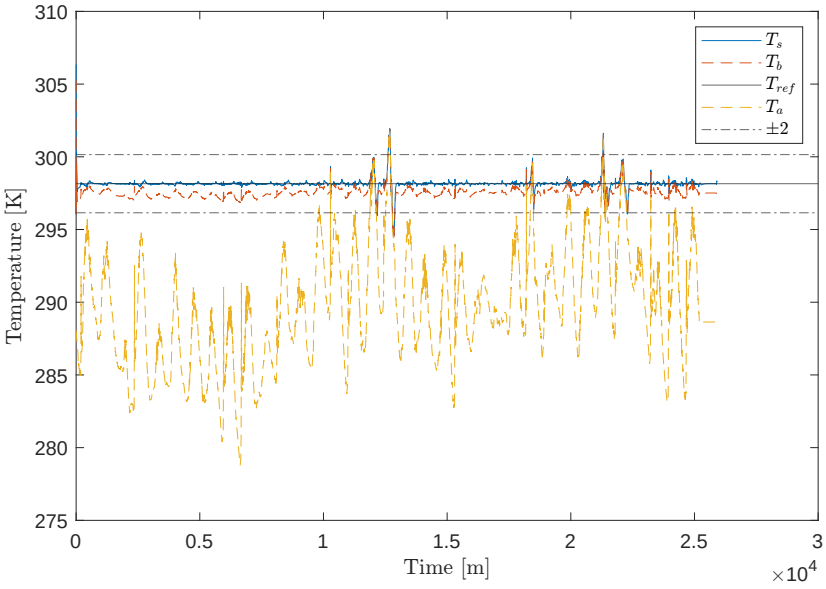

Figure 6.7: Temperature results from LQI simulation with Mosegaarden summer data set.

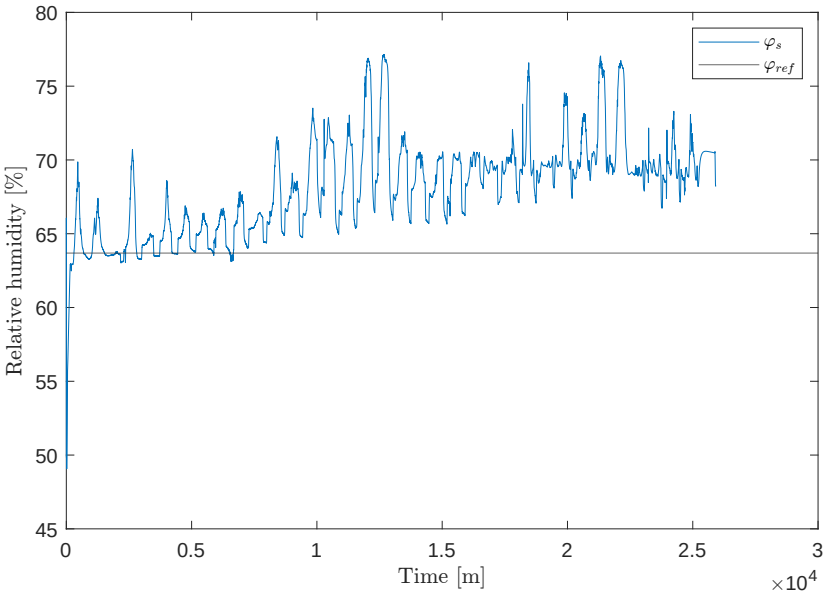

Figure 6.8: Humidity results from LQI simulation with Mosegaarden summer data set.

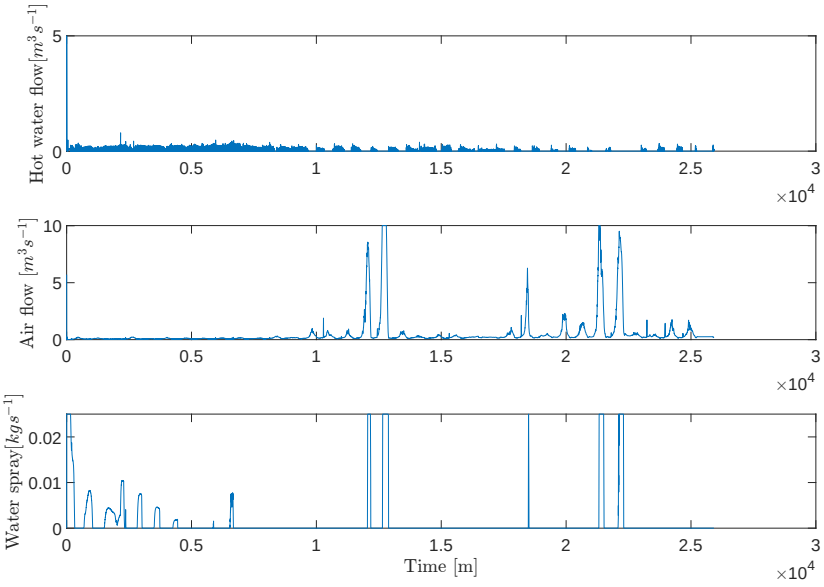

Figure 6.9: Inputs from LQI simulation with Mosegaarden summer data set.

Chapter 7

Implementation

To test the controller designed in chapter 6, SKOV A/S granted us access to their Air Physical Laboratory, which were described in section 2.5. Here a number of tests were done in the week, we were given. These test will be described in this chapter. The test are:

- Test No. 1 - Mosegaarden LQQ with 25 °C reference - subsection 7.2.1
- Test No. 2 - SKOV Laboratory LQQ with 33 °C reference - subsection 7.2.2
- Test No. 3 - SKOV Laboratory LQQ with 17 °C reference - subsection 7.2.3
- Test No. 4 - SKOV Laboratory LQI with 25 °C reference - subsection 7.2.4
- Test No. 5 - SKOV Laboratory LQI with 17 °C reference - subsection 7.2.5
- Test No. 6 - LQI test with chicken disturbance - subsection 7.2.6
- Test No. 7 - SKOV Laboratory LQI with 25 °C reference - subsection 7.2.7

Note that the LQI in section 6.5 was designed during testing at SKOV A/S. Therefore the first three tests are with we LQG controller.

7.1 Test Setup

In this section the test setup used at SKOV A/S for the air Physical laboratory will be described. In this description is included changes to the model caused by differences between the laboratory and real production houses and how the controller interfaced with SKOV's systems.

7.1.1 Relative Humidity to Absolute Humidity

The sensor DOL 114 outputs the humidity in relative humidity, which is defined as

$$x_{a,s,relative} = \frac{p_{a,s}}{p_{ws}}. \tag{7.1}$$

where

$x_{a,s,relative}$	[%]	is the relative humidity of the outside a or production house s,
$p_{a,s}$	[Pa]	is the pressure of water vapour at current humidity for a or s.

Using this definition to derive an expression for $p_{a,s}$, and combining that with an expression for the absolute humidity an expression for converting relative humidity to absolute humidity is derived in Equation 7.2. [24]

$$x_{a,s} = \lambda_{wd} \cdot \frac{p_{a,s}}{p_0 - p_{a,s}} = \lambda_{wd} \cdot \frac{x_{a,s,relative} \cdot p_{ws}}{p_0 - x_{a,s,relative} \cdot p_{ws}} \tag{7.2}$$

where

$x_{a,s}$	$[\frac{\text{kg water vapour}}{\text{kg dry air}}]$	absolute humidity of the outside a or production house s.

7.1.2 The heater

As mentioned in section 2.5 the heating method in the laboratory and a normal production house differs. Therefore the model required a small change, before the controller could be tuned for the laboratory. In Equation 3.27 and 3.26 Q_{heater} is defined as being controlled by the water flow w_{sh}. But the laboratory does not have heating pipes with water flow, only fan heaters. Therefore the model was simply changed, so Q_{heater} is treated as a direct actuator input, which the controller can adjust.

Multiple fan heaters were utilised. 3x 9 kW fan heaters were placed inside the air physical laboratory, while the 55 kW fan heater was permanently mounted on the ceiling in link with the air inlet to the laboratory. Therefore the 55 kW heater required a constant air flow otherwise the heat it supplied would not enter the laboratory.

Furthermore a secondary ventilator was utilised to create a big enough pressure drop across the 55 kW fan heater, since it required a minimum air flow or it would shut off as to not overheat and damage itself. The secondary ventilator is placed in link with the fan heater and was set to a constant air flow not controlled by the controller.

7.1.3 The Air Physical Laboratory

In Figure 2.3 it was shown that the room could be raised to an angle or lowered to be completely flat. During this test the roof was lowered to be flat given a maximum overall height of 2505 mm. Given this setup the volume of the main room is calculated in Equation 7.3.

$$V_{lab} = 19.8\,\mathrm{m} \cdot 14.1\,\mathrm{m} \cdot 2.502\,\mathrm{m} \approx 698.51\,\mathrm{m}^3 \tag{7.3}$$

Furthermore it was illustrated in Figure 2.2 that a corridor could be used to simulate the outside environment. This was not true during the test. The air heated by the 55 kW fan heater first enters the corridor, and then the main room. The reason being that the room is mostly used to test the DA 1211 air inlets in different conditions. Therefore the corridor was not used to simulate the outside during this test. Instead air from the actual outside was pumped through the fan heater, then into the corridor from there is entered the main room.

The corridor was therefore seen as part of the piping transporting the heated air into the main room, and not as an extension of the main room. Another reason for this specific distinction was, that the spray cooling only were mounted inside of the main room, and therefore did not affect the temperature in the corridor.

7.1.4 Poultry Simulation

In subsection 2.5.5 it was written that the poultry would be simulated with floor heating transporting hot water. This were partially true. Instead of hot water floor heating, electric floor heating is used. Here six circuits of floor heating were used each delivering 1410 W giving a total potential heat output of 8460 W.

7.1.5 Bryson's Rule Controller Adjustment

After the changes to the heater in the model, the input were now in watts with a max input of 82 000 W. This was far greater a number than the former maximum input of $1.1097\,\mathrm{m}^3\,\mathrm{s}^{-1}$

found in Table 4.1. Therefore Bryson's Rule described in subsection 6.3.2 was utilised to find new values for the R matrix in Equation 7.4. The Q matrix was kept as in subsection 6.3.2.

$$R = \begin{bmatrix} 1.49 \cdot 10^{-9} & 0 & 0 \\ 0 & 0.00690 & 0 \\ 0 & 0 & 9.07 \cdot 10^{3} \end{bmatrix} \tag{7.4}$$

7.1.6 Anti Windup Implementation

In test no. 4 to 7 an integral were used to keep track of the error. To avoid an aggressive overshoot anti-windup is implemented as described in section 6.5. Normally anti-windup works by deactivating the integral if any of the actuator inputs are saturated.

However this would happen every time the controller tried to heat or cool down the laboratory. Cooling down the heater would be turned off, thereby saturated at 0, and vice versa for heating up, where the water spray would be turned off.

Therefore anti-windup was implemented for the test by having the integral being deactivated only if all actuator inputs were saturated.

In section 6.5

7.1.7 Interfacing with SKOV equipment

As mentioned in section 2.5 both the heater, ventilation and sensors communicates via a 0 V–10 V analogue signal.

For this purpose a USB-6001 from National Instruments has been utilised. It has eight analogue read and two analogue write ports, which all can handle 0 V–10 V. Furthermore it has 13 digital write/read ports which can deliver 3.3 V at 20 mA. [40]

The "Data Acquisition Toolbox" from Matlab directly support the NI USB-6001 through a support package meaning the controller in Matlab can directly control the air physical laboratory. [41][42]

Four of the analogue read ports are used for two DOL 114 sensors described in subsection 2.5.6. One is placed directly outside, the other inside the main room of the laboratory. Both measure humidity and temperature.

The two DA 820 chimneys described in subsection 2.5.2 are connected in parallel, thereby requiring only one 0 V–10 V control signal.

The 55 kW fan heater can be linearly controlled with a 0 V–10 V as mentioned in subsection 2.5.4.

The three 9 kW fan heaters and the spray cooling pump can only be turned on/off with a 3.3 V digital signal controlling a relay. Since the actuator input calculated by the controller is a flow rate for both the heater ($\mathrm{W\,s^{-1}}$) and spray cooling ($\mathrm{kg\,s^{-1}}$), the flow rate is converted to a duty cycle for each time step. The duty cycle is found in Equation 7.5 based on the maximum flow rate for each system, the sample-rate t_s and the controller generated actuator input.

$$t_d = \frac{u_{actuator,n} \cdot t_s}{u_{max,n}} \tag{7.5}$$

where

$t_{d,n}$	[s]	duty cycle for actuator n,
$u_{actuator,n}$	[·]	input to actuator n,
$u_{max,n}$	[·]	maximum output of actuator n.

Furthermore there are six sprinklers connected to the cooling pump. With each sprinkler having a flow rate of $6.3\,\mathrm{L\,h^{-1}}$ the total flow rate is $37.8\,\mathrm{L\,h^{-1}}$ or $10.5 \cdot 10^{-3}\,\mathrm{L\,s^{-1}}$.

7.2 Tests

In this section all test carried out at the Air Physical Laboratory at SKOV A/S will be described and their results presented.

7.2.1 Test No. 1 - Mosegaarden LQG with 25 °C reference

For the first test the LQG controller designed in chapter 6 was utilised. This LQG were tuned based on data from Mosegaarden production house, and were therefore not tuned for the laboratory at SKOV.

The reference temperature was set to 25 °C. The result of the test are plotted in Figure 7.1, 7.2 and 7.3.

Note, that the DOL 114 was affected by the sun directly hitting it, thereby causing the measurement of the outside temperature T_a to reach upwards of 31 °C as shown in Figure 7.1.

The Mosegaarden LQG is able to keep the temperature T_s just under reference T_{ref} inside the margin of error with a bias of around $-0.43\,\mathrm{K}$ as seen in Figure 7.1.

The relative humidity plotted in Figure 7.2 does not lie close to reference, but given that the LQG attaches more importance to the temperature than the humidity this is to be expected. For this reason as can be seen in Figure 7.3 the LQG turns off both ventilation and spraying, only utilising the heating to regulate the temperature. Thereby the only source of humidity will be that from the outside air.

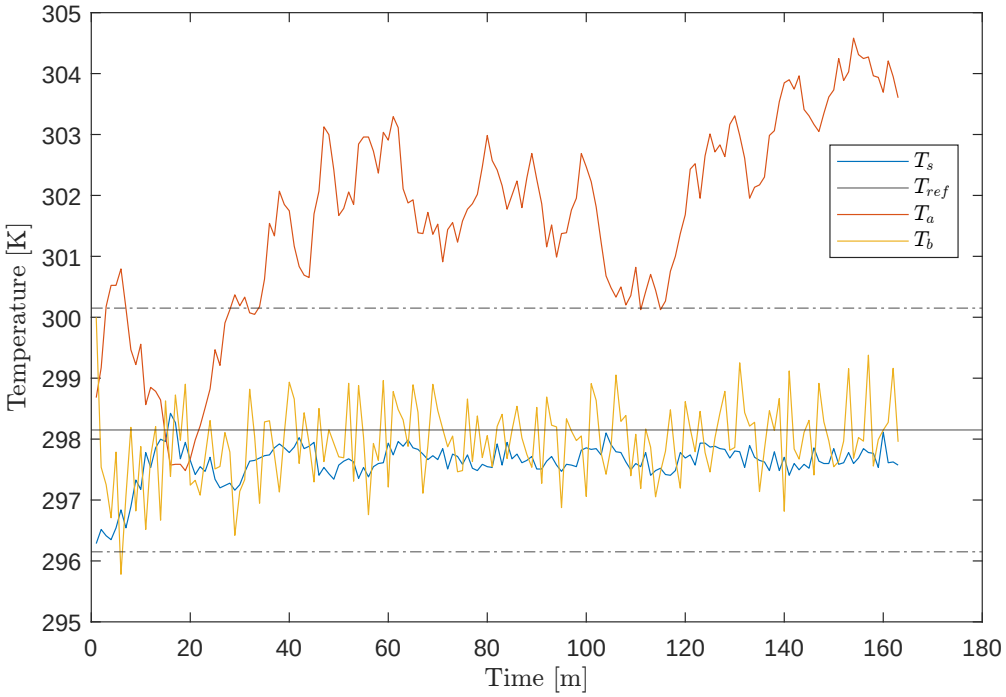

Figure 7.1: Temperature results from test no. 1 with Mosegaarden LQG.

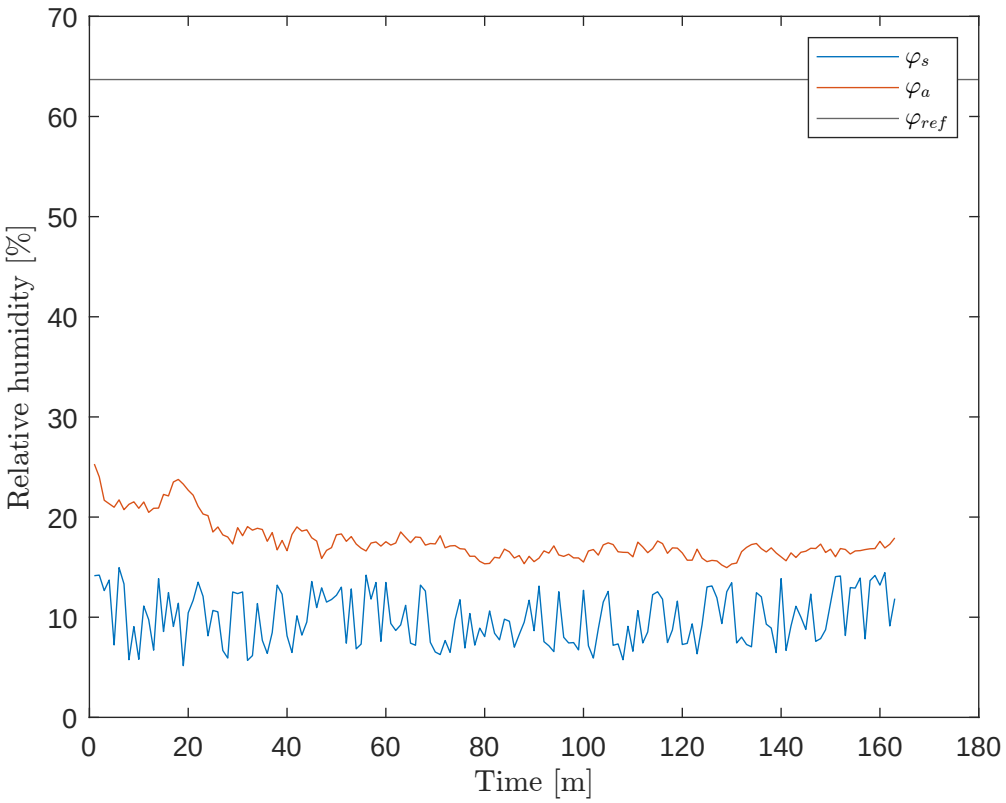

Figure 7.2: Humidity results from test no. 1 with Mosegaarden LQG.

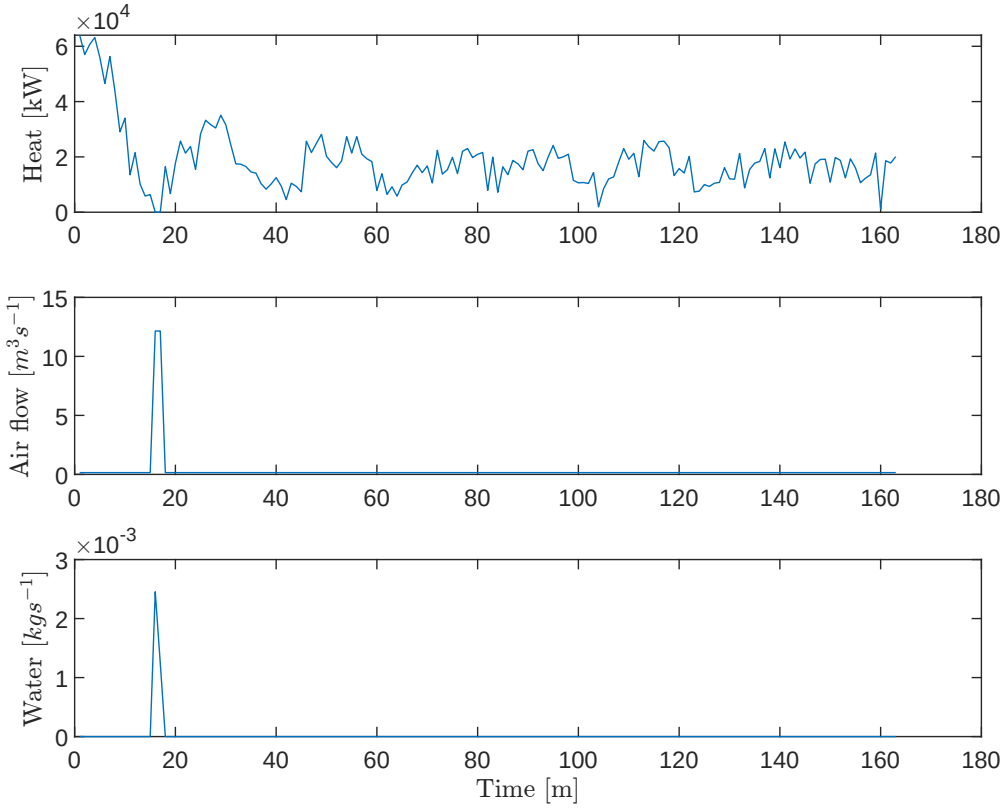

Figure 7.3: Inputs from test no. 1 with Mosegaarden LQG.

7.2.2 Test No. 2 - SKOV Laboratory LQG with 33 °C reference

In this test a controller designed for the laboratory at SKOV was utilised. The design was done by firstly conducting a new parameter estimation based on data from the laboratory, followed by the tuning of the EKF and finally the tuning of the LQR. This process is described in detail in Appendix D.

To test the reaction time of the new controller together with its stability a script in Matlab were programmed to automatically change the reference temperature between 33 °C and 17 °C. The change would happen 30 min after T_s first hits the current reference giving the controller time to stabilise. The two references were chosen from Table 2.1. Since the time it takes to reach the reference points currently are unknown, the test will run for a undetermined number of cycles.

Note that, between this test and test no. 1 it was noticed that the DA 820 chimneys would turn off if the pressure difference between the laboratory and the outside became to great. A limit of $9\,\mathrm{m^3\,s^{-1}}$ has therefore been implemented for this test. Furthermore a minimum ventilation of $0.15\,\mathrm{m^3\,s^{-1}}$ were added to ensure that heated air from the corridor would move into the laboratory.

Additionally the humidity reference was lowered to keep the controller from spraying too much water, lowering the temperature.

The results for the test are plotted in Figure 7.4, 7.5 and 7.6.

The test was stopped prematurely as it was noticed that even after passing the reference temperature, the input to the system was still the maximum allowed heating input. This could be due to the controller not taking the error over time into account.

Furthermore the safety switch of the 9 kW fan heaters were noticed to have been activated, properly during a previous test. The safety switch would activate if the fan were suddenly turned off while the heating element were at maximum. Thereafter only the fans would turn on, not the heating elements.

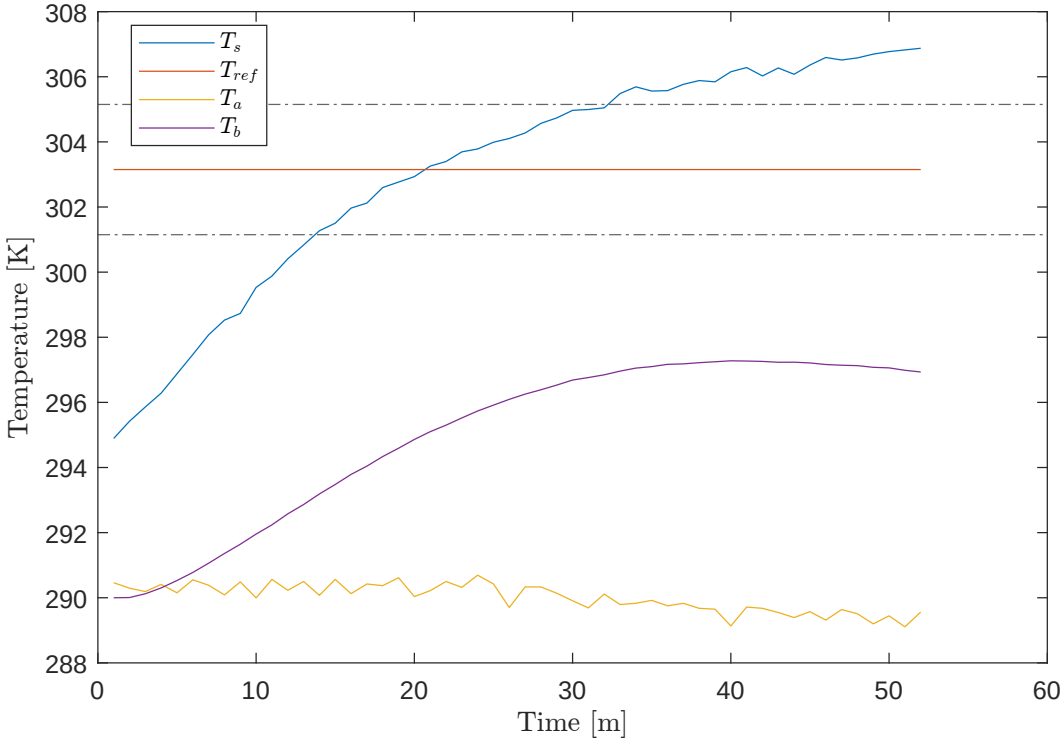

Figure 7.4: Temperature results from test no. 2 with SKOV laboratory LQG and reference of 33 °C.

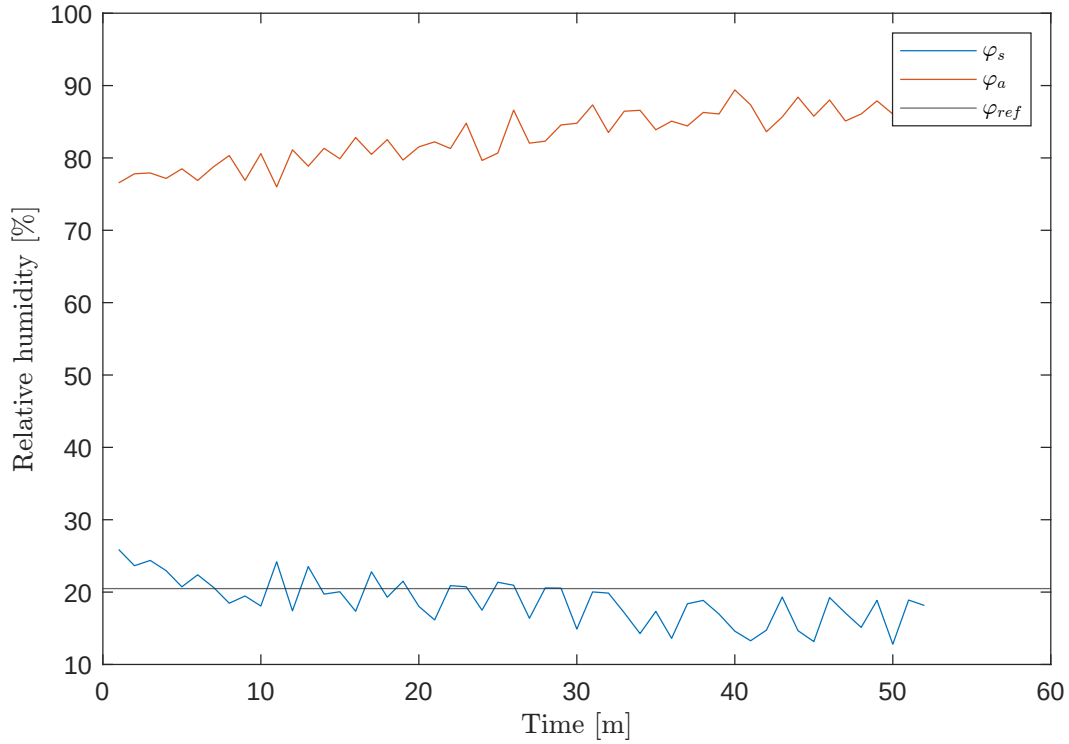

Figure 7.5: Humidity results from test no. 2 with SKOV laboratory LQG and reference of 33 °C.

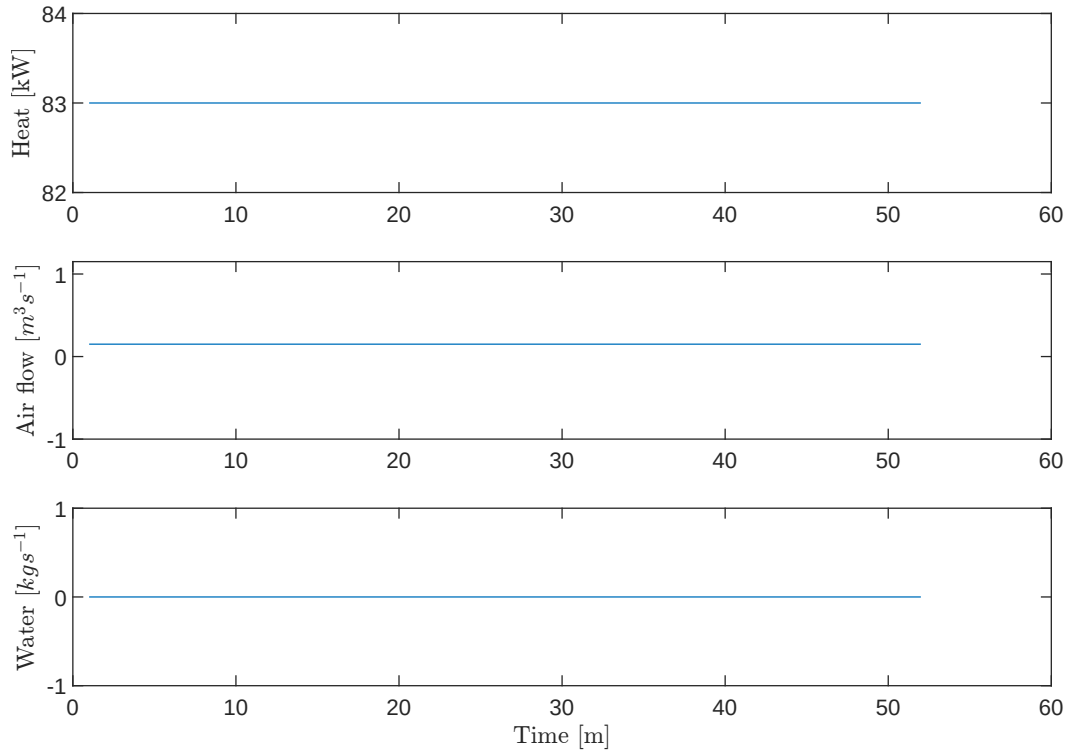

Figure 7.6: Inputs from test no. 2 with SKOV laboratory LQG and reference of 33 °C.

7.2.3 Test No. 3 - SKOV Laboratory LQG with 17 °C reference

In test no. 3 the same controller and test setup as for test no. 2 were utilised, only changing the reference temperature to 17 °C. The result are plotted in Figure 7.7, 7.8 and 7.9.

Like test no. 2, this test was stopped prematurely as it was noticed that the temperature T_s was slowly stabilising at a bias of about 3.6 K.

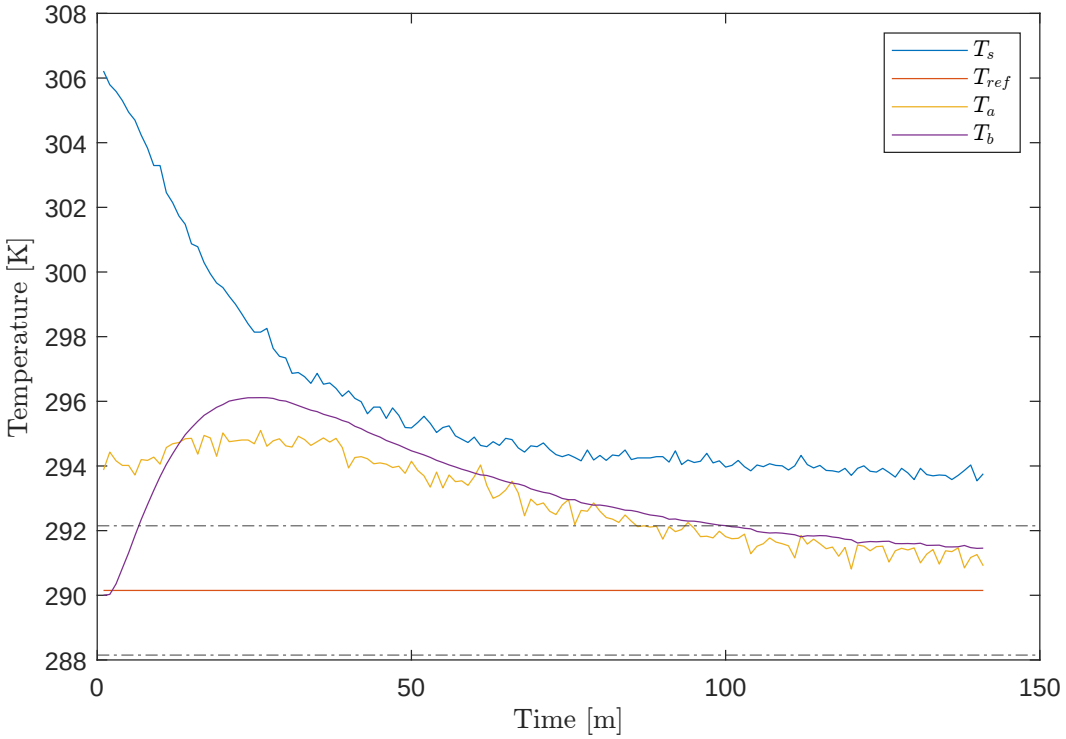

Figure 7.7: Temperature results from test no. 3 with SKOV laboratory LQG and reference of 17 °C.

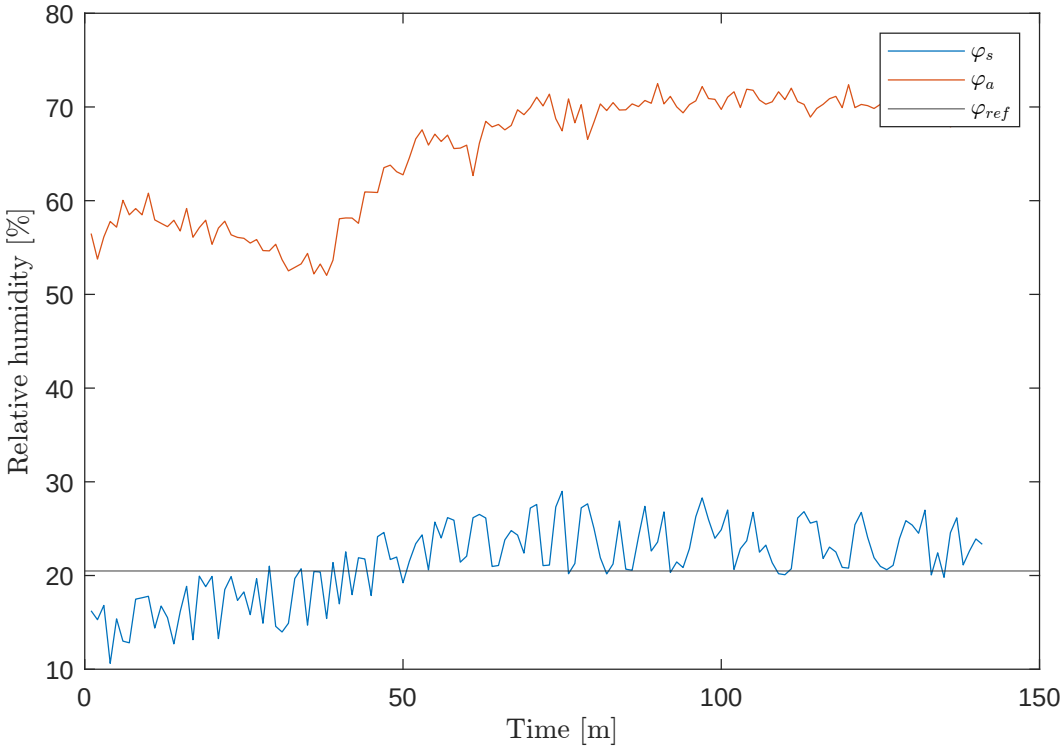

Figure 7.8: Humidity results from test no. 3 with SKOV laboratory LQG and reference of 17 °C.

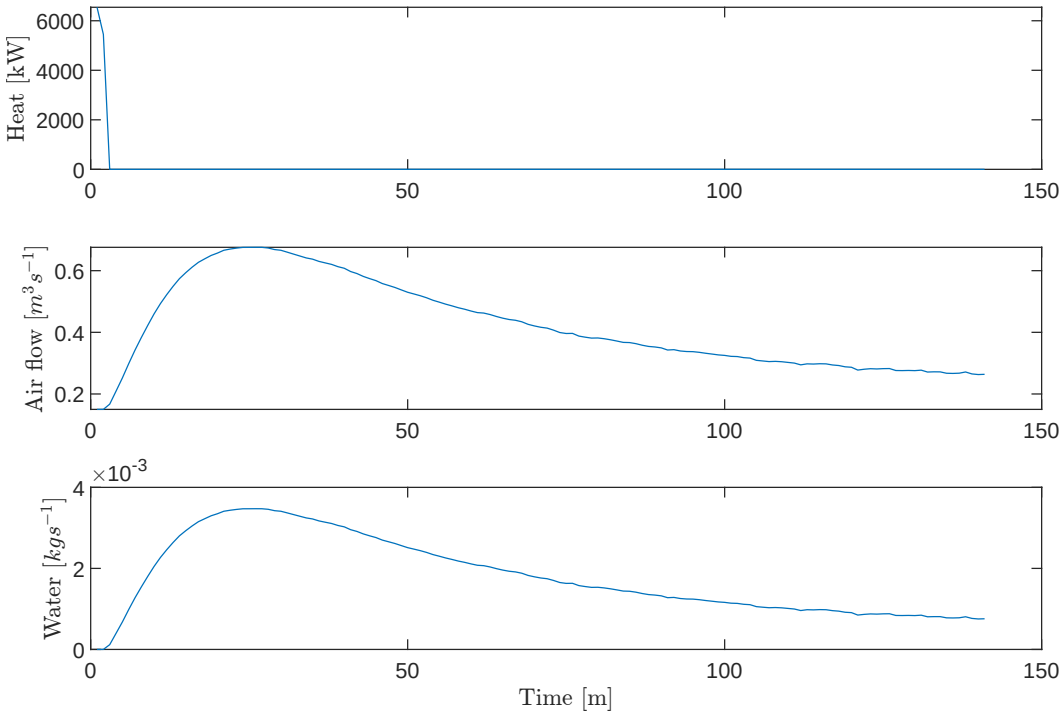

Figure 7.9: Inputs from test no. 3 with SKOV laboratory LQG and reference of 17 °C.

7.2.4 Test No. 4 - SKOV Laboratory LQI with 25 °C reference

Based on the results from test no. 2 and no. 3 it was decided to implement a integral with the LQR creating an LQI. The general design can be found in section 6.5 and tuning for the SKOV laboratory in Appendix D. The result of the test is plotted in Figure 7.10, 7.11 and 7.12.

Compared to the first three test, the new LQI performed better and the bias was eliminated. In Figure 7.10 it is seen that the temperature T_s follows the reference well keeping just below it, while staying inside the margin of error. The humidity is furthermore keeping to the reference in Figure 7.11.

However, looking at the inputs in Figure 7.12 it is seen that the controller is aggressively tuned for the spray. The spray is either on or off and shows a bang-bang type performance. When the error in temperature T_s is small and the humidity is below reference, the spray turns on, before turning off again in the next timestep, where the temperature has been lowered and the humidity increased.

For the next test some tuning is required.

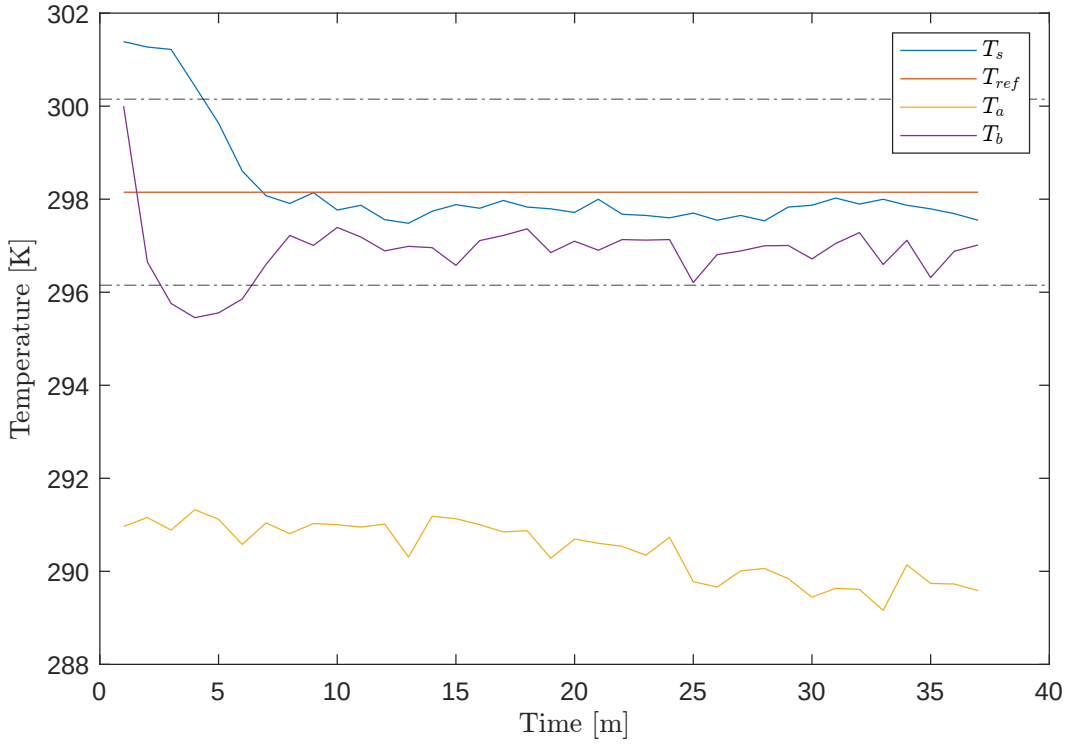

Figure 7.10: Temperature results from test no. 4 with SKOV laboratory LQI and reference of 25 °C.

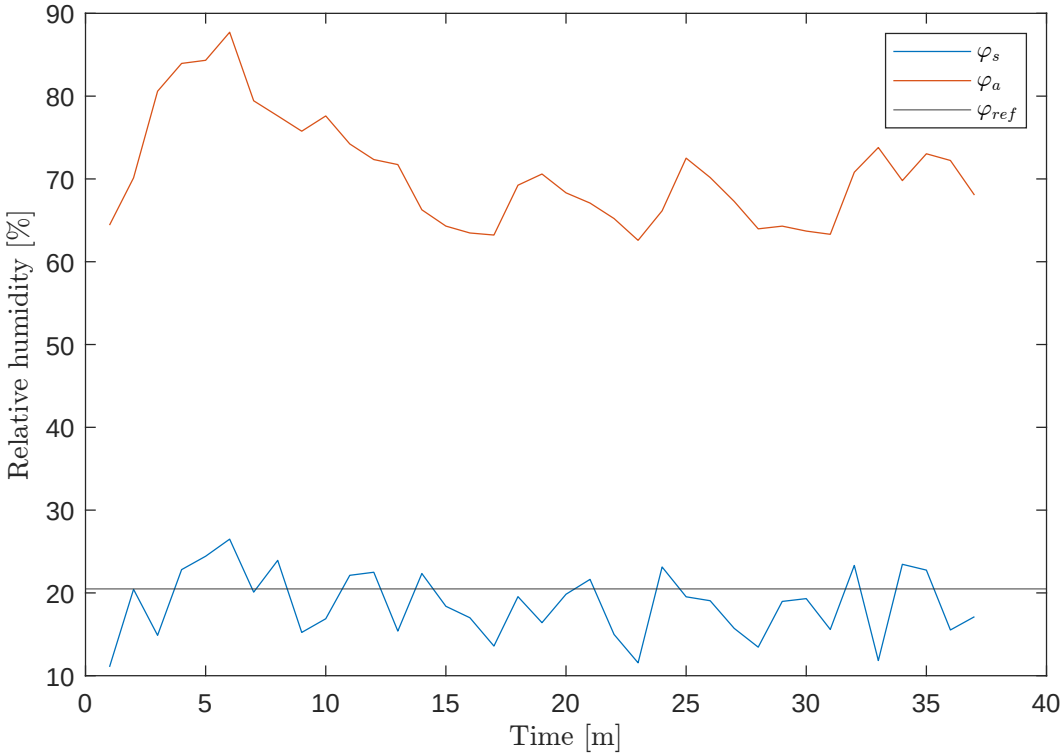

Figure 7.11: Humidity results from test no. 4 with SKOV laboratory LQI and reference of 25 °C.

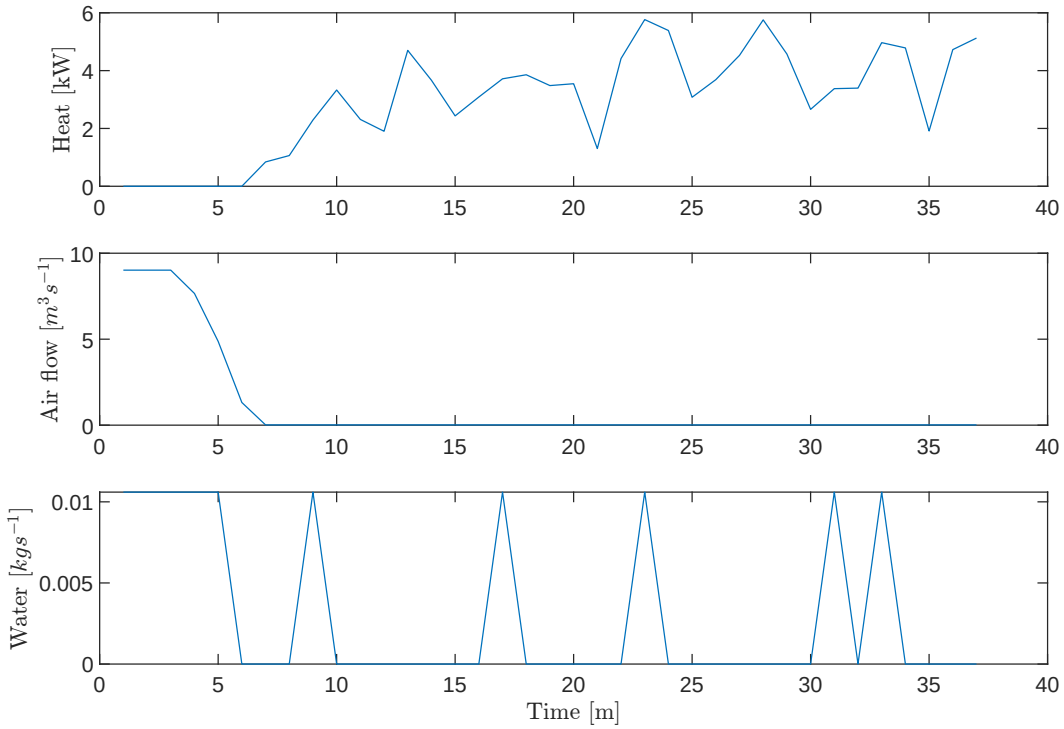

Figure 7.12: Inputs from test no. 4 with SKOV laboratory LQI and reference of 25 °C.

7.2.5 Test No. 5 - SKOV Laboratory LQI with 17 °C reference

In an effort to make the LQI less aggressive the heater input was changed from being in watts to being in kilowatts. Thereby the R matrix where changed to

$$R = \begin{bmatrix} 1.49 \cdot 10^{-3} & 0 & 0 \\ 0 & 0.00690 & 0 \\ 0 & 0 & 9.07 \cdot 10^{3} \end{bmatrix}. \tag{7.6}$$

Now the weight for the spray and heater had the same scale. The test was then run with the temperature reference set at 17 °C. The results for the test are plotted in Figure 7.13, 7.14 and 7.15.

The test was stopped prematurely as the temperature began to settle around 21 °C, while the spray input and ventilation gradually was lowered. But an important takeaway from this test is that the controller managed to get the temperature T_s below the outside temperature T_a for the first time.

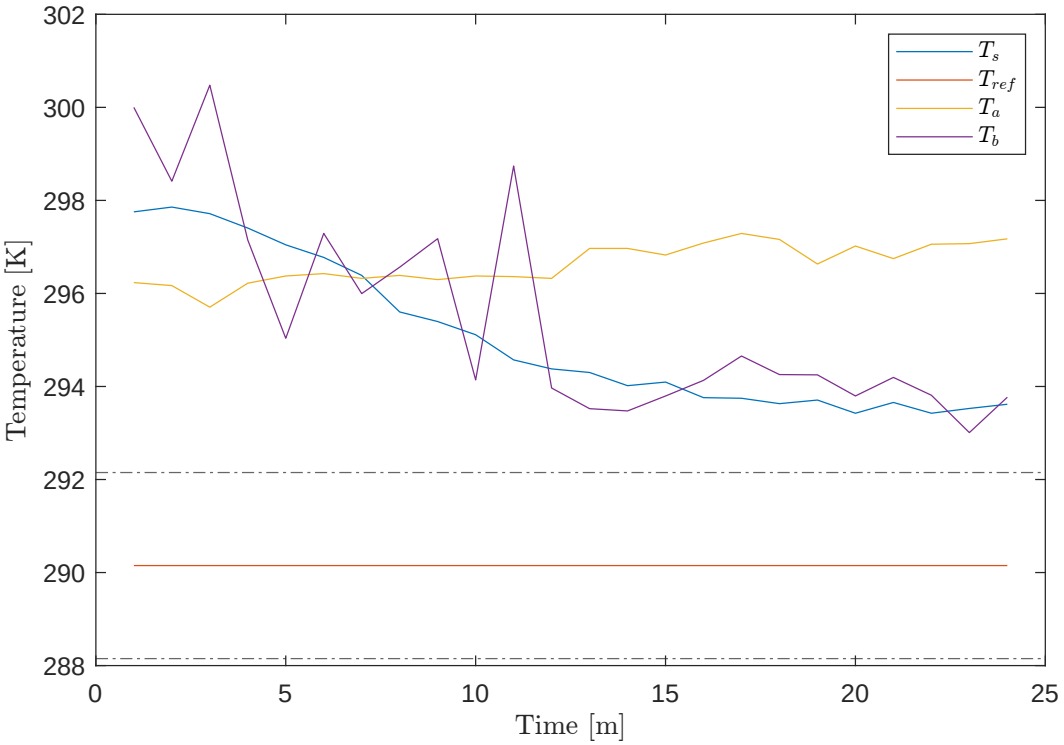

Figure 7.13: Temperature results from test no. 5 with SKOV laboratory LQI and reference of 17 °C.

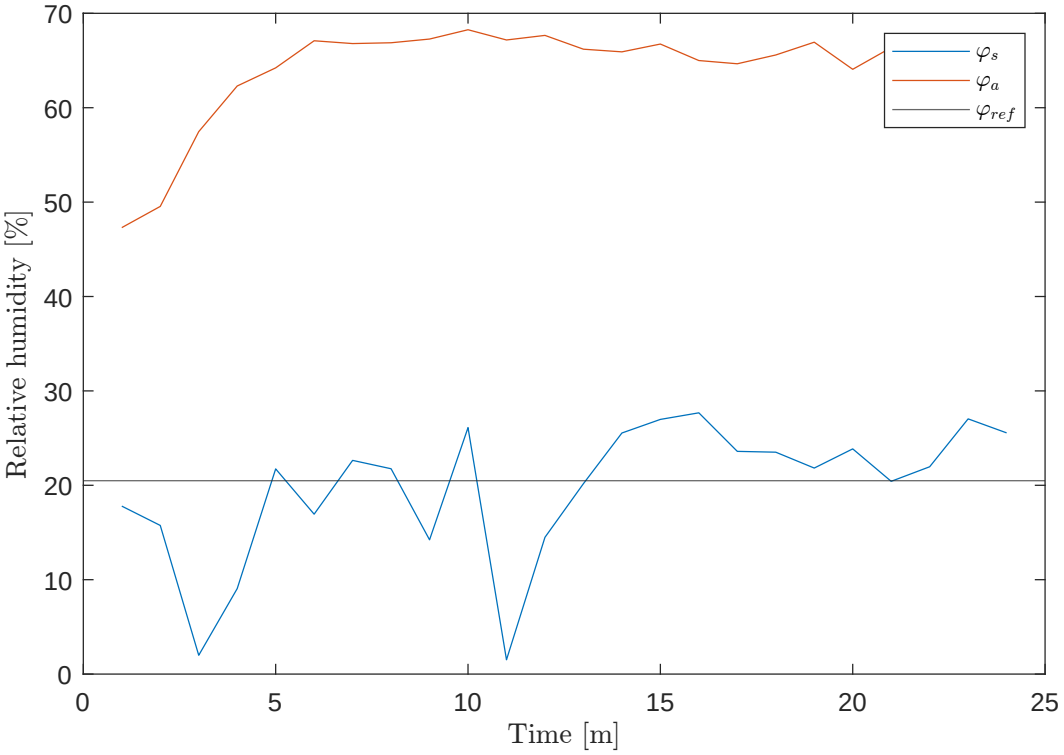

Figure 7.14: Humidity results from test no. 5 with SKOV laboratory LQI and reference of 17 °C.

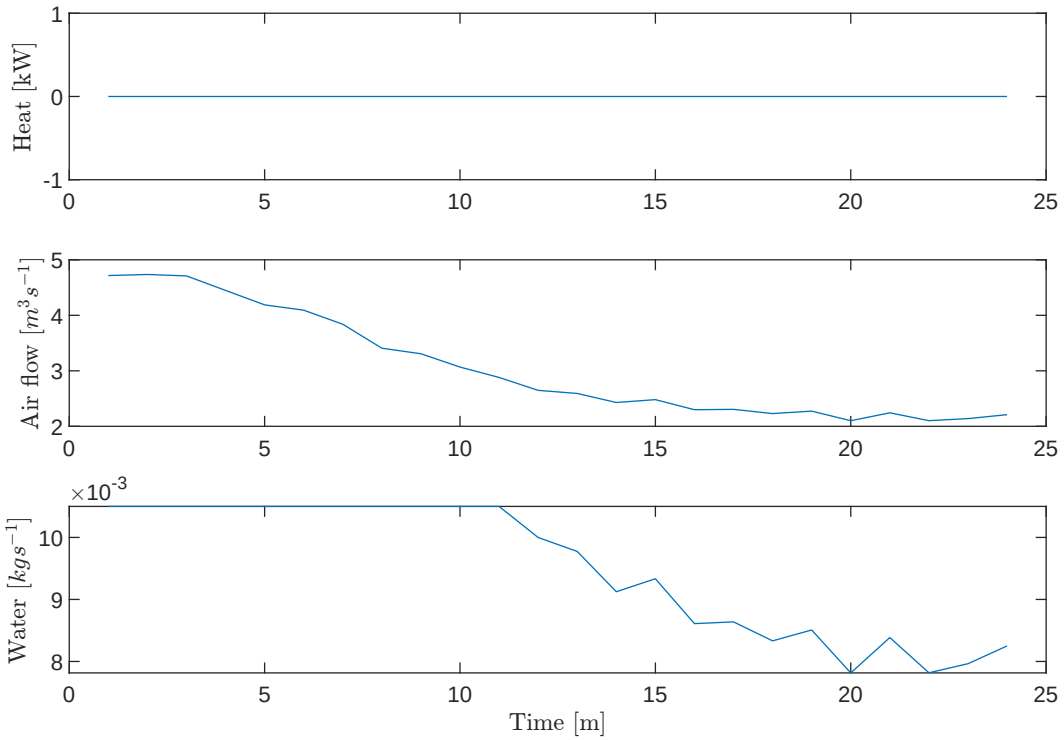

Figure 7.15: Inputs from test no. 5 with SKOV laboratory LQI and reference of 17 °C.

7.2.6 Test No. 6 - LQI test with chicken disturbance

The purpose of this test was to see how the LQI would handle sudden change in reference together with disturbance rejection. The disturbance in this case being the six 1401 W floor heating elements simulating the heat output from poultry. The results of the test is plotted in Figure 7.16, 7.17 and 7.18.

In Figure 7.16 it can be seen that the LQI keeps the temperature T_s close to reference inside the margin of error with a 1.08 K offset, and reacts as expected when the reference is changed from 26 °C to 20 °C.

Furthermore the LQI reacts to the changes in temperature T_s caused by the poultry simulation being turned off and then on again. In Figure 7.18 it is seen that the water spray input is decreased when the poultry is deactivated, and again slightly increased when the poultry is activated.

Additionally, the humidity in Figure 7.17 keeps to reference.

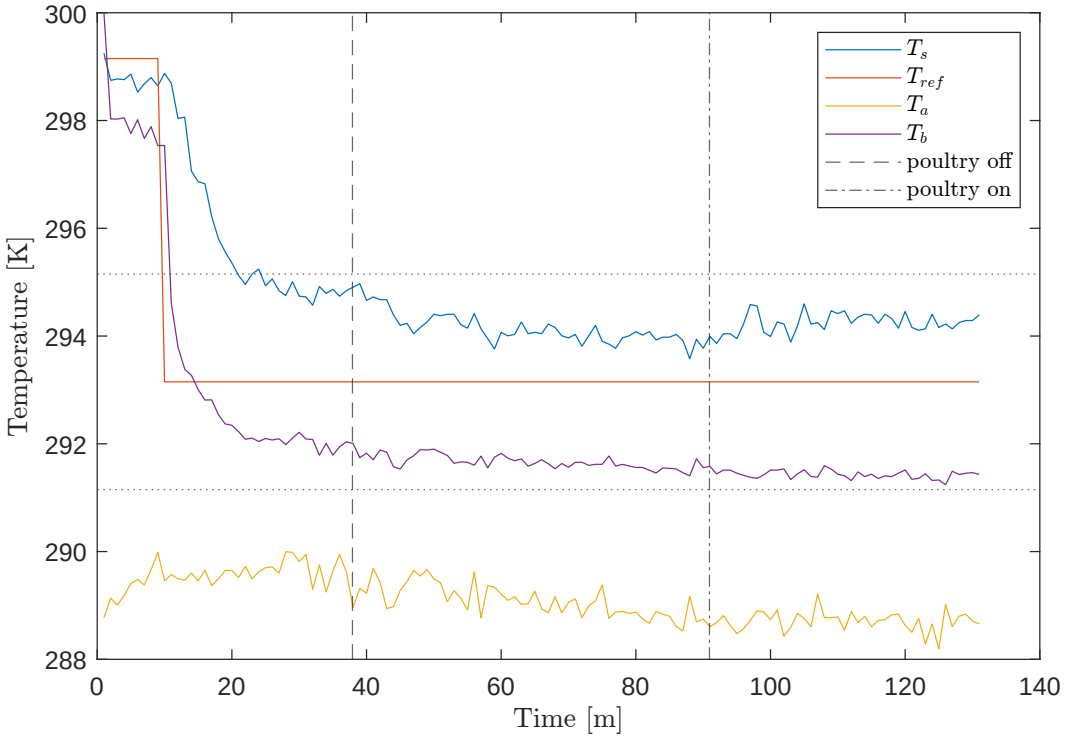

Figure 7.16: Temperature results from test no. 6 with SKOV laboratory LQI with disturbances.

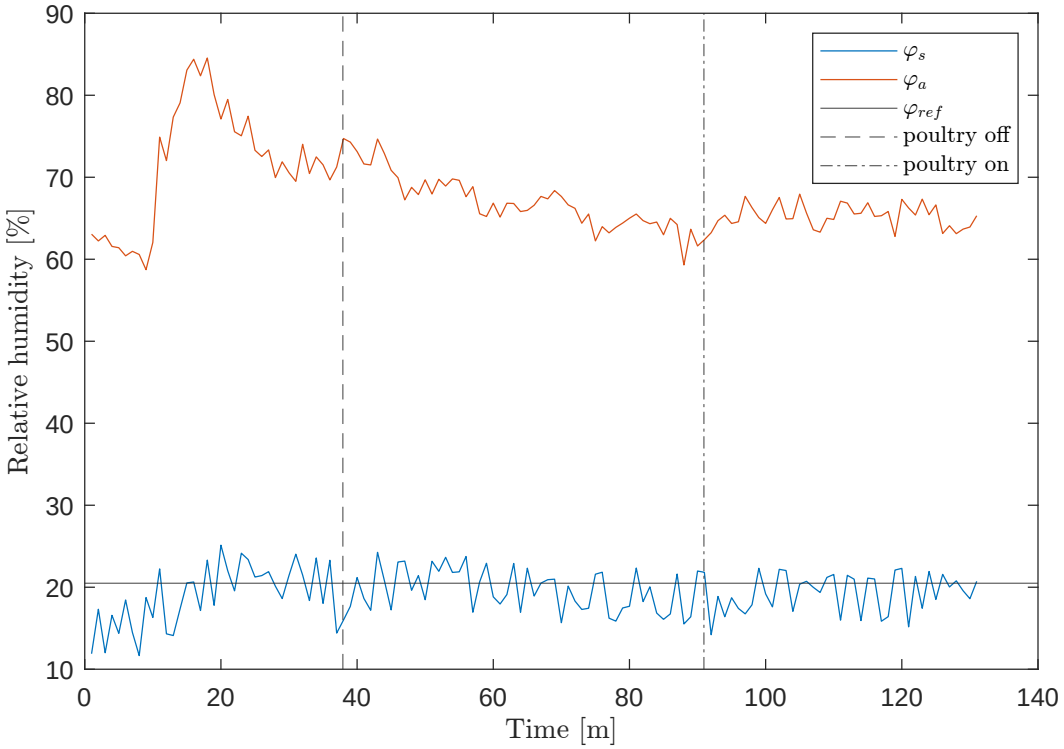

Figure 7.17: Humidity results from test no. 6 with SKOV laboratory LQI with disturbances.

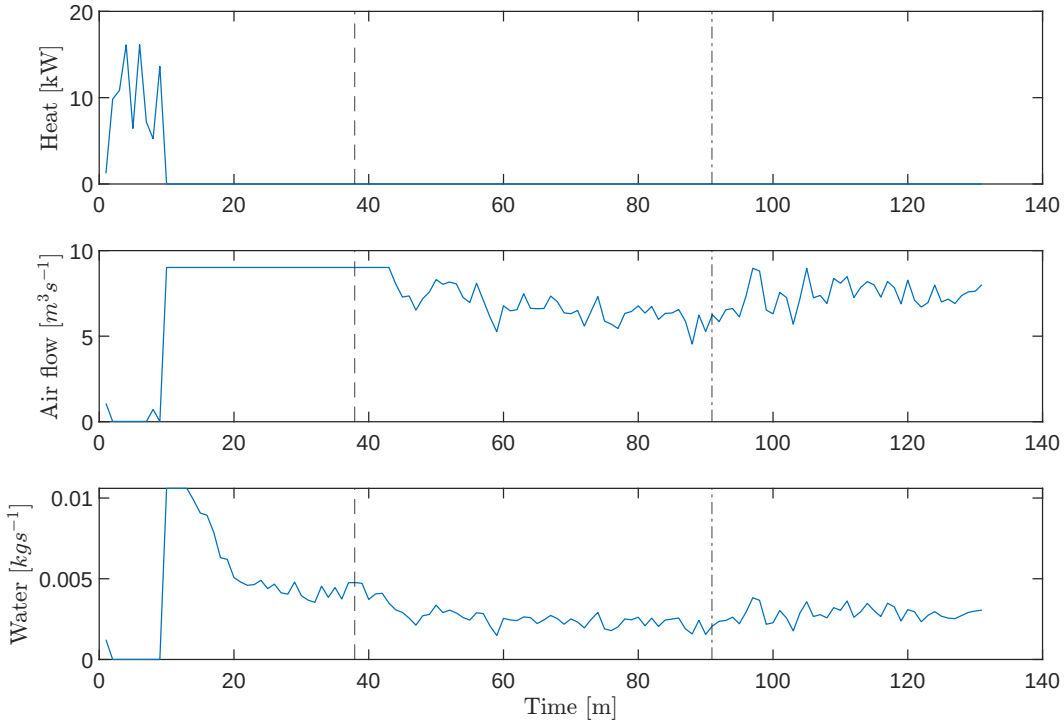

Figure 7.18: Inputs from test no. 6 with SKOV laboratory LQI with disturbances.

7.2.7 Test No. 7 - SKOV Laboratory LQI with 25 °C reference

Before this test was started the safety in the 55 kW heating element was activated and could not be deactivated again. Therefore some changes needed to be made. The maximum heat input for the LQI was changed to that of the three 9 kW fan heaters given a maximum heat input of 27 kW. This required the R matrix to be changed to

$$R = \begin{bmatrix} 1 \cdot 10^{-2} & 0 & 0 \\ 0 & 0.5 & 0 \\ 0 & 0 & 170 \end{bmatrix}. \tag{7.7}$$

Furthermore, the secondary ventilator described in subsection 7.1.2 was turned off, since the 55 kW heater no longer required the extra air flow.

This test was performed remotely. Therefore the poultry disturbance was not activated as it required a person to turn on breakers inside the laboratory. The results for the test is plotted in Figure 7.19, 7.20 and 7.21.

In Figure 7.19 the best results yet is seen. The temperature is at reference inside the margin of error with a bias of -0.23 K offset and the same goes for the humidity in Figure 7.20. Furthermore looking at the inputs in Figure 7.21 it is seen how all inputs are dynamically utilised in controlling the temperature and humidity inside the laboratory.

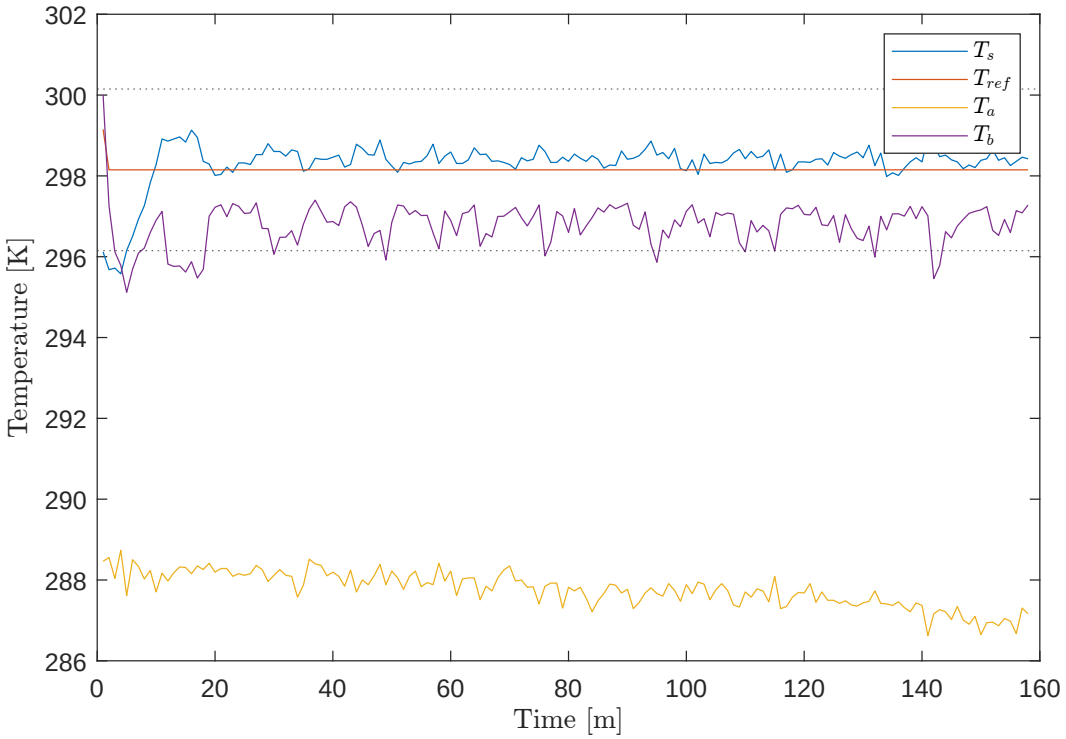

Figure 7.19: Temperature results from test no. 7 with SKOV laboratory LQI and reference 25 °C.

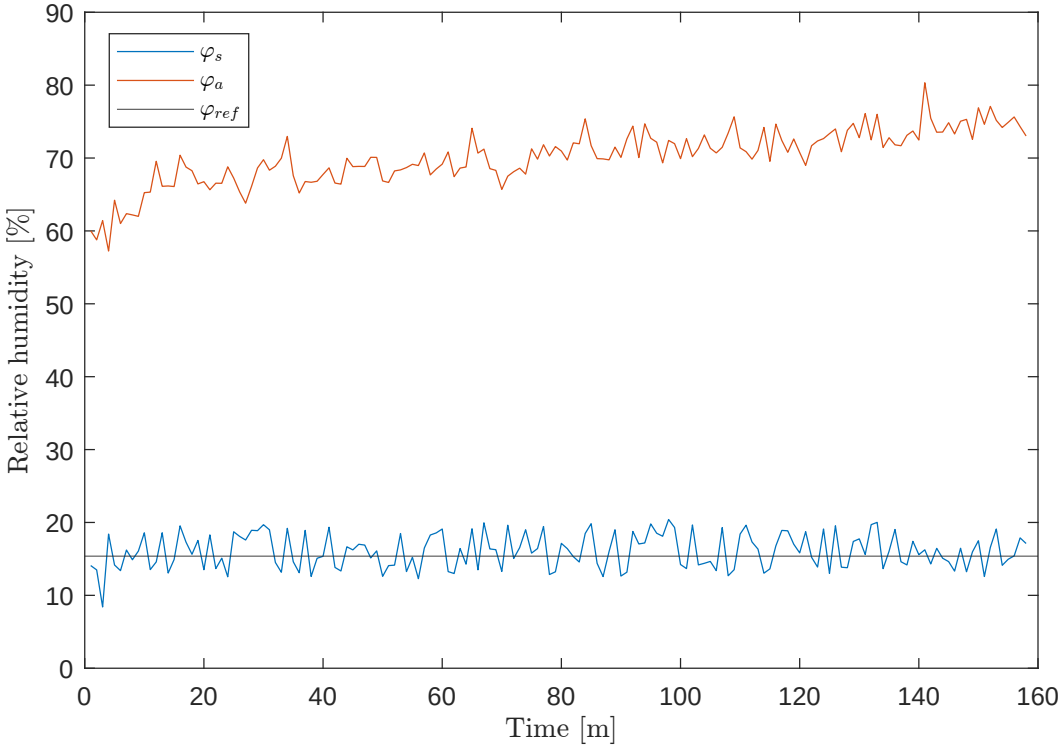

Figure 7.20: Humidity results from test no. 7 with SKOV laboratory LQI and reference 25 °C.

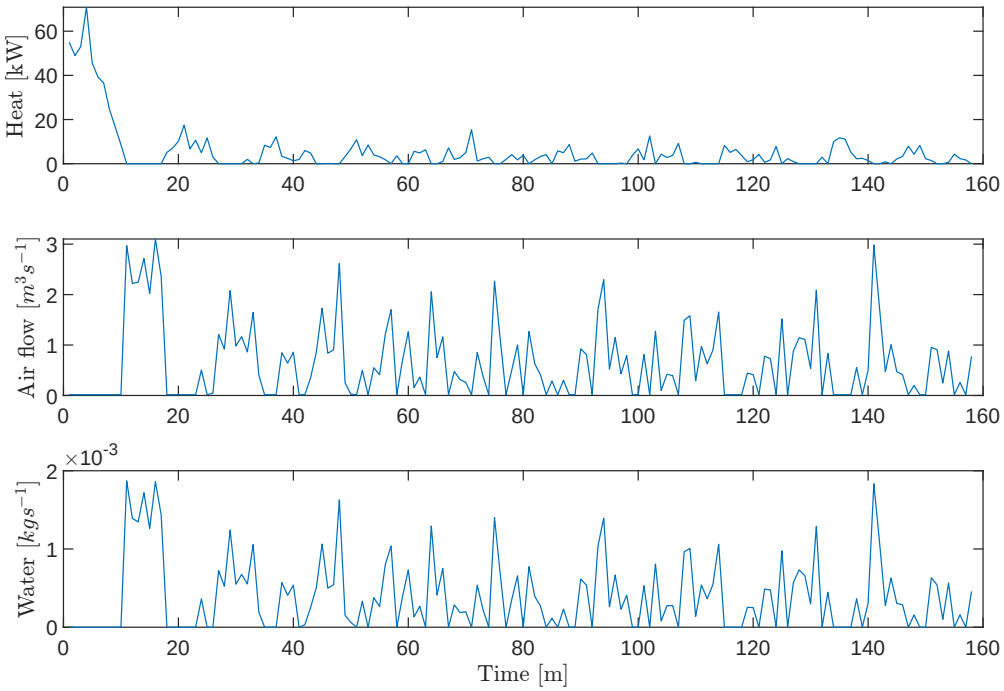

Figure 7.21: Inputs from test no. 7 with SKOV laboratory LQI and reference 25 °C.

With all the performed test presented the combined results will further be discussed in chapter 8.

Part IV

Discussion & Conclusion

Chapter 8

Discussion

In this chapter the discussion of some of the problems and decisions during the project is presented. The subjects are

- Exclusion of the Archimedes Number from the final model in section 8.1,
- Model Shortcomings in section 8.2,
- Problems during testing at SKOV in section 8.3,
- Comparison between the controllers tested at SKOV A/S in section 8.4,
- Alternative Control Strategies in section 8.5

8.1 Exclusion of the Archimedes Number from the final model

The expression for the corrected Archimedes number Ar_c derived in Equation 3.1 in section 3.1 was not included in the final state space model.

This was due to the fact, that the final problem statement defined that the temperature T_s would be the focus of this report.

Therefore the control of the position of the DA 1211 flaps described in subsection 2.5.1 was not included in the controller. Instead the flaps were adjusted to a constant position. This might have affected air resistance, which the model then did not account for.

8.2 Model Shortcomings

The model did not include the humidity produced by the bedding in the production house as mentioned in section 4.5. This did however not affect the test at SKOV Air Physical Laboratory, since the vapour produced by either poultry or bedding were not simulated.

8.3 Problems during testing at SKOV

In this section some of the problems and challenge encountered when testing at SKOV Air Physical Laboratory and the effect they had on the test results are described.

8.3.1 Placement of the 55 kW fan heater

The 55 kW fan heater was not located inside the laboratory as expected but rather in continuation with the ventilation system. Only two configurations for the heater were possible, either air from the outside or air pumped out of the laboratory were circulated through the fan heater and into the laboratory.

The controller in chapter 6 was designed to use the ventilation as a cooling factor by pumping out the water vapour or pumping in colder air from the outside. Therefore the configuration pulling air from the outside through the fan heater was the best option. Otherwise the water vapour would have kept being recirculated into the laboratory until saturation was reached.

This configuration caused another problem. If any heat was to enter the laboratory during heating an air flow was needed through the fan heater. Since the controller would turn ventilation down to the minimum ventilation of $0.15\,\mathrm{m^3\,s^{-1}}$ during heating, a second ventilator was required keeping an constant airflow. Thereby air from the outside entered the laboratory, when it was not supposed to.

These factors affected the controllers ability to keep the temperature T_s at reference. This is seen in test no. 7 in subsection 7.2.7. Before this test the 55 kW fan heater shut down. Therefore the controller was set to only use the three 9 kW fan heaters located inside the laboratory, while the second ventilator was turned off. With these disturbances removed, the best results were seen during this test.

8.3.2 DOL 114 in the sun

During test no. 1 in subsection 7.2.1 it was noticed that the sun was hitting the DOL 114 sensor, thereby measuring a temperature of 31 °C. Fortunately this problem was easy to mitigate by provide shade for the sensor.

It should though be mentioned, that the temperature T_b is greatly affected by the temperature T_a, which the controller expects will affect T_s. Therefore the results for test no. 1 showing the temperature T_s being close to reference might be caused by the controller reducing the heat input to counteract the increased outside temperature.

8.3.3 Placement of the Air Physical Laboratory inside a building

The model for the system was designed with three temperature zones. The outside temperature T_a, the temperature of the wall T_b and the temperature inside the laboratory / production house T_s.

The laboratory however was not located directly outside, but were constructed inside another building, and was thereby not in direct contact with the outside air.

However, since the parameter l_{hb} in Equation 4.6 describing the heat transfer between the wall and laboratory air was estimated based on data from the laboratory, the building the laboratory was placed inside could be viewed as part of the wall.

Bear in mind, that the building was heated, which the controller did not account for.

8.3.4 Power outage prevented further testing

It was planned to carry out further testing remotely during the weekend after test no. 7 in subsection 7.2.7. Unfortunately the computer running the test died due to a power outage. Since it was the weekend no personal was on site to help mitigate this issue. Therefore no further experiments could be carried out.

8.4 Comparison between the controllers tested at SKOV A/S

In this section the error between the reference and temperature T_s for test no. 1, 3 and 7 in subsection 7.2.1, 7.2.3 and 7.2.7 respectively, is plotted in Figure 8.1.

It can be seen that the LQG controller tuned for the laboratory performed worse than the controller tuned for Mosegaarden. However the advantage of the introduction of an integral

is clearly seen as it reduces the error to generally being lower than the Mosegaarden LQG.

However low error seen for the Mosegaarden might be caused by the sun hitting the sensor during the test as mentioned in subsection 8.3.2. This is not the case with the LQI from test no 7.

Therefore it can be concluded that the LQI was the best performing controller among the ones tested in the Air Physical Laboratory.

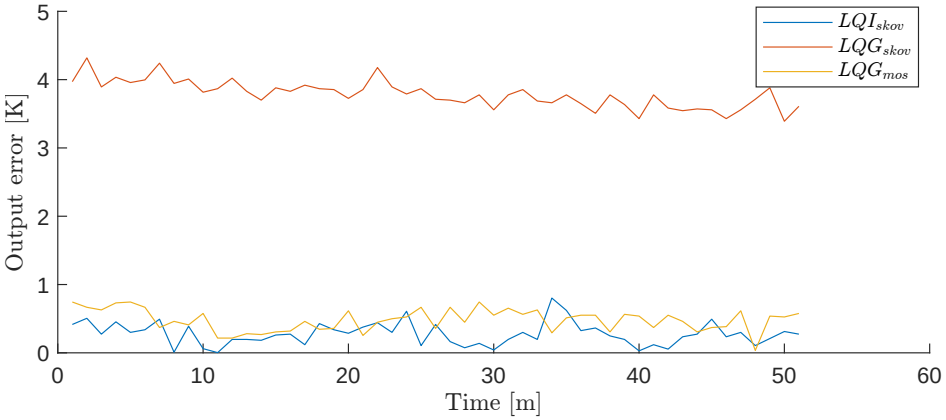

Figure 8.1: Output error for T_s from test no. 1, 3 and 7 in subsection 7.2.1, 7.2.3 and 7.2.7 respectively.

8.5 Alternative Control Strategies

A concern for the LQI is its ability to handle saturation of the actuators. While clamping was used in this project to disable the integrator it was not investigated how this affect controller performance. As design of atiwindup for MIMO system is not trivial to do.

Model Predictive Control was considered as an alternative control strategy with simpler constraint implementation. In short terms it works by predicting the future states given some inputs. Here actuator constraints can be included, when the MPC tries to minimise the inputs required to reach a reference. The MPC is furthermore capable of including disturbance predictions into its state predictions

Unfortunately the MPC strategy was not viable at the time of this project. It requires a lot of tuning, and since no data was available from the Air Physical Laboratory before the testing began, it would not have been possible to tune the MPC and thoroughly test it in the short time given.

However, given that the MPC can predict future states, while including the disturbances it would possibly perform better than the LQI. Looking at the problem with the light schedule affecting the heat or weather forecast, the LQI is only able to react to these changes when they happen. The MPC would on the other hand be able to predict the changes and adjust its actuator inputs accordingly.

For future work it is therefore recommended to explore the possibility of implementing a MPC.

Chapter 9

Conclusion

In this project is was attempted to design a MIMO controller for a livestock production house with a focus on poultry.

Based on the findings in the problem analysis, the problem statement was in section 2.7 defined as:

"How can a MIMO climate controller for a poultry production house be designed, which keeps the internal temperature at a reference between 17 ℃–33 ℃ *with a maximum deviation of* 2 ℃*."*

A physics based model was derived for the mass and energy balance of a livestock production house. Parameter estimation was performed for the model using data from both Mosegaarden production house and the Air Physical laboratory. In both cases the model was shown to fit real data in open loop simulation.

For MIMO control it was chosen to design a Linear Quadratic Regulator (LQR) in combination with an Extended Kalman Filter (EKF) as observer and a integral to keep track of the error. The EKF was tuned for both Mosegaarden and the Air Physical Laboratory. In both cases it was shown that the EKF was capable of tracking both the hidden and non-hidden states accurately.

The non-linear continuous model was linearised and discritised for use in the EKF and LQR/LQI. The LQG/LQI was simulated with data from Mosegaarden where in both cases the performance was acceptable. Furthermore the LQG/LQI was adjusted and tuned to fit the Air Physical Laboratory located at SKOV A/S Glyngøre, where the testing was carried out.

In test no. 7 in subsection 7.2.7 is was shown that the LQI was able to keep the internal temperature T_s at the reference temperature inside the 2 °C margin of error. The result is plotted in Figure 9.1.

The LQG tuned for a data set from Mosegaarden production house and the LQG tuned for the Air Physical Laboratory were also implemented and tested at SKOV A/S. Both controllers performed worse than the LQI.

A block diagram of the final EKF and LQI can be found in Figure 9.2.

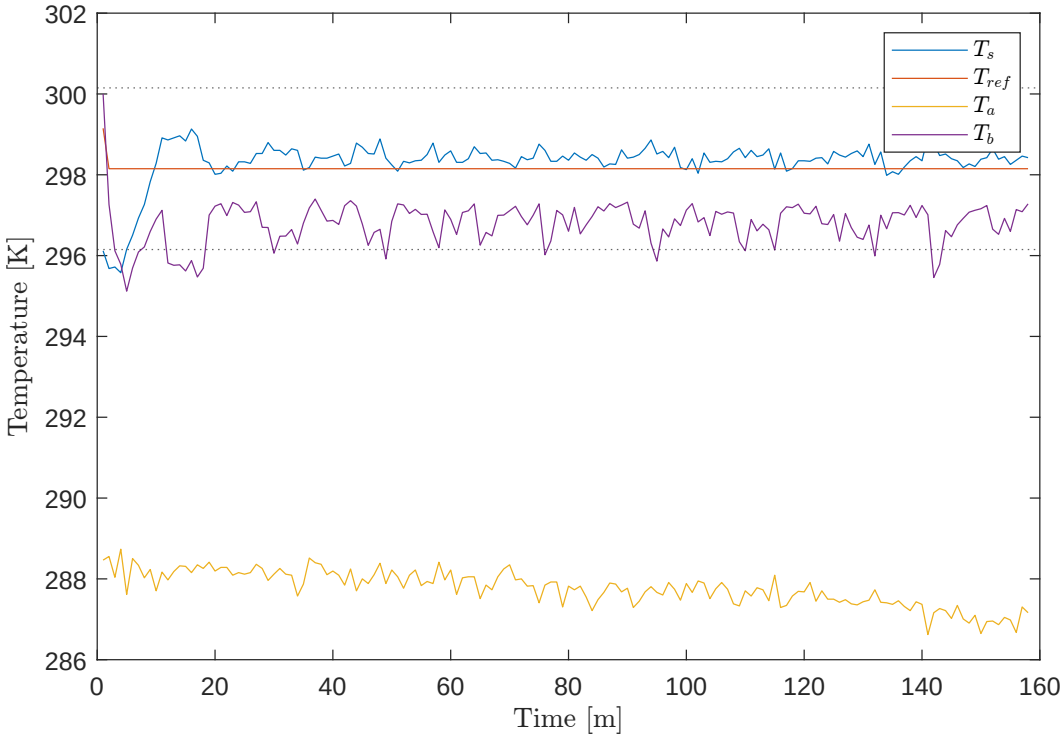

Figure 9.1: Temperature results from test no. 7 with SKOV laboratory LQI and reference 25 °C. Replica of Figure 7.19.

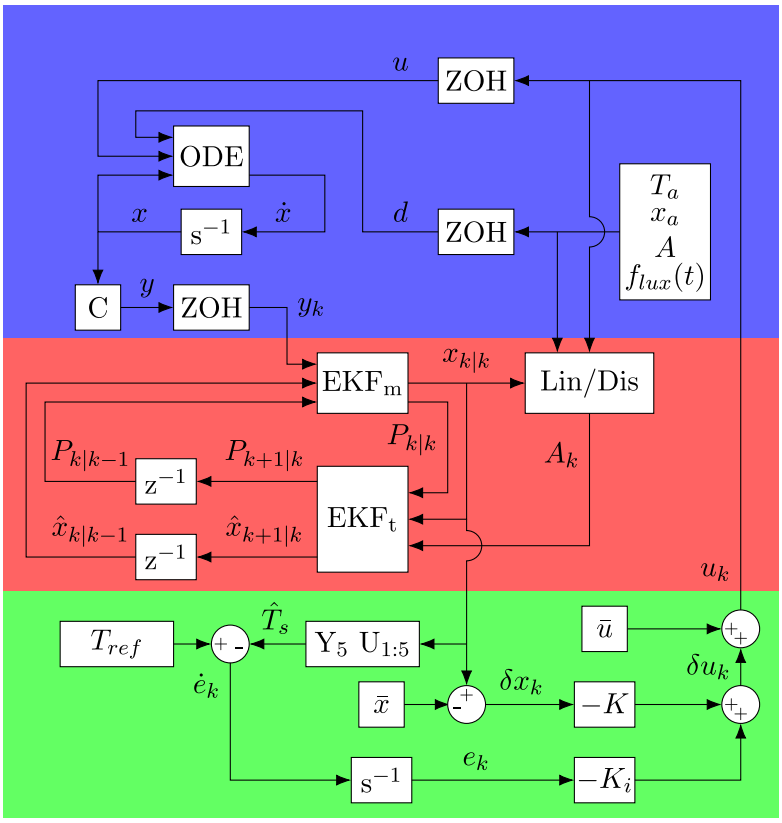

Figure 9.2: Block Diagram over the EKF, LQI and simulation setup used at SKOV A/S.

Bibliography

[1] Unknown, "Example domain," *http:// example.com/*, UNKOWN, last viewed: February 24th 2022.

[2] Food and Agriculture Organization of the United Nations, "Global agriculture towards 2050," https://www.fao.org/fileadmin/templates/wsfs/docs/Issues_papers/HLEF2050_Global_Agriculture.pdf, 2009, last visited: Martch 30th 2022.

[3] ——, "Crops and livestock products - statistics," https://www.fao.org/faostat/en/#data/QCL, last viewed: March 30th 2022.

[4] COMPASSION in world farming, "Do you live in a factory farm hotspot?" https://www.ciwf.org.uk/factory-farm-map/, last visited: Martch 30th 2022.

[5] Sentience Institute, "Us factory farming estimates," https://www.sentienceinstitute.org/us-factory-farming-estimates, 2019, last visited: Martch 30th 2022.

[6] H. Poulsen and S. Pedersen, *Klimateknik - ventilation, isolering og opvarmning*, 4th ed. Landbrugsforlaget, 2007.

[7] SKOV A/S, "Lpv system for poultry," https://www.skov.com/climate/poultry/lpv/, last viewed: April 29th 2022.

[8] ——, "Equal pressure system for poultry," https://www.skov.com/climate/poultry/equal-pressure/, last viewed: April 29th 2022.

[9] ——, "Tunnel system for poultry," https://www.skov.com/climate/poultry/tunnel/, last viewed: April 29th 2022.

[10] ——, "Combi-tunnel system for poultry," https://www.skov.com/climate/poultry/combi-tunnel/, last viewed: April 29th 2022.

[11] ——, "Skov systems for poultry," https://www.skov.com/climate/poultry/, last viewed: April 29th 2022.

[12] M. Hansen, P. D. Hansen, and S. B. Madsen, "Climate control for livestock stables," Master's thesis, Aalborg University, 2009.

[13] SKOV A/S, "Da 1211/1911 wall inlet," https://www.skov.com/products/air-inlet/da-1211-1911-wall-inlet/, last visited: April 8th 2022.

[14] ——, "Da 174 winch motor datasheet," Handed out by SKOV A/S, last visited: April 19th 2022.

[15] ——, "Da 600/820/920 chimney," https://www.skov.com/products/air-outlet/da-600-820-920-chimney/, last visited: April 14th 2022.

[16] ——, "Spiraflex," https://www.skov.com/products/heating/spiraflex/, last visited: April 14th 2022.

[17] ——, "Dol 114 temperature & humidity sensor," https://www.skov.com/products/climate-sensors/dol-114-temperature-and-humidity-sensor/, last visited: April 14th 2022.

[18] ——, "Dol 119 co2 sensor," https://www.skov.com/products/climate-sensors/dol-119-co2-sensor/, last visited: April 14th 2022.

[19] ——, "Dol 53 nh3 sensor," https://www.skov.com/products/climate-sensors/dol-53-ammonia-sensor/, last visited: April 14th 2022.

[20] ——, "Dol 16 light sensor," https://www.skov.com/products/climate-sensors/dol-16-light-sensor/, last visited: April 14th 2022.

[21] J. Vlachopoulos and V. Sidiropoulos, "Polymer film blowing: Modeling," in *Encyclopedia of Materials: Science and Technology*, K. J. Buschow, R. W. Cahn, M. C. Flemings, B. Ilschner, E. J. Kramer, S. Mahajan, and P. Veyssière, Eds. Oxford: Elsevier, 2001, pp. 7296–7301. [Online]. Available: https://www.sciencedirect.com/science/article/pii/B0080431526012997

[22] A. M. Alkhedhair, "Modelling and experimental study of spray cooling systems for inlet air pre-cooling in natural draft dry cooling towers," https://espace.library.uq.edu.au/view/UQ:373607/s4189716_phd_submission.pdf, 2015.

[23] J. Huang, "A simple accurate formula for calculating saturation vapor pressure of water and ice," *Journal of Applied Meteorology and Climatology*, vol. 57, no. 6, pp. 1265 – 1272, 2018.

[24] Engineering ToolBox, "Air - humidity ratio," https://www.engineeringtoolbox.com/humidity-ratio-air-d_686.html, 2004, last viewed: March 23th 2022.

[25] ——, "Reynolds number," https://www.engineeringtoolbox.com/reynolds-number-d_237.html, 2003, last viewed: April 29th 2022.

[26] ——, "Dimensionless numbers," https://www.engineeringtoolbox.com/dimensionless-number-quantity-symbol-application-d_1982.html, 2017, last viewed: April 29th 2022.

[27] "Reynolds number," https://www.oxfordreference.com/view/10.1093/acref/9780199233991.001.0001/acref-9780199233991-e-2654, 2009.

[28] C. Schaschke, "Schmidt number," https://www.oxfordreference.com/view/10.1093/acref/9780199651450.001.0001/acref-9780199651450-e-2565, 2014.

[29] J. S. Strøm, *Varmeafgivelse fra kvæg, svin og fjerkræ som grundlag for varmetekniske beregninger*, ser. SBI-landbrugsbyggeri. SBI forlag, 1978, no. 55.

[30] J.-M. Aerts, D. Berckmans, P. Saevels, J. Buyse, and E. Decuypere, "Quantification of the order dynamics of heat production response of broiler chickens to steps in temperature and light intensity," *Transactions of the American Society of Agricultural Engineers*, vol. 46, 01 2001.

[31] O. Brastein, D. Perera, C. Pfeifer, and N.-O. Skeie, "Parameter estimation for grey-box models of building thermal behaviour," *Energy and Buildings*, vol. 169, pp. 58–68, 2018. [Online]. Available: https://www.sciencedirect.com/science/article/pii/S0378778817331791

[32] Mathworks, "nlgreyest - estimate nonlinear grey-box model parameters," https://www.mathworks.com/help/ident/ref/iddata.nlgreyest.html?s_tid=doc_ta, last viewed: May 12, 2022.

[33] ——, "Loss function and model quality metrics," https://se.mathworks.com/help/ident/ug/model-quality-metrics.html, last viewed: May 2, 2022.

[34] ——, "nlgreyestoptions - option set for nlgreyest," https://se.mathworks.com/help/ident/ref/nlgreyestoptions.html?s_tid=doc_ta, last viewed: May 2, 2022.

[35] J. Nocedal and S. J. Wright, *Numerical Optimization*, 2nd ed. New York, NY, USA: Springer, 2006.

[36] M. Grewal and A. Andrews, "Kalman filtering: theory and practice using matlab," *New York: John Wiley and Sons*, vol. 14, 01 2001.

[37] A. Packard, K. Poolla, and R. Horowitz, *Dynamic Systems and Feedback*. Andrew Packard, 2002.

[38] Mathworks, "jacobian," https://se.mathworks.com/help/symbolic/sym.jacobian.html, last viewed: May 30, 2022.

[39] G. F. Franklin, J. D. Powell, and M. L. Workman, *Digital Control of Dynamic Systems*, 3rd ed. Addison-Wesley, 1998.

[40] N. Instruments, "Ni usb-6001 specifications," https://www.ni.com/pdf/manuals/374369a.pdf, last viewed: May 2, 2022.

[41] Mathworks, "Data acquisition toolbox," https://se.mathworks.com/help/daq/index.html, last viewed: May 18, 2022.

[42] ——, "Ni-daqmx support from data acquisition toolbox," https://se.mathworks.com/hardware-support/nidaqmx.html, last viewed: May 18, 2022.

Appendix A

Nomenclature

Table A.1: Notations introduced during Air Flow Model in section 3.1.

D_d	m	jet drop distance
Ar	·	Archimedes Number
Ar_c	·	corrected Archimedes Number
g	$\mathrm{m\,s^{-2}}$	gravitational acceleration
C_d	·	discharge coefficient
a	m	vertical dimension of the inlet
b	m	horizontal dimension of the inlet
W	m	width of the livestock production house
H	m	height of the livestock production house
T_s	K	livestock production house temperature
T_a	K	ambient temperature outside
$q_{inlet,i}$	$\mathrm{m^3\,s^{-1}}$	volumetric airflow through inlet no. i

Table A.2: Notations for flows introduced during Humidity & Temperature Models in section 3.2.

$w_{v,in}$	$\mathrm{kg\,s^{-1}}$	flow rate of water vapour into the production house
$w_{v,out}$	$\mathrm{kg\,s^{-1}}$	flow rate of water vapour out of the production house
$w_{evaporation}$	$\mathrm{kg\,s^{-1}}$	rate of water evaporating
$w_{livestock}$	$\mathrm{kg\,s^{-1}}$	rate of water vapour from the livestock
$w_{d,in}$	$\mathrm{kg\,s^{-1}}$	mass flow of dry air into the production house
$w_{d,out}$	$\mathrm{kg\,s^{-1}}$	mass flow of dry air out of the production house
w_a	$\mathrm{kg\,s^{-1}}$	flow rate of air into the production house

Table A.3: Notations for energy introduced during Humidity & Temperature Models in section 3.2.

U_s	J	internal energy inside the production house
Q_{in}	$\mathrm{J\,s^{-1}}$	heat transfer from the air outside to the production house air
Q_{out}	$\mathrm{J\,s^{-1}}$	heat transfer from the production house air to the outside air
Q_{evap}	$\mathrm{J\,s^{-1}}$	heat loss in production house air from water evaporation
Q_{heater}	$\mathrm{J\,s^{-1}}$	heat transfer from heater to production house air
Q_b	$\mathrm{J\,s^{-1}}$	heat transfer from the production house air to the production house walls
$Q_{sensible}$	$\mathrm{J\,s^{-1}}$	heat transfer from the broilers to the production house air

Table A.4: Notations for states introduced during Humidity & Temperature Models in section 3.2.

M_v	kg	mass of water vapour inside the production house
M_w	kg	mass of water inside the production house
$T_{sh,out}$	K	temperature of the water exiting the heater
T_b	K	temperature of the production house walls
T_s	K	temperature of air in the production house (aka. the stable)

Table A.5: Notations for inputs introduced during Humidity & Temperature Models in section 3.2.

w_{sh}	$\mathrm{kg\,s^{-1}}$	water flow rate through the heater
$\dot{V}(t)$	$\mathrm{m^3\,s^{-1}}$	volumetric flow rate of air into and out of the production house
w_{spray}	$[\mathrm{kg\,s^{-1}}]$	flow rate of water from the sprinkler system
f_{lux}	·	light correction factor

Table A.6: Notations for disturbances introduced during Humidity & Temperature Models in section 3.2.

$T_{sh,in}$	K	temperature of the water entering the heater
T_a	K	temperature of the air outside
x_a	$\frac{\text{kg water vapour}}{\text{kg dry air}}$	absolute humidity of the outside air (sensor reading)
A	$week$	age of the broiler in weeks

Table A.7: Notations for broiler introduced during Humidity & Temperature Models in section 3.2.

y	$\mathrm{J\,s^{-1}}$	total heat produced by one broiler in 20°C production house
f_t	·	temperature correction factor
T_s	°C	temperature in the production house
F	·	sensible heat ratio
T_s	°C	temperature in the production house
$Q_{sensible}$	$\mathrm{J\,s^{-1}}$	sensible heat produced by one broiler corrected for by the production house temperature.
$w_{livestock}$	$\mathrm{kg\,s^{-1}}$	water vapour produced by one broiler corrected for by the production house temperature.
$n_{broilers}$	·	number of broilers in production house

Table A.8: Notations introduced during Humidity & Temperature Models in section 3.2.

x_s	$\frac{\text{kg water vapour}}{\text{kg dry air}}$	absolute humidity of the production house air
M_d	kg	mass of dry air inside the production house
M_{drop}	kg	mass of water droplet
M_b	kg	mass of the production house walls
V_s	m^3	volume of the production house
h_m	$\mathrm{m\,s^{-1}}$	mass transfer coefficient
γ_{ws}	$\mathrm{mol\,m^{-3}}$	molar concentration of water vapour at saturation
γ_s	$\mathrm{mol\,m^{-3}}$	molar concentration of water vapour at current humidity x_s
$\aleph_v$	$\mathrm{g\,mol^{-1}}$	molar mass of water vapour
R	$\mathrm{J\,K^{-1}\,mol^{-1}}$	the universal gas constant
p_{ws}	Pa	pressure of water vapour at saturation
p_s	Pa	pressure of water vapour at current humidity x_s
p_0	Pa	standard air pressure at sea level
λ_{wd}	·	ratio between the molar mass of water and dry air
sh	·	Sherwood number
Re	·	Reynolds number
Sc	·	Schmidt number
D_v	$\mathrm{m^2\,s^{-1}}$	mass diffusion coefficient of vapour
d_{drop}	m	diameter of a drop
u_r	$\mathrm{m\,s^{-1}}$	flow speed air relative to droplet
μ_s	$\mathrm{N\,s\,m^{-2}}$	general viscosity of air
P_{sh}	m	outer perimeter of the heater
l_{sh}	m	length of the stable heater
c_d	$\mathrm{J\,kg^{-1}\,K^{-1}}$	specific heat capacity of dry air
c_v	$\mathrm{J\,kg^{-1}\,K^{-1}}$	specific heat capacity of water vapour
c_{pw}	$\mathrm{J\,kg^{-1}\,K^{-1}}$	specific heat capacity of water
c_{pi}	$\mathrm{J\,kg^{-1}\,K^{-1}}$	specific heat capacity of iron
c_{pb}	$\mathrm{J\,kg^{-1}\,K^{-1}}$	specific heat capacity of the production house walls
c_s	$\mathrm{J\,kg^{-1}\,K^{-1}}$	specific heat capacity of production house air given a humidity
ρ_s	$\mathrm{kg\,m^{-3}}$	general density of air
ρ_i	$\mathrm{kg\,m^{-3}}$	density of iron
ρ_w	$\mathrm{kg\,m^{-3}}$	density of water
A_m	m^2	surface area of a mist
A_d	m^2	surface area of a water droplet
A_i	m^2	cross-sectional area of iron in the heating pipe
A_w	m^2	cross-sectional area of water in the heating pipe
A_b	m^2	area of the inside walls of the production house
h_e	$\mathrm{J\,kg^{-1}}$	latent heat of evaporation
h_b	$\mathrm{W\,m^{-2}\,K^{-1}}$	heat transfer coefficient between the production house air and walls
h_a	$\mathrm{W\,m^{-2}\,K^{-1}}$	heat transfer coefficient between the production house walls and outside air,
h_{sh}	$\mathrm{W\,m^{-2}\,K^{-1}}$	convection heat transfer coefficient between the heater and air

Table A.9: Notations introduced during parameter estimation.

θ_{hsh}	$\mathrm{W\,K^{-1}}$	$h_{sh} \cdot P_{sh} \cdot l_{sh}$
θ_{msh}	$\mathrm{J\,K^{-1}}$	$l_{sh} \cdot (\rho_i \cdot c_{pi} \cdot A_i + \rho_w \cdot c_{pw} \cdot A_w)$
θ_{hb}	$\mathrm{W\,K^{-1}}$	$h_b \cdot A_b$
θ_{ha}	$\mathrm{W\,K^{-1}}$	$h_a \cdot A_b$
θ_{Mb}	$\mathrm{J\,K^{-1}}$	$c_{pb} \cdot M_b$
θ_{evap}	$\mathrm{m^3\,K\,J^{-1}\,s^{-1}}$	$(A_d \cdot \mathrm{sh} \cdot D_v \cdot \aleph_v) \cdot (M_{drop} \cdot R \cdot d_{drop})^{-1}$
N	$\cdot$	number of data samples
$e(t, \theta)$	$\cdot$	the error between the model and measured output
t	$\cdot$	discrete time t
θ	$\cdot$	vector of parameters to be estimated
W	$\cdot$	positive semi-definite weighting matrix
ψ	$\cdot$	nonlinear constraints
λ	$\cdot$	Lagrangian multiplier
fit	%	Fit
y	$\cdot$	Measured output
$\hat{y}$	$\cdot$	Model output

Table A.10: Notations introduced during State Observer in chapter 5.

x_k	$[\cdot]$	state at time k
u_k	$[\cdot]$	input at time k
d_k	$\cdot$	disturbance at discrete time k
w_k	$[\cdot]$	random dynamic disturbance at time k
v_k	$[\cdot]$	random sensor noise at time k
$\hat{y}_{k\|k-1}$	$\cdot$	output prediction at time k
$\tilde{y}_{k\|k-1}$	$\cdot$	output prediction error at time k
$\hat{x}_{k\|k}$	$\cdot$	state estimate at time k
$\hat{x}_{k+1\|k}$	$\cdot$	state prediction at time k
H_k	$\cdot$	linearisation of the output function $h(x, u)$
F_k	$\cdot$	linearisation of the state function $f(x, u)$
I	$\cdot$	identity matrix
K_k	$\cdot$	Kalman gain at time k
$P_{k\|k}$	$\cdot$	estimate of the state covariance at time k
$P_{k+1\|k}$	$\cdot$	prediction of the state covariance at time k
R_k	$\cdot$	sensor noise weighting matrix
Q_k	$\cdot$	process noise weighting matrix
f_c	$\cdot$	continuous time function
A_c	$\cdot$	continuous time state matrix
B_c	$\cdot$	continuous time input matrix
$\bar{x}$	$\cdot$	state equilibrium point(s)
$\bar{u}$	$\cdot$	input equilibrium point(s)
$\bar{d}$	$\cdot$	disturbance equilibrium point(s)
A_k	$\cdot$	discrete time state matrix
B_k	$\cdot$	discrete time input matrix
Q_k	$\cdot$	observer weight matrix for process noise
R_k	$\cdot$	observer weight matrix for sensor noise

Table A.11: Notations introduced during Control Strategy in chapter 6.

Q	·	the state weight matrix
R	·	the input weight matrix
K	·	controller gain
e_k	·	error between state and reference
A_{aug}	·	error augmented matrix A
B_{aug}	·	error augmented matrix B
K_i	·	integral gain for the error

Table A.12: Notations introduced during Implementation in chapter 7.

$x_{a,s,relative}$	%	is the relative humidity of the outside a or production house s
$p_{a,s}$	Pa	is the pressure of water vapour at current humidity for a or s
$x_{a,s}$	$\frac{\text{kg water vapour}}{\text{kg dry air}}$	absolute humidity of the outside a or production house s
V_{lab}	m^3	the volume of the laboratory
$t_{d,n}$	s	duty cycle for actuator n
$u_{actuator,n}$	·	input to actuator n
$u_{max,n}$	·	maximum output of actuator n

Appendix B

Initial Guess for Parameter Estimation for Mosegaarden

Table B.1: Values of model parameters found before parameter estimation.

Parameter	**Initial Guess**	**Unit**	**Origin**
h_{sh}	64.9	$\mathrm{W\,m^{-2}\,K^{-1}}$	Old production house from [12]
P_{sh}	0.279	m	Old production house from [12]
l_{sh}	186.3	m	Old production house from [12]
A_i	0.0057	$\mathrm{m^2}$	Old production house from [12]
A_w	0.0005	$\mathrm{m^2}$	Old production house from [12]
A_b	410.65	$\mathrm{m^2}$	Old production house from [12]
h_a	7.5	$\mathrm{W\,m^{-2}\,K^{-1}}$	Old production house from [12]
h_b	58.9	$\mathrm{W\,m^{-2}\,K^{-1}}$	Old production house from [12]
ρ_i	7870	$\mathrm{kg\,m^{-3}}$	From look-up table
ρ_w	992.3	$\mathrm{kg\,m^{-3}}$	From look-up table at 313 K
ρ_s	1.205	$\mathrm{kg\,m^{-3}}$	From look-up table at 293 K
c_{pi}	412	$\mathrm{J\,kg^{-1}\,K^{-1}}$	From look-up table
c_{pw}	4179.6	$\mathrm{J\,kg^{-1}\,K^{-1}}$	From look-up table at 313 K
c_d	1006	$\mathrm{J\,kg^{-1}\,K^{-1}}$	From look-up table at 293 K
c_v	1864	$\mathrm{J\,kg^{-1}\,K^{-1}}$	From look-up table at 293 K
h_e	2453500	$\mathrm{J\,kg^{-1}}$	From look-up table at 293 K
p_0	101325	Pa	From look-up table at sea level
$\aleph_v$	0.018	$\mathrm{kg\,mol^{-1}}$	From look-up table
D_v	$2.42 \cdot 10^{-5}$	$\mathrm{m^2\,s^{-1}}$	From look-up table at 293 K
R	8.31	$\mathrm{J\,K^{-1}\,mol^{-1}}$	From look-up table
sh	2	·	Calculated at zero relative velocity in Equation 3.17
λ_{wd}	0.62	·	From look-up table
$T_{sh,in}$	313.15	K	From Mosegaard
V_s	9000	$\mathrm{m^3}$	From Mosegaard
M_b	1000	kg	Guess
c_{pb}	1000	$\mathrm{J\,kg^{-1}\,K^{-1}}$	Guess
$n_{broilers}$	8000	·	Guess
d_{drop}	$1 \cdot 10^{-4}$	m	Guess
M_{drop}	$1.04 \cdot 10^{-5}$	kg	$M_{drop} = 4 \cdot 3^{-1} \cdot \pi \cdot \left(d_{drop} \cdot 2^{-1}\right)^2 \cdot \rho_w$
A_d	$3.14 \cdot 10^{-8}$	$\mathrm{m^2}$	$A_d = 4 \cdot \pi \cdot \left(d_{drop} \cdot 2^{-1}\right)^2$

Appendix C

Forward Euler Discritisation

Before using Backwards Euler for discritisation, an attempt was made with Forwards Euler. Given an ODE

$$\dot{x} = f(t, x), \tag{C.1}$$

both sides of the ODE is integrated over the interval $[t_0, t_1]$ in Equation C.2.

$$\begin{gathered} \int_{t_0}^{t_1} \dot{x}\mathrm{d}t = \int_{t_0}^{t_1} f(t,x)\mathrm{d}t = x(t_1) - x(t_0) \\ \Downarrow \\ x(t_1) = x(t_0) + \int_{t_0}^{t_1} f(t,x)\mathrm{d}t \end{gathered} \tag{C.2}$$

To solve $\int_{t_0}^{t_1} f(t,x)\mathrm{d}t$ the numeric integration method the rectangular rule is utilised with stepsize $h = t_1 - t_0$.

$$\begin{gathered} \int_{t_0}^{t_1} f(t,x)\mathrm{d}t \approx hf(t_0, x(t_0)) \\ \Downarrow \\ x(t_1) = x(t_0) + hf(t_0, x(t_0)) \end{gathered} \tag{C.3}$$

The results from the Extended Kalman Filter utilizing the Forward Euler method for discritisation are plotted in Figure C.1, C.2, C.3, C.4 and C.5. Looking at these plots it is clear that the EKF performs badly when utilising the Forward Euler method.

Furthermore the biggest eigenvalue for the Forward Euler equation are plotted in Figure C.6. Since it is bigger than one, then the system is unstable.

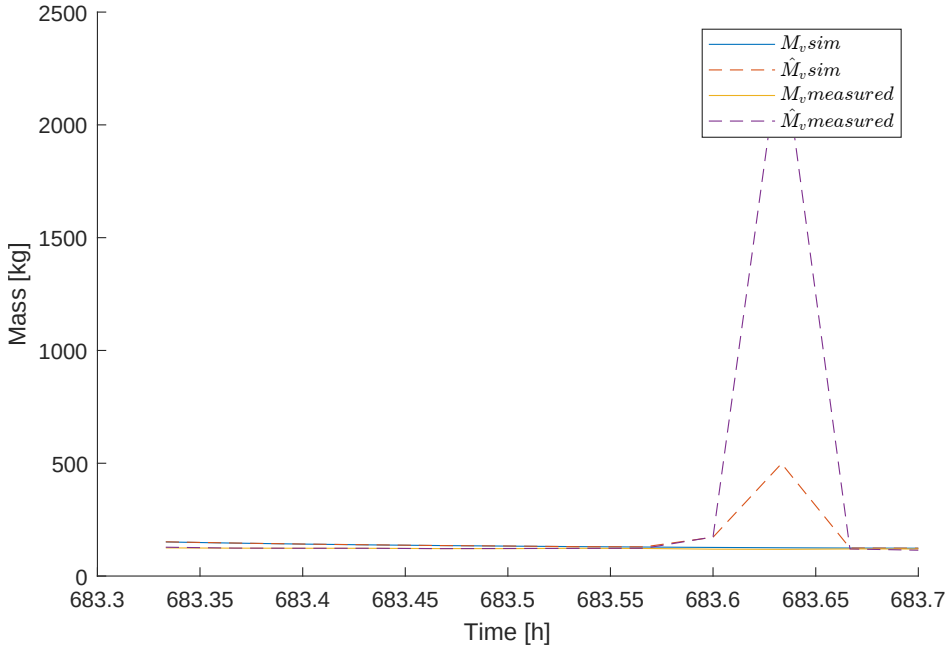

Figure C.1: Results for M_v from the EKF using Forward Euler discritisation.

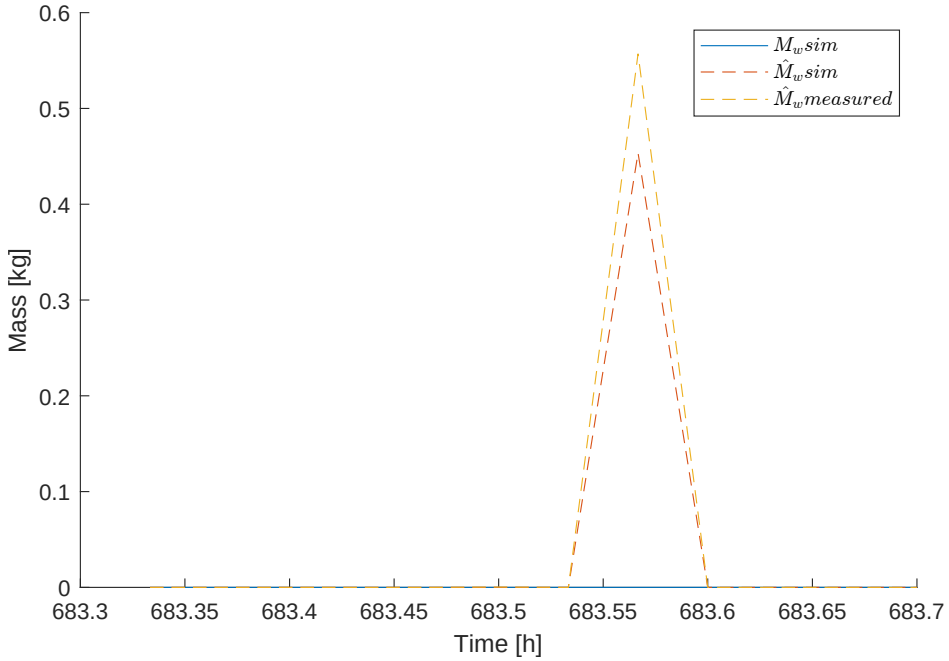

Figure C.2: Results for M_w from the EKF using Forward Euler discritisation.

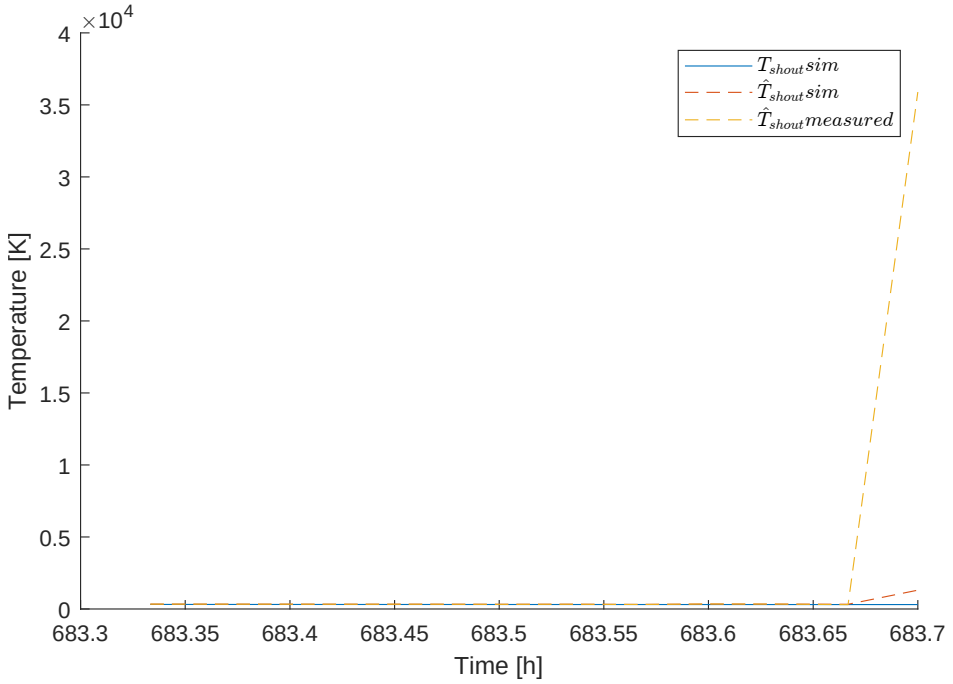

Figure C.3: Results for $T_{sh,out}$ from the EKF using Forward Euler discritisation.

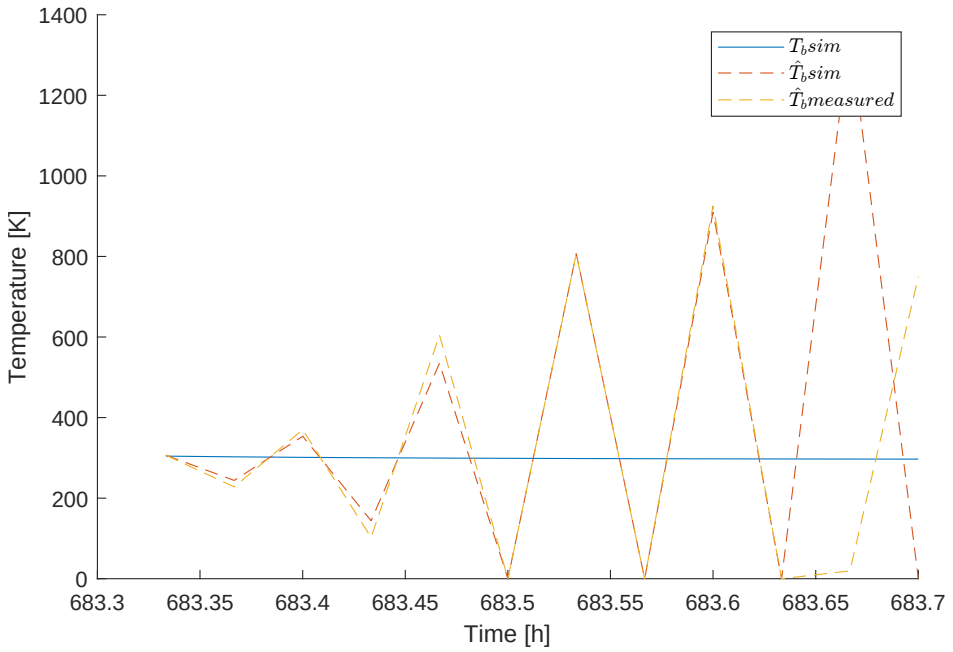

Figure C.4: Results for T_b from the EKF using Forward Euler discritisation.

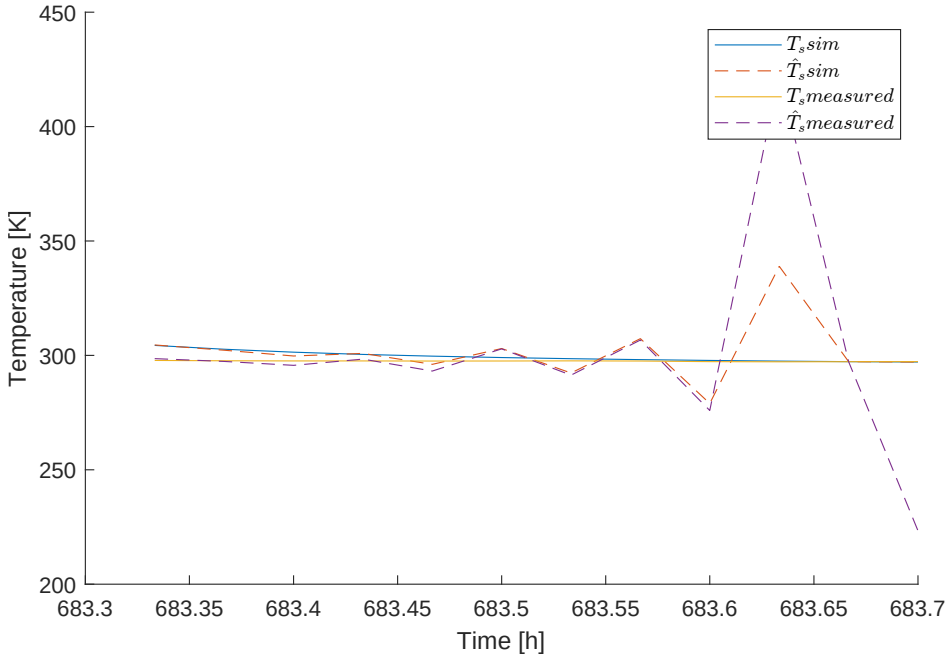

Figure C.5: Results for T_s from the EKF using Forward Euler discritisation.

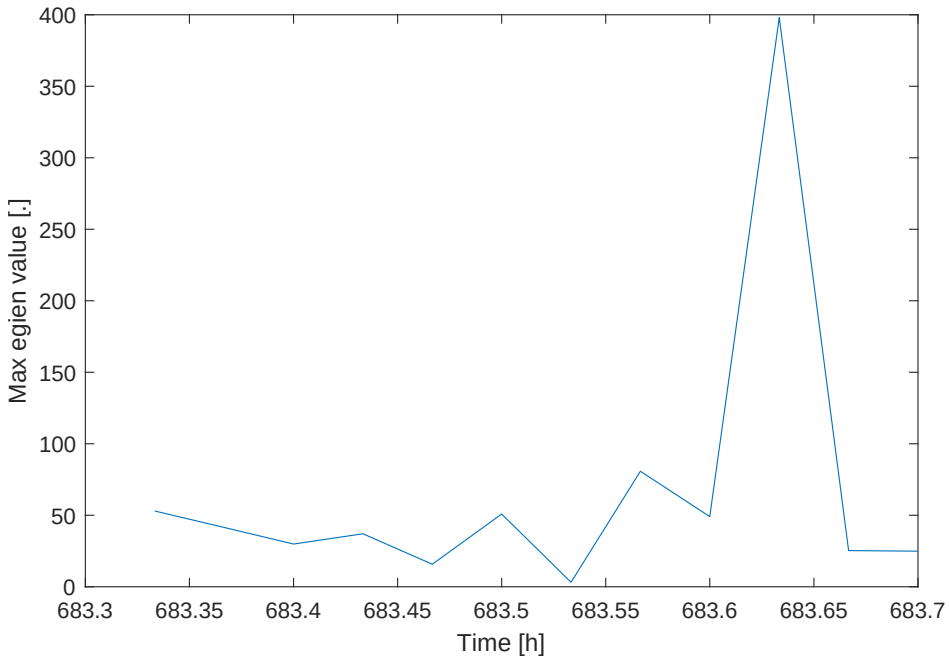

Figure C.6: Biggest eigenvalue for the Forward Euler equation.

Appendix D

Parameter Estimation for the Air Physical Laboratory

No data for the Air Physical Laboratory located at SKOV A/S was available. Therefore it was necessary to generate some data in the beginning of the week used for testing as to design an observer and controller tuned for the laboratory.

This meant repeating the steps:

- Parameter estimation,
- Observer design and tuning,
- LQG design and tuning,
- LQI design and tuning.

In section D.1 and section D.2 the results of the parameter estimation and observer tuning done for the Air Physical Laboratory are shown. The results for the LQG and LQI can be seen in the test results under implementation in chapter 7.

D.1 Parameter Estimation for the Air Physical Laboratory

The first step is the parameter estimation. To be able to do parameter estimation data demonstrating the dynamics of the system are needed. This data was collected at SKOV A/S and are plotted in Figure D.1, D.2 and D.3.

Changing only the volume of building the same initial guesses for parameters from Table 4.1 are utilised. These initial guesses together with the final parameters are listed in Table D.1.

The resulting fit of the model is plotted in Figure D.4, showing the temperature T_s and humidity x_s having acceptable results for observer and controller design.

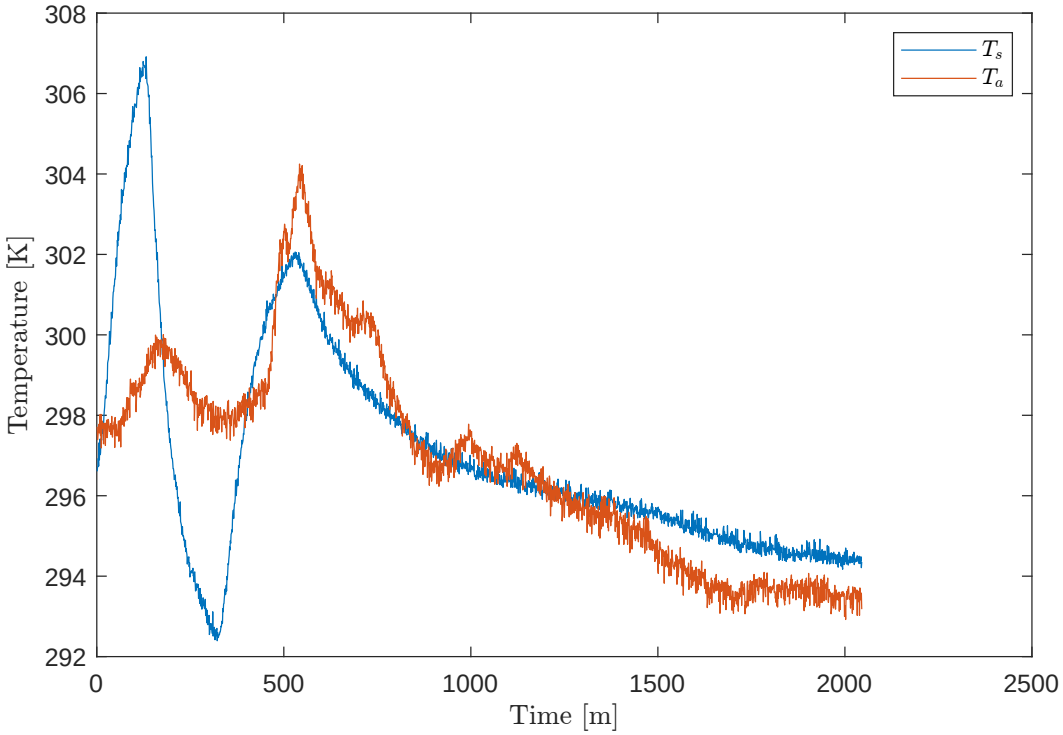

Figure D.1: Measured temperature from the Air Physical Laboratory and from the outside.

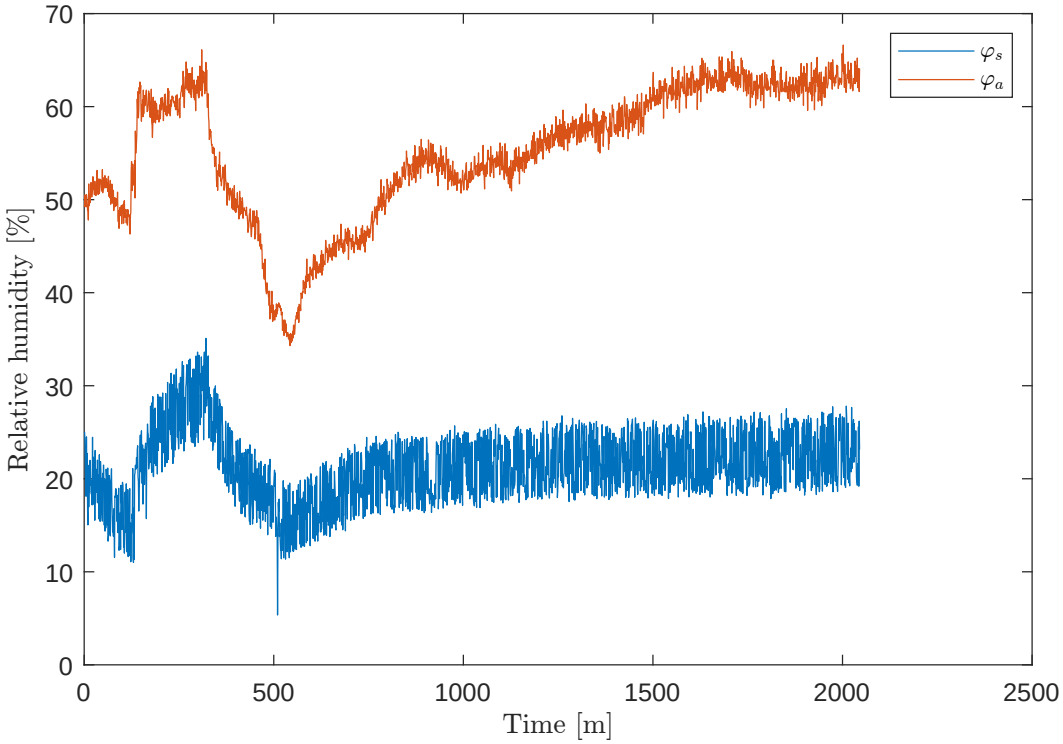

Figure D.2: Measured humidity from the Air Physical Laboratory and from the outside.

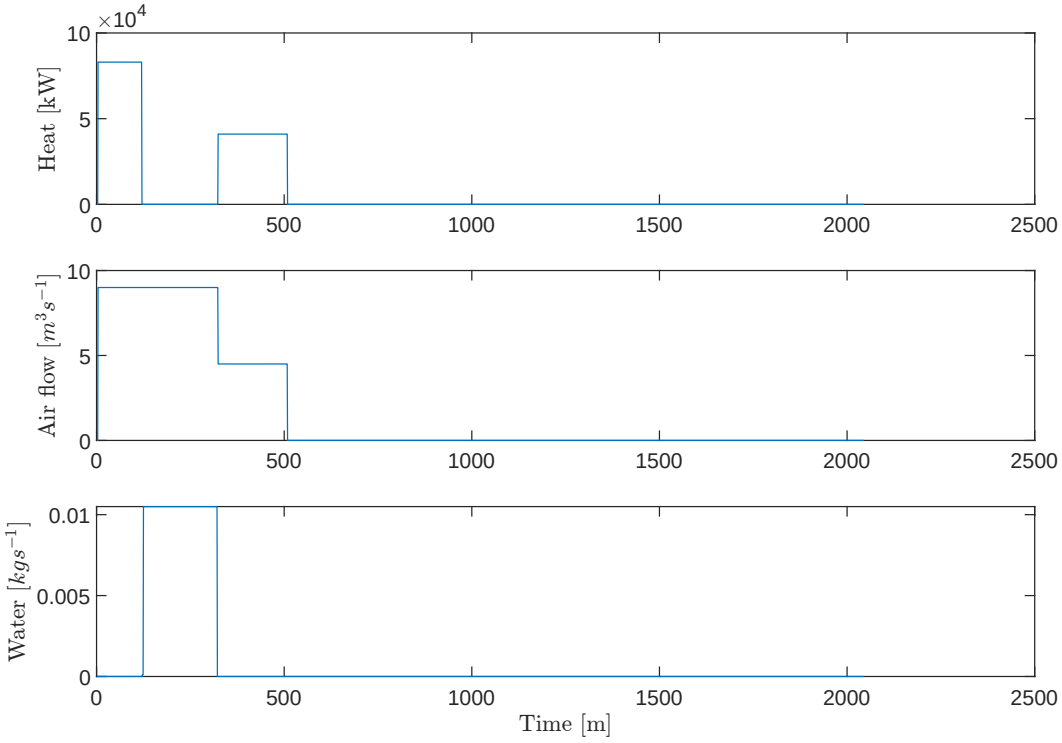

Figure D.3: Applied input to the Air Physical Laboratory.

Table D.1: Parameters to be estimated with initial guess and final value for the Air Physical Laboratory.

Parameter	**Initial Guess**	**Final Value**	**Unit**
h_e	2453500	2453601.09821	$\mathrm{J\,kg^{-1}}$
θ_{evap}	0.06341	0.065646	$\mathrm{m^3\,K\,J^{-1}\,s^{-1}}$
λ_{wd}	0.62198	0.68109	·
p_0	101325	101325	Pa
c_d	1006	1053.24035	$\mathrm{J\,kg^{-1}\,K^{-1}}$
c_v	1864	11759.2829	$\mathrm{J\,kg^{-1}\,K^{-1}}$
ρ_s	1.205	1.24978	$\mathrm{kg\,m^{-3}}$
V_s	600	829.8848	$\mathrm{m^3}$
θ_{hb}	24187.285	22713.1723	$\mathrm{W\,K^{-1}}$
θ_{ha}	3079.875	1641.7425	$\mathrm{W\,K^{-1}}$
θ_{Mb}	10000000	325597.8095	$\mathrm{J\,K^{-1}}$

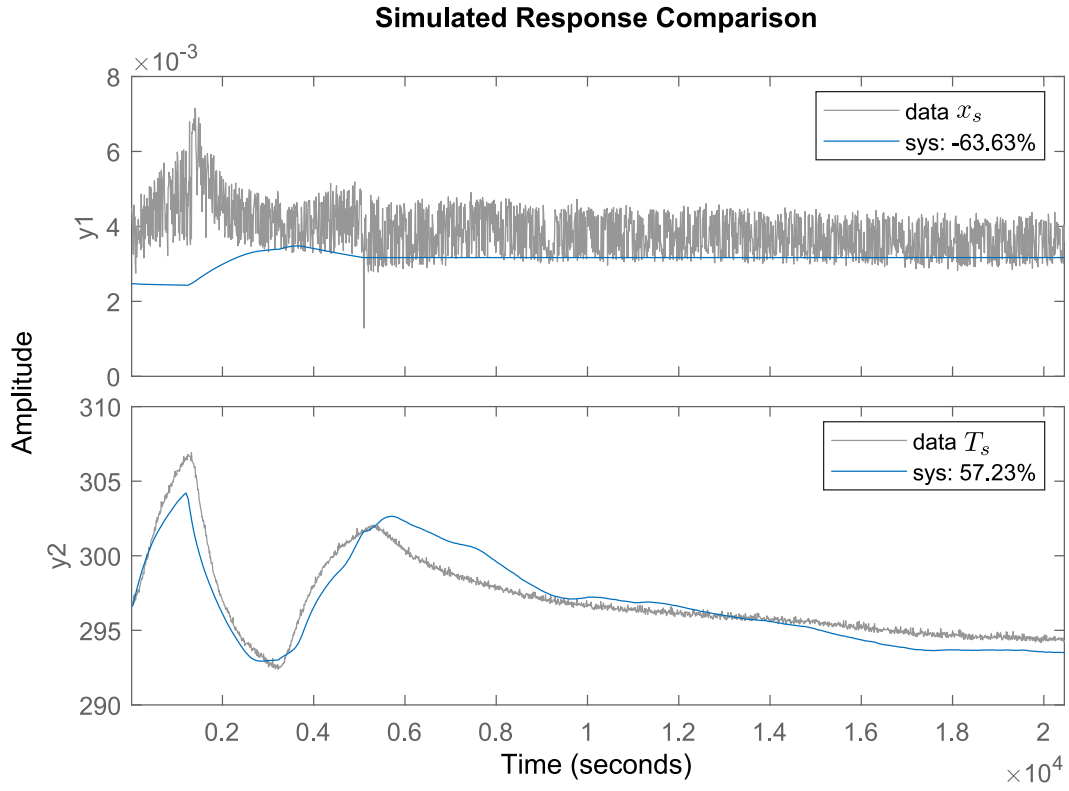

Figure D.4: Comparison between the model and measured data given the estimated parameters in Table D.1 for an open-loop simulation of the data from the Air Physical Laboratory.

D.2 Observer design and tuning

Based on the parameters found for the Air Physical Laboratory, an EKF is tuned. In Figure D.5, D.6, D.7 and D.8 the results for the states M_v, M_w, T_b and T_s are plotted respectively. In all plots are included a test based on simulation output and measured output.

In Figure D.5 the estimate for M_v is shown to converge on the measured output while filtering the noise.

In Figure D.6 the estimate of M_w from measured does not seem to get as big as simulation.

Both Figure D.7 and D.8 shows similar looking estimates. T_s follows the measurement well.

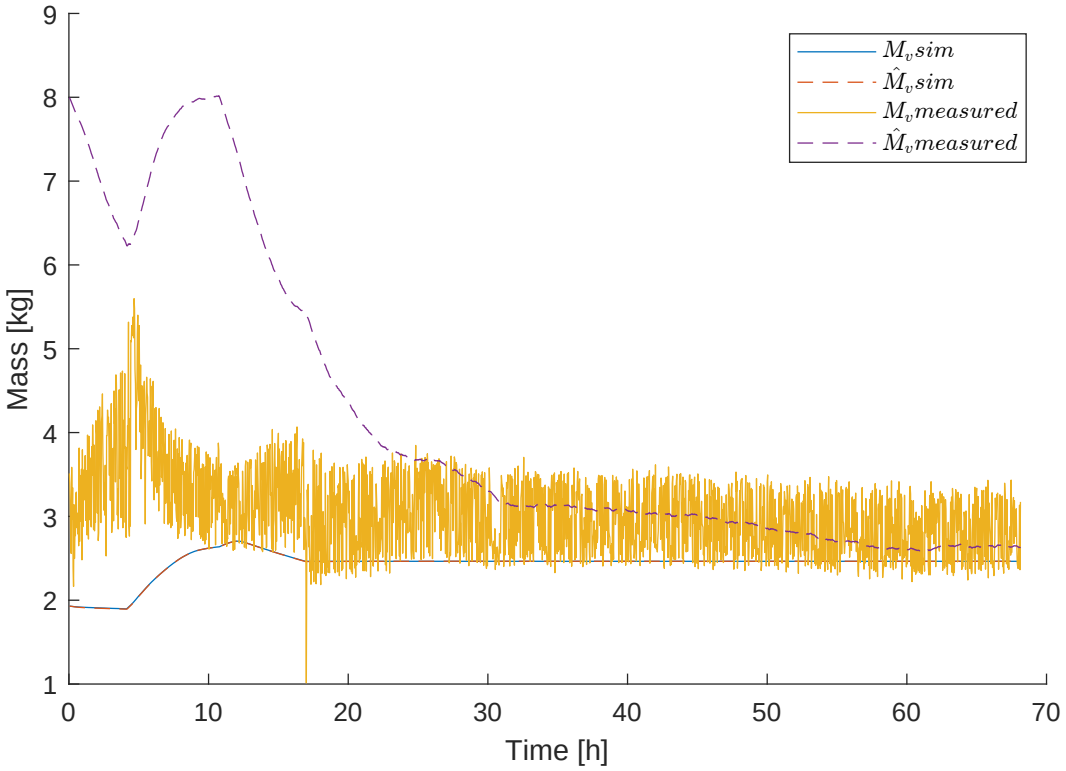

Figure D.5: Estimate of M_v given data from simulation output and measured data from Air Physical Laboratory.

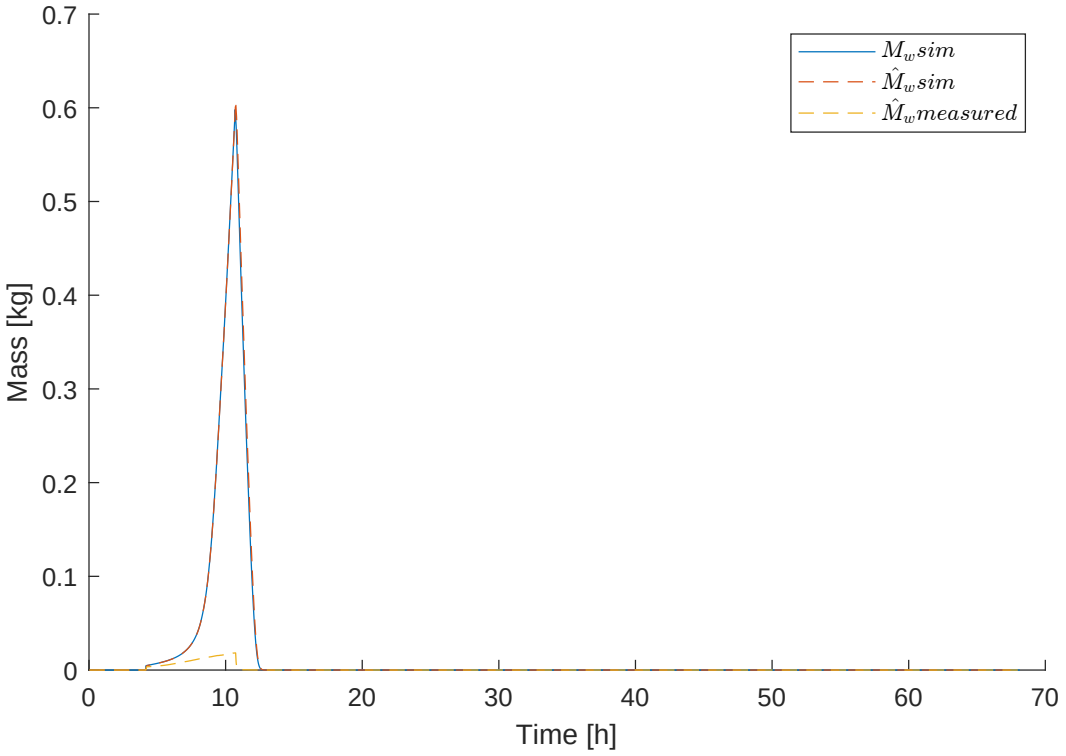

Figure D.6: Estimate of M_w given data from simulation output and measured data from Air Physical Laboratory.

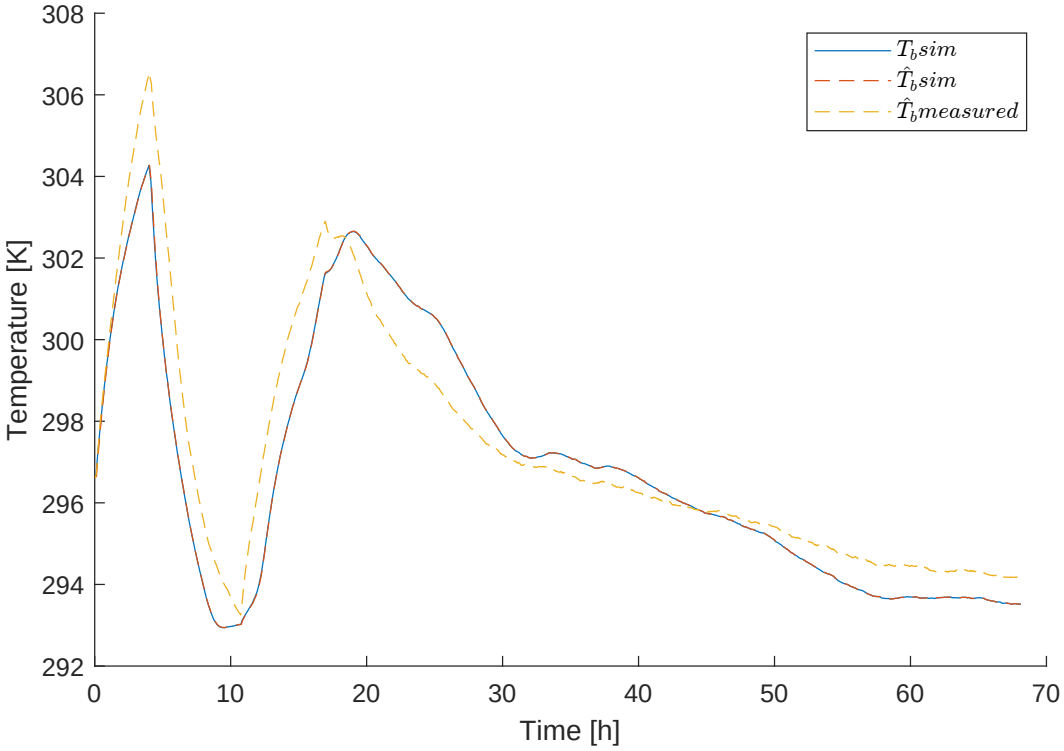

Figure D.7: Estimate of T_b given data from simulation output and measured data from Air Physical Laboratory.

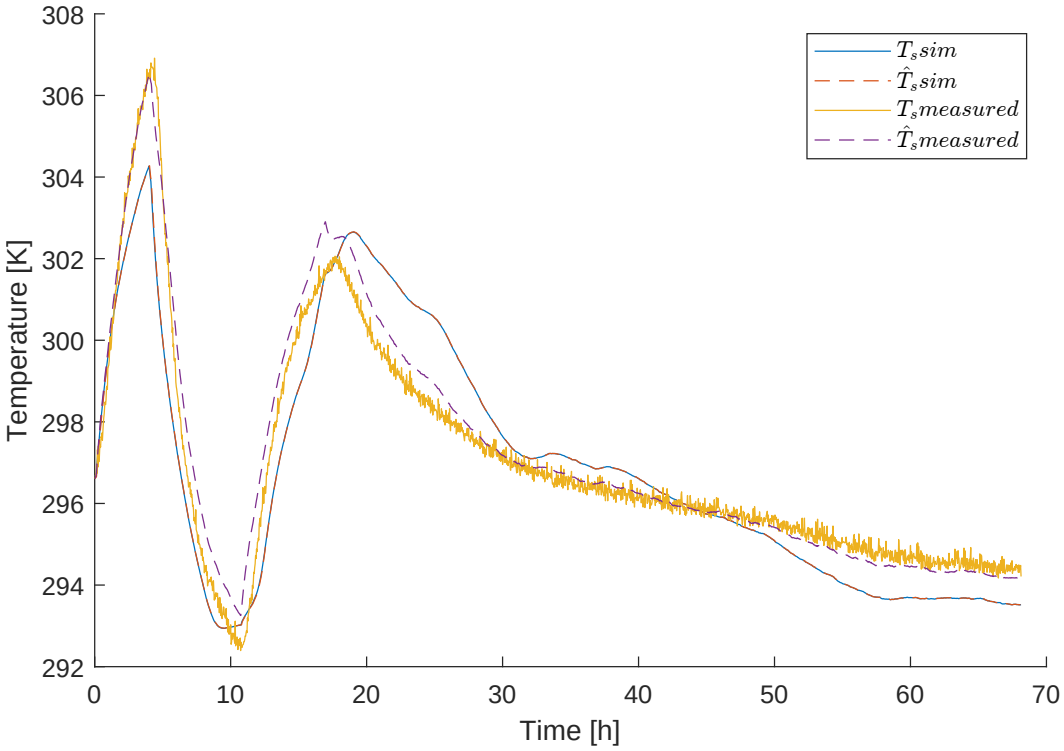

Figure D.8: Estimate of T_s given data from simulation output and measured data from Air Physical Laboratory.